Information Circular 43

STATE OF ARKANSAS

ARKANSAS GEOLOGICAL SURVEY
BEKKI WHITE, DIRECTOR AND STATE GEOLOGIST

INFORMATION CIRCULAR 43

UNCONVENTIONAL RESERVIOR CHARACTERISTICS OF THE BROWN DENSE MUDSTONE (LOWER SMACKOVER FORMATION), SESSIONS NO. 1 WELL, UNION COUNTY, ARKANSAS

by

Peng Li, Michael Ratchford, Marc Charette, Bradley Walls, and Richard Philp

Little Rock, Arkansas

2016

STATE OF ARKANSAS
Asa Hutchinson, Governor

ARKANSAS GEOLOGICAL SURVEY
Bekki White, Director and State Geologist

COMMISSIONERS

Dr. Richard Cohoon, Chairman……..Russellville

William Willis, Vice Chairman……..Hot Springs

Quin Baber III……Benton

Bill Cains……...Altus

Ken Fritsche……Greenwood

Gus Ludwig……..Quitman

David Lumbert……...Maumelle

Table of Contents

List of Figures and Tables

Introduction

The Arkansas Geological Survey (AGS) has undertaken a 3-year research project to explore the reservoir characteristics and resource potential of the Brown Dense Mudstone in southern Arkansas under the USGS Grant No. G12AC20245 (Supplement #0002). This mudstone, a lower member of the Smackover Formation, is an unconventional oil reservoir found in southern Arkansas and northern Louisiana. The Brown Dense has been of interest since 2009, when the first wildcat well, Endsley 1-24H was vertically drilled and cored by Border Exploration into this interval in Lafayette County, Arkansas.

The formation ranges in vertical depths from 8,000 to 11,000 ft and appears to be laterally extensive over a large area ranging in thickness from 300 to 550 ft. The Lower Smackover Brown Dense (LSBD) member is an Upper Jurassic age, kerogen-rich carbonate source rock found across the Gulf Coast region of the southern United States from Texas to Florida. The oil industry extensively reviewed the Brown Dense across the region and has indications that the right mix of reservoir depth, thickness, porosity, matrix permeability, sealing formations, thermal maturity and oil characteristics occur in the area of southern Arkansas and northern Louisiana. This region of Arkansas and Louisiana has produced oil and gas from the Upper Smackover since the 1920s. The LSBD member is the source rock for these Upper Smackover fields. It has the critical properties necessary to be a successful play and compares favorably to other productive oil plays in the United States.

Current State of Exploration

Southwestern Energy (SWN) is the top drilling exploration company in the LSBD member. As of December 31, 2014, SWN held approximately 304,371 net acres in the area at an average cost of $831 per acre and had drilled 14 wells in the area, 6 of which were currently producing in northern Louisiana and 2 of which were drilled in southern Arkansas. Late in 2014, SWN acquired 75 miles of 3-D seismic data and is currently in the process of analyzing that data and the results to date.

As of July 2015, 9 LSBD wells have been drilled in southern Arkansas, 4 of which are horizontal wells and 1 of which is currently producing small amount of oil (Appendix 1). Cabot Oil & Gas Corporation disclosed that its first LSBD well, Denny 1-32H well, in Union County, Arkansas, reached a peak production rate of 206 barrels of oil per day from a 10-stage hydraulic fracturing job. The well has been plugged and abandoned since April 16, 2015, as shown on the Arkansas Oil and Gas Commission database. Roberson 18-19 1-15H, which was the first LSBD well drilled by SWN in Columbia County, Arkansas, had an initial production rate of 103 barrels of oil and 200 mcf of

natural gas for 24 hours. This well has been temporarily abandoned since October 25, 2012. SWN's second attempt in southern Arkansas is McMahen 19-21 1-7, a vertical well in Columbia County, which had a peak daily production of 17 barrels of oil and 299 mcf of natural gas. It has been temporarily abandoned since October 23, 2014. The only current LSBD producing well in southern Arkansas is SWF Red River Land 1 well, which was drilled in Union County by Weiser-Brown Operating Company and then transferred to Roil Energy, LLC. The initial production of the well was 6 barrels of oil per day. Since September 2012 through April 2015, it has cumulatively produced 786 barrels of oil.

Samples and Experimental Methods

By signing a confidentiality agreement with the Betsy Production Company, the AGS obtained the cores, crude oil, and completion reports of the Sessions #1 well (API: 03-139-13401-00-00) located in Union County, Arkansas, which was vertically drilled and cored in the Brown Dense Mudstone in 2013 for testing its unconventional reservoir potential (Figure 1).

Using petrophysical, petrographic, and rock mechanics techniques, the AGS has been able to evaluate the reservoir characteristics of the Brown Dense Mudstone. The Sessions #1 core was initially sent to Delta Core Analysts in Shreveport, LA for routine porosity, permeability, and basic core descriptions. Delta Core Analysts also measured oil and gas saturations. The Sessions #1 core was then sent to Weatherford Laboratories located in Houston, TX to perform a series of analyses as listed below. Note that three plugs were selected for mercury injection capillary pressure tests, but the process failed due to insufficient pores. A crude oil sample was sent to the Petroleum Geochemistry and Environmental Forensics Laboratory at the University of Oklahoma for biomarker and stable carbon isotopic analyses.

Helical CT Scanning

Helical computed tomography (CT) scanning is one of the very first procedures performed on core arriving at the lab. It provided high resolution imaging of internal features throughout the core that can be visualized in the videos of mp4 format. CT scanning helps characterize reservoir types, improve slab and plug orientations/sampling locations, and identify fracture geometries and relationships, orientation of bedding planes and location of induced artifacts. Bulk density (RHOB) values were derived from CT numbers (Hounsfield units) as shown on the whole core bulk density plots (Appendix 2).

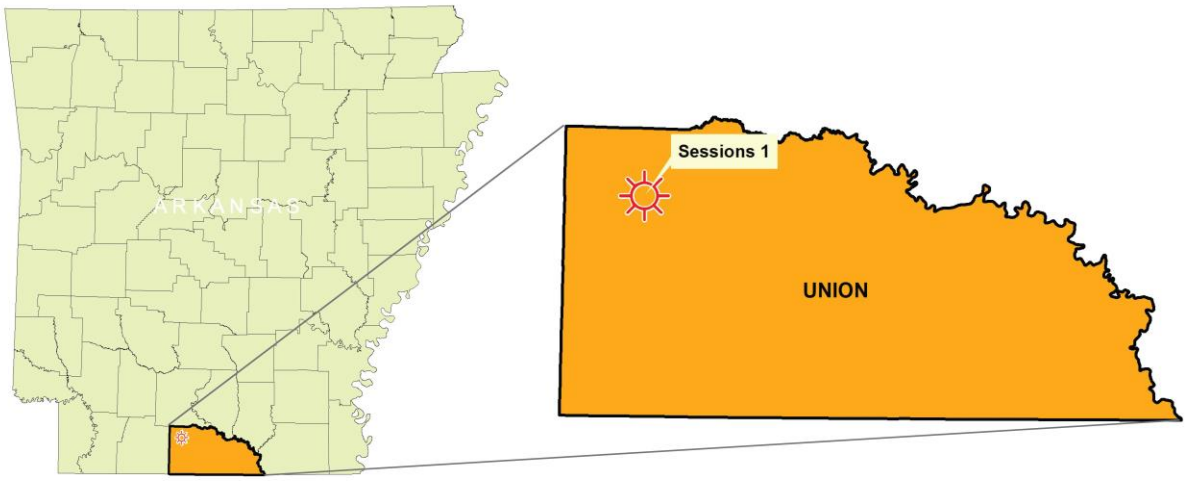

Figure 1. Location map of the Sessions #1 well, Union County, Arkansas.

Thin Sections

Standard sized thin sections were prepared with fluorescent-spiked, blue-dyed epoxy impregnation and dual carbonate staining. These thin sections were photographed using a high resolution petrographic microscope set at specified magnifications (50X and 200X) in plane polarized light. The thin sections were then described qualitatively including a mineralogical and textural thin section description of grain size, sorting, porosity types, and mineral abundances.

Core Description

Detailed core descriptions provided information on lithologies, textures, fossil assemblages, sedimentary structures, and depositional environments.

Geochemical Analysis

Geochemical analysis was performed in the form of total organic carbon (TOC) and Rock-Eval pyrolysis to evaluate the organic richness, kerogen type, and thermal maturity of the sampled cores.

Field Emission Scanning Electron Microscopy

Weatherford was retained to perform argon ion milling (AIM) and field emission scanning electron microscopy (FE-SEM). AIM is an electron microscopy sample preparation service which produces a debris-free surface for optimum examination of micro to nanopores, which was of particular interest for this study. FE-SEM provides high resolution, high magnification SEM imaging capabilities that are especially beneficial for characterizing micro- to nano-sized pores in shale samples.

Rock Mechanics Analysis

Rock mechanics tests were performed including X-ray diffraction (XRD), a quantitative analysis of bulk (whole rock) and clay mineralogy, triaxial compressive strength, and acoustic (ultrasonic) velocity.

Shale Rock Properties Analysis

Shale rock properties analysis provided as-received bulk density, dry bulk density, dry grain density, as-received fluid saturations (water, oil, and gas), dry helium porosity, and dry press decay permeability.

Thin Section Images and Descriptions

Introduction

Eighteen (18) thin sections were prepared and described by Weatherford Laboratories. The samples have been impregnated with fluorescent-spiked, blue-dyed epoxy at ambient conditions and dual carbonate staining. The photomicrographs show the standard-sized thin sections prepared at 27mm x 46mm with magnifications 50X (A) and 200X (B). Exception is for Plate 8 that has additional photomicrographs of (C) and (D), showcasing different matrix materials and organic matter within the sample. Each set of thin section images is followed by the mineralogic and textural description of grain size, sorting, porosity types, and mineral abundances (Plates 1-18).

Mineralogical and Textural Characteristics

The Dunham classification system for carbonate rocks was used to describe the detailed textural components in thin sections. The types of lithology present in the samples include: (1) slightly silty/sandy limestone ranging in texture from mudstone to wackestone (Plates 2, 7, 8, 9, 12, 15, and 17); (2) slightly silty/sandy, bioclastic limestone with texture ranging from crystalline, wackestone to packstone (Plates 4, 5, 6, 10, 11, 16, and 18); (3) slightly silty limestone with an algal boundstone texture (Plates 13 and 14); (4) slightly sandy peloidal limestone with a wackestone texture (Plate 1); and (5) slightly sandy, oolitic limestone with a grainstone texture (Plate 3). Detrital grains are comprised of quartz sand/silt, feldspar, muscovite, and phosphatic fragments. Allochems include peloids, ooids, limestone lithoclasts, spherules, foraminifera, brachiopod fragments, echinoderm fragments, and algal fragments/laminites.

The matrix of all samples has been mostly replaced by fine sparry calcite. Organic material and undifferentiated detrital clays are associated with the microstylolites, dissolution seams, and mudstone laminations. Calcite is the primary authigenic mineral in all samples. Many allochems have been fully micritized which makes identification impossible. Dolomite, baroque dolomite, anhydrite, and gypsum are sparse and occur as pore and vug-filling cement. Pyrite is sparse and present as a replacement of calcite and organic material. Authigenic quartz is rare and replaces calcite. Rare authigenic kaolinite locally occludes vugs. Pores are rare for most of the samples. Some of the pores and fractures are sampling-induced.

7376.65’ - 7376.80’
Plate 1

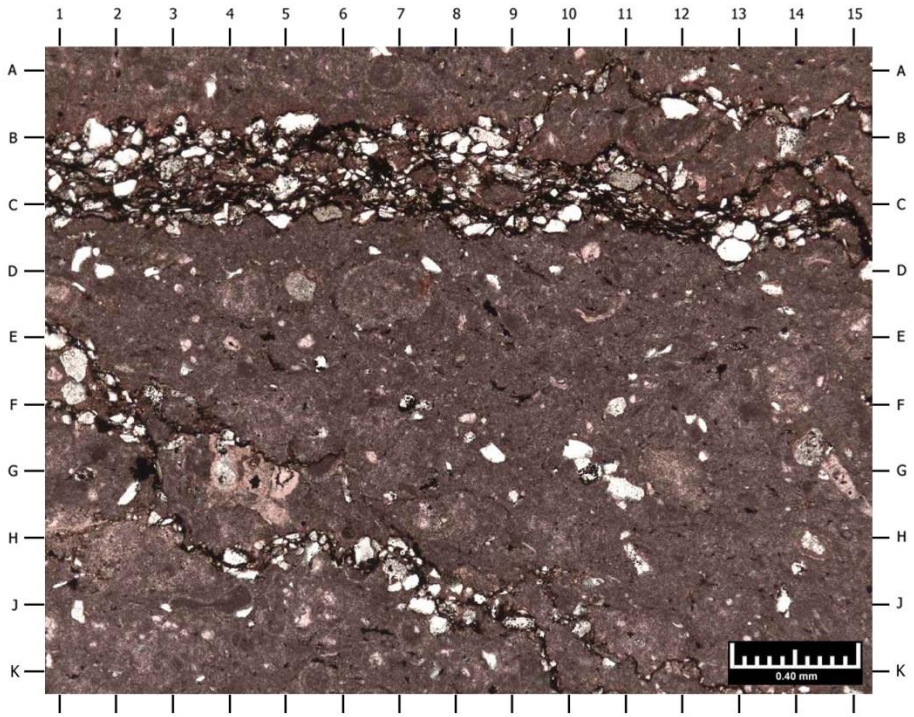

A

50X

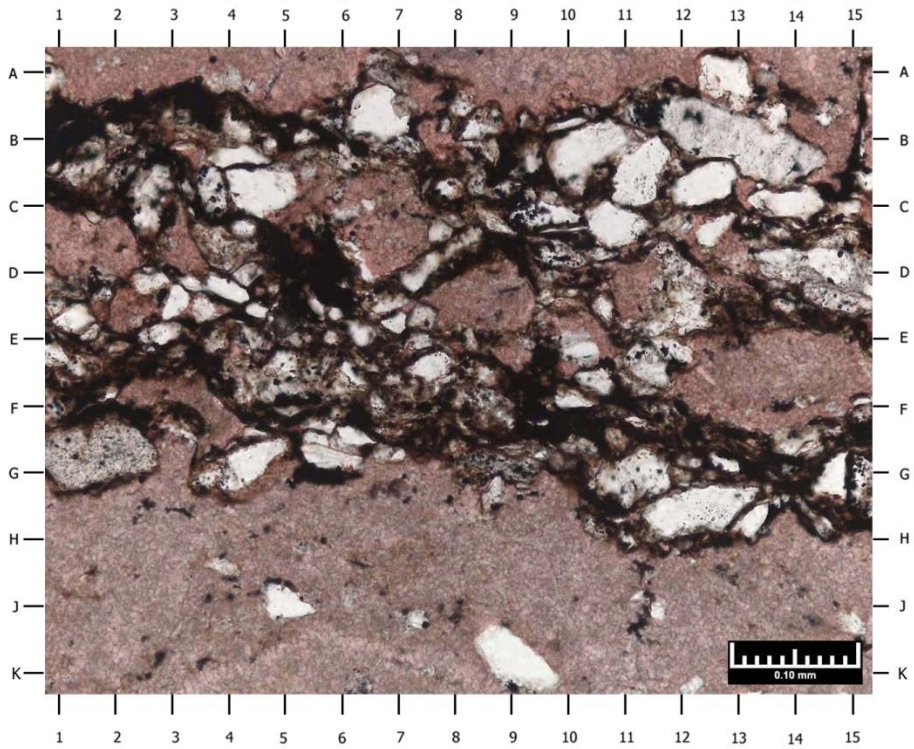

B

200X

SAMPLE DEPTH: 7376.65 – 7376.80 FEET
PLATE 1

Lithology: Slightly sandy peloidal limestone
Sedimentary Fabric: Limestone texture is a wackestone; moderately common stylolites
Compaction: Moderate to high (based on the presence of stylolites)

Detrital Grains / Allochems:

Major: Peloids
Minor: Quartz sand; quartz silt; foraminifera; potassium feldspar; plagioclase feldspar
Accessory: Ooids; muscovite; brachiopod fragments; limestone lithoclasts; undifferentiated heavy minerals

Matrix: The matrix has been mostly replaced to fine sparry calcite; organic material and undifferentiated detrital clays are associated with the microstylolites.

Cement / Replacement: Calcite is the primary authigenic mineral in this sample and occurs in a variety of ways: replacement/recrystallization of allochems, pore- and vug-filling cement, micritization of allochems, and fine spar replacement of the matrix. Many allochems have been micritized fully making identification impossible. Dolomite and baroque dolomite are sparse and occur as cement. Pyrite is sparse and occurs as a replacement of calcite and organic material.

Porosity Types: Rare fracture porosity; it is possible that organic material originally occluding these pores have been leached by the sampling process. Rare sampling induced cracks.

Magnification: A: 50X B: 200X

A) Photomicrograph 1A depicts a slightly sandy wackestone. Stylolites are common in this field of view (BC1-CD15, EF1-K10, AB10-AB15) and contain higher concentrations of siliciclastic grains. Detrital grains include quartz (AB12, AB1.7, FG10), feldspar (C5.7, DE5.2, FG14), and muscovite (C3.2, BC3.8, B7.8). Undifferentiated allochems (D6-7, F11.8, G14.8) have been almost completely micritized, making identification difficult. Authigenic minerals include calcite (stained pink; G4.8, E5.3, EF3.2), dolomite (unstained; G3.8), and pyrite (G4.3, FG1.8, DE8.6). The matrix (A3, K3, E2) has been recrystallized to fine sparry calcite. Organic material and undifferentiated detrital clays are associated with the stylolites.

B) High magnification view of Photomicrograph 1A at D7 depicts several stylolites (AG1-AH15). Detrital grains, which include quartz (AB6.5, JK9, BC12-13), feldspar (G1-2, CD3.8), and muscovite (CD10), are concentrated within the stylolites. Undifferentiated detrital clays and organic material are also more common within the stylolites. The matrix has been recrystallized to fine sparry calcite (stained pink; A2.5, A9.5, H1). Authigenic pyrite (A3.8, A14.9, C3.7) partially replaces calcite.

7389.20’ - 7389.30’
Plate 2

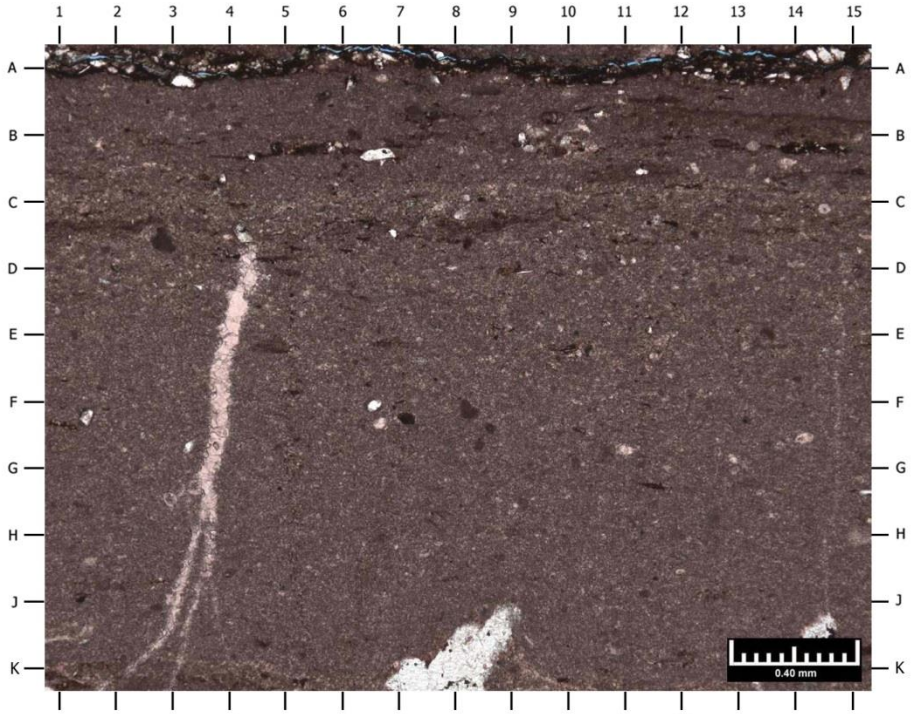

A

50X

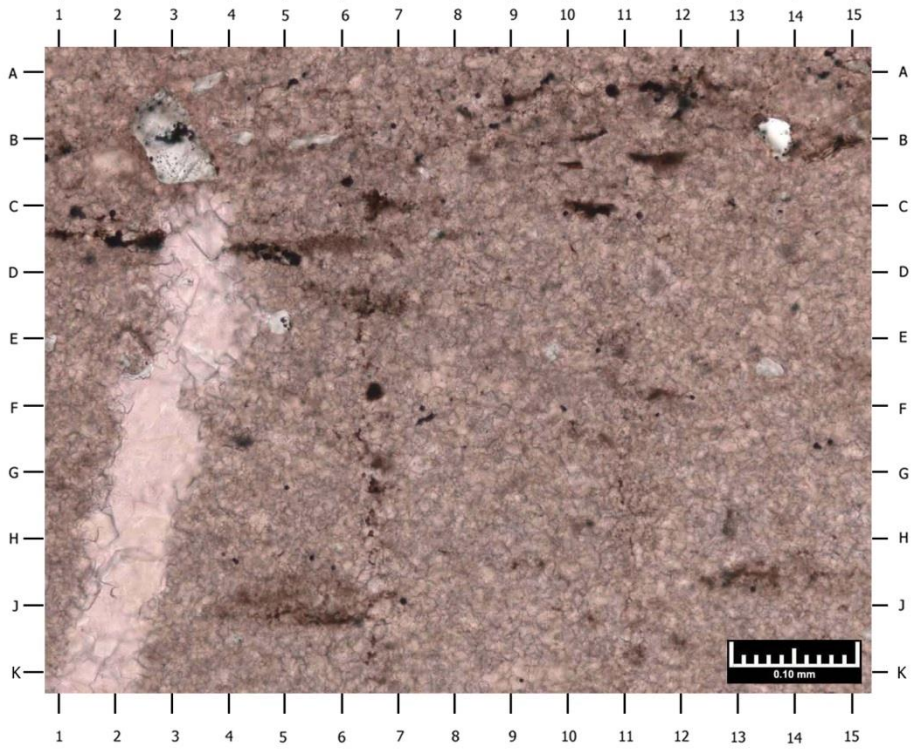

B

200X

SAMPLE DEPTH: 7389.20 – 7389.30 FEET
PLATE 2

Lithology: Slightly silty limestone

Sedimentary Fabric: The limestone texture ranges from a mudstone to a wackestone; several microstylolites and calcite-filled fractures are present; faint laminations are moderately common

Compaction: Moderate to high (based on the presence of incipient microstylolites)

Detrital Grains / Allochems:

Major: N/A

Minor: Peloids; quartz silt

Accessory: Quartz sand; muscovite; spherules; miliolid foraminifera; plagioclase feldspar

Matrix: The matrix has been mostly replaced to fine sparry calcite; organic material and undifferentiated detrital clays are associated with the microstylolites.

Cement / Replacement: Calcite is the primary authigenic mineral in this sample and occurs in a variety of ways: replacement/recrystallization of allochems, filling fractures, micritization of allochems, and fine spar replacement of the matrix. Many allochems have been micritized making complete identification impossible. Gypsum is rare and occurs as a vug-filling cement. Dolomite is rare occurring as a replacement of calcite. Pyrite is sparse and occurs as a replacement of calcite and organic material.

Porosity Types: Rare pores associated with organic material and clays within microstylolites; rare sampling-induced cracks

Magnification: A: 50X B: 200X

A) Photomicrograph 2A depicts a slightly silty lime mudstone to wackestone. A calcite-filled fracture extends from CD4.3 to K2 (calcite stained pink). Peloids (CD2.7, EF4-5, F8.2) are the primary allochem in this sample. These allochems have been micritized making identification difficult. Spherules (C14.4) and miliolid foraminifera (AB9.7) are also present. Detrital grains include quartz silt (F6.6, FG3.3, CD6.8), muscovite (A1.4, D9.3), and quartz sand (AB3.2, BC6.7). An incipient microstylolite extends from A1-15. Organic material and detrital clays are associated with the stylolite. Pyrite (A6, K7.9, JK14.6) partially replaces organic material and calcite and is disseminated throughout the matrix. Gypsum cement is also present (JK14.3, JK7-9).

B) High magnification view of Photomicrograph 2A at E6 depicts a calcite-filled fracture (stained pink; C3-K2). The matrix of this sample contains fine calcite spar. Peloids (J4-6, CD5-7, HJ13-14) are the primary allochem in this sample. Quartz silt (AB3.7, B13.7, DE4.8) is moderately common. Organic material (AB11-12, C10-11, CD2-3) has been partially replaced by pyrite. Authigenic dolomite is rare (BC2-4).

7391.60’ - 7391.70’
Plate 3

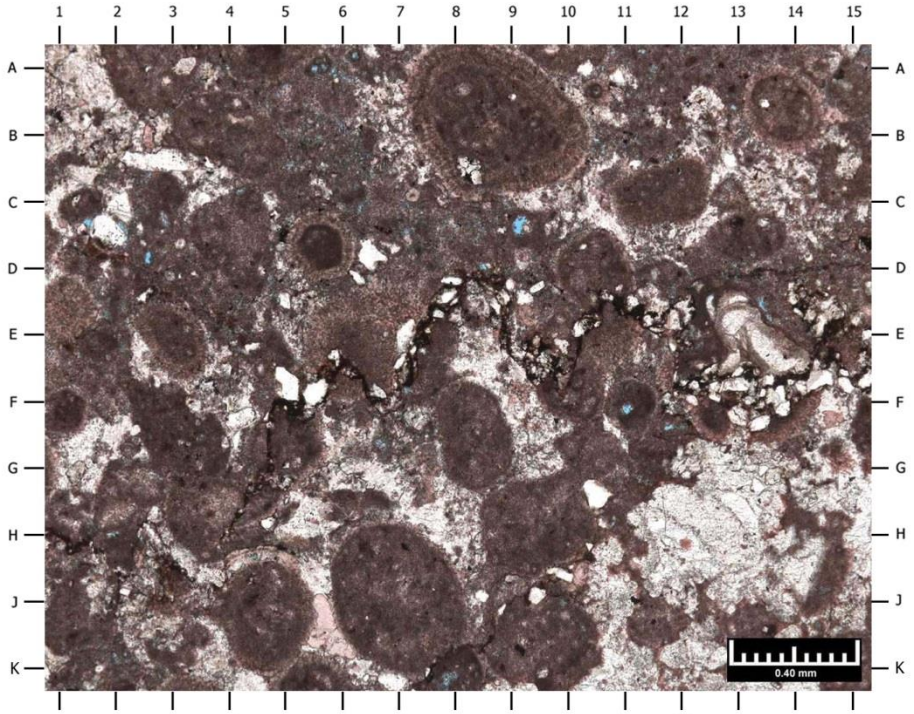

A

50X

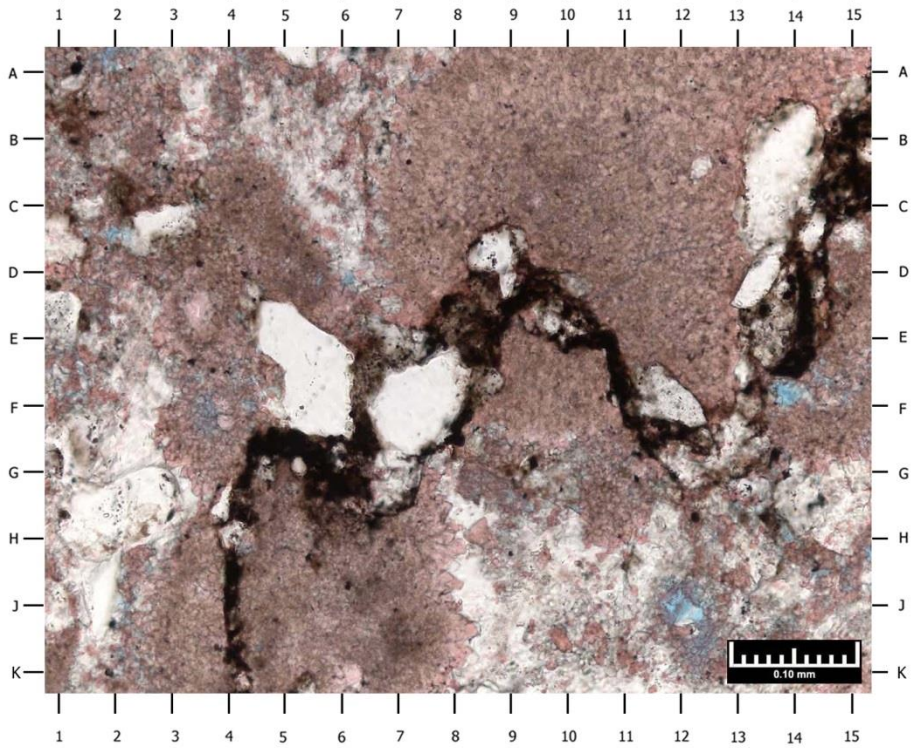

B

200X

SAMPLE DEPTH: 7391.60 – 7391.70 FEET
PLATE 3

Lithology: Slightly sandy, oolitic limestone

Sedimentary Fabric: Limestone texture is a packstone to a grainstone; rare incipient microstylolites

Compaction: Moderate to high (based on the presence of microstylolites)

Detrital Grains / Allochems:

Major: Ooids

Minor: Quartz sand; quartz silt

Accessory: Plagioclase feldspar; muscovite; phosphatic fragments

Matrix: The matrix has been mostly replaced to fine sparry calcite; organic material and undifferentiated detrital clays are associated with the microstylolites.

Cement / Replacement: Calcite is the primary authigenic mineral in this sample and occurs in a variety of ways: replacement/recrystallization of allochems, isopachous pore-filling cement, coarse pore- and vug-filling cement, micritization of allochems, and fine spar replacement of the matrix. Many allochems have been micritized making complete identification impossible. Dolomite, baroque dolomite, and anhydrite are common and occur as a pore-filling cement and as a replacement of allochems. Pyrite is sparse and occurs as a replacement of calcite and organic material. Authigenic quartz is rare and replaces calcite.

Porosity Types: Moderately common matrix micropores; sparse moldic pores; rare intraparticle pores

Magnification: A: 50X B: 200X

A) Photomicrograph 3A depicts an oolitic grainstone. A stylolite extends from H1-EF15. Ooids are the primary allochem of this sample (AC7-10, AB13-14, CD5-6). Some of these allochems have been so micritized, identification is difficult (JK9-10, GH9-10, J1). Quartz (GH10.6, CD6.4, EF4.9) is the primary detrital grain in this sample. Most of the interparticle porosity has been occluded by anhydrite (HK10.8, GJ12-13, GJ15, BC2-3), baroque dolomite (GH7.6, EF8.5, FG1-2), and calcite (stained pink; J5.8). Pore types include matrix micropores (AB6, DE13.2), moldic pores (CD9.2, FG10.9), and interparticle pores (CD1.6). Authigenic quartz is rare (AB13.4, BC8.3).

B) High magnification view of Photomicrograph 3A at F6 depicts part of a stylolite (K4-B15). Quartz (EF5-6, EF7-8, D13.4) is the primary detrital grain in this sample. A possible ooid (AF7-12) has been cross-cut by the stylolite. Interparticle pore has been occluded by baroque dolomite cement (FG2.4, J1.7, J9). The ooid fragment has been mostly micritized. The matrix contains fine calcite spar (E4, GH10.8, K1). Authigenic pyrite is also present (K1.8, K1.3, G13.8).

7401.40’ - 7401.50’
Plate 4

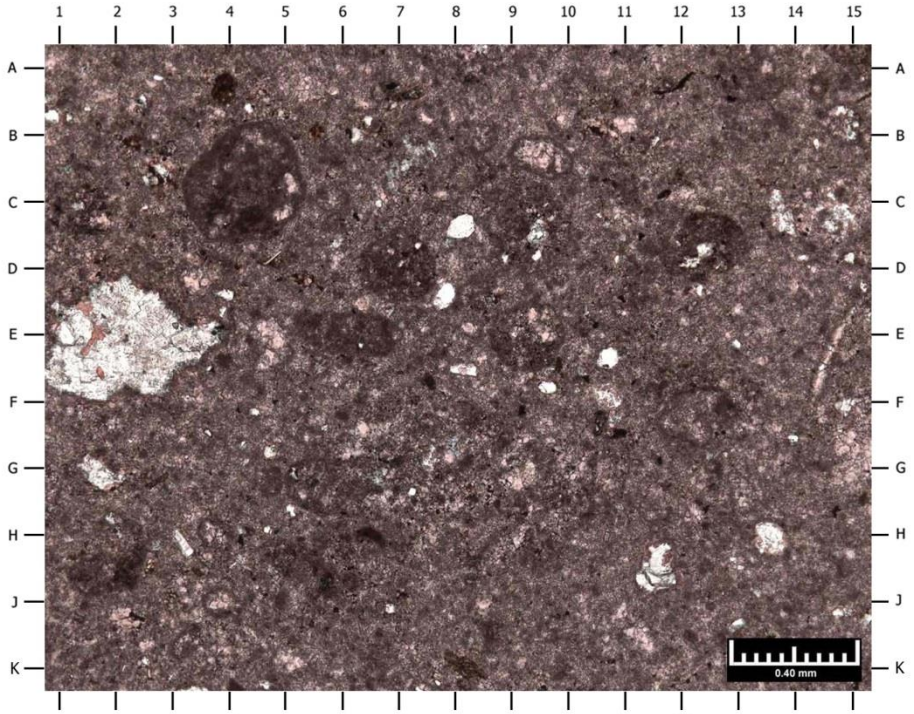

A

50X

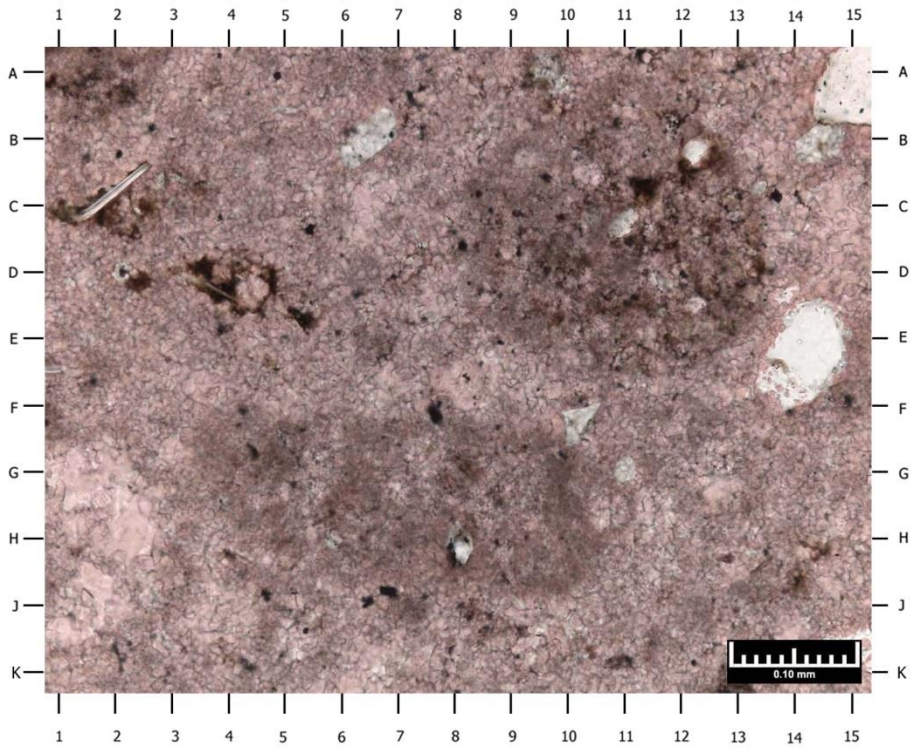

B

200X

SAMPLE DEPTH: 7401.40 – 7401.50 FEET
PLATE 4

Lithology: Slightly sandy, bioclastic limestone
Sedimentary Fabric: The limestone texture is a wackestone; rare, faint laminations
Compaction: Moderate

Detrital Grains / Allochems:

Major: Undifferentiated, partially micritized allochems; peloids
Minor: Quartz sand; quartz silt
Accessory: Muscovite; foraminifera; brachiopod fragments; plagioclase feldspar; mudstone lithoclasts

Matrix: The matrix has been mostly replaced to fine sparry calcite

Cement / Replacement: Calcite is the primary authigenic mineral in this sample and occurs in a variety of ways: replacement/recrystallization of allochems, pore- and vug-filling cement, micritization of allochems, and fine spar replacement of the matrix. Many allochems have been micritized making complete identification impossible. Dolomite and baroque dolomite are sparse and occur as a cement. Pyrite is sparse and occurs as a replacement of calcite and organic material. Rare quartz cement.

Porosity Types: Rare grain-moldic pores and intercrystalline pores

Magnification: A: 50X B: 200X

A) Photomicrograph 4A depicts a slightly sandy, bioclastic wackestone. Undifferentiated, partially micritized allochems (BC3-5, CD12-13, D7) are common. Peloids (F12.8, EF7.4, HJ4.9) are also present. Most of these allochems have been partially to completely micritized making identification difficult. Sparry calcite also replaces allochems (EF14.7, BC9.3, E4.7). Baroque dolomite cement is also present (E1.2, EF1, E2.5). Detrital grains include quartz sand (CD8, DE7.9, EF10.7), muscovite (D4.8), and quartz silt (JK13, GH5.2, AB2.7).

B) High magnification view of Photomicrograph 4A at D6 depicts several undifferentiated micritized allochems (BE9-13, A1-3, FH4-10). Detrital grains include quartz sand (A15, E14), quartz silt (FG10, B12.3), and muscovite (C1.3-BC2.7). The matrix contains fine calcite spar (A3.3, E2, C15). Organic material (DE3.7, FG7.7, BC13.6) has been partially replaced by pyrite. Pyrite also replaces calcite and is disseminated throughout the matrix. Quartz overgrowth cement is also present, but is not common (B14.5).

7404.00' - 7404.10'
Plate 5

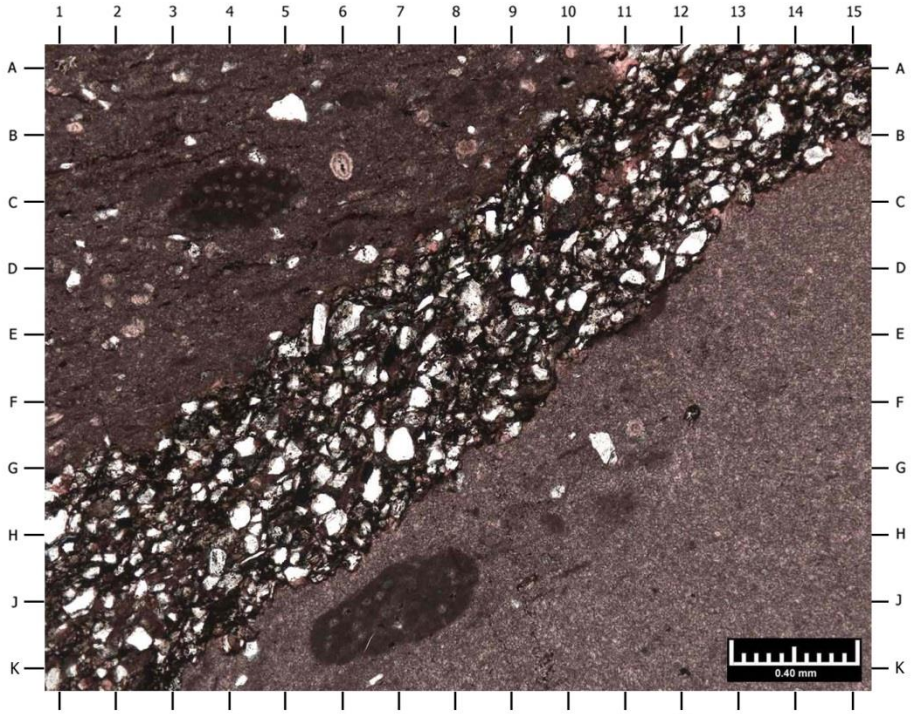

A

50X

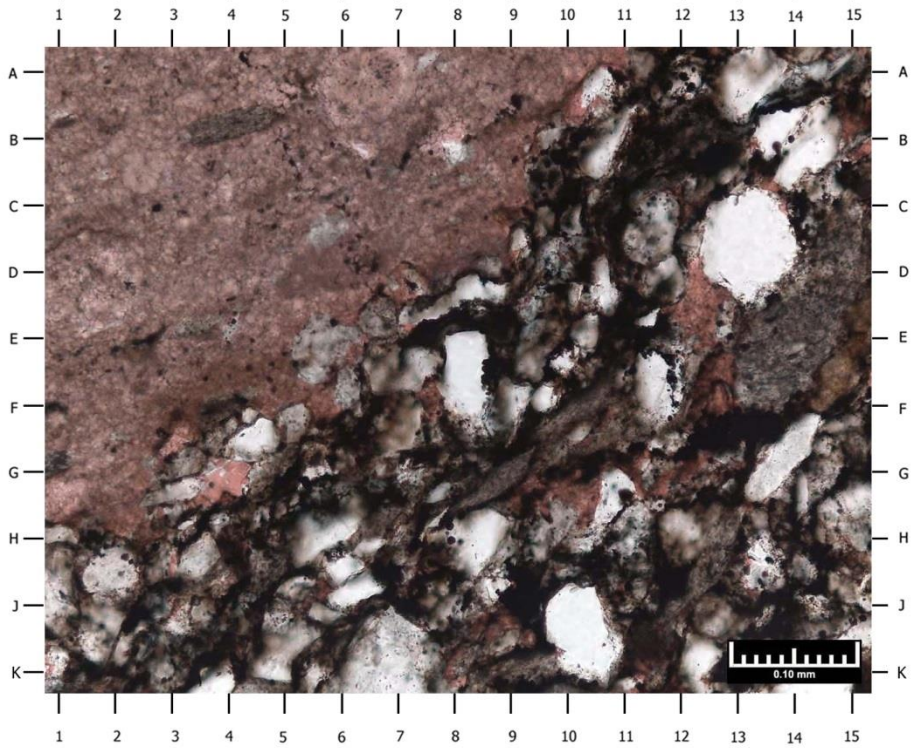

B

200X

SAMPLE DEPTH: 7404.00 – 7404.10 FEET
PLATE 5

Lithology: Variably silty/sandy, bioclastic limestone

Sedimentary Fabric: Limestone texture ranges from a crystalline limestone to a wackestone; several subvertical, thin fractures partially to completely healed by organic material; sparse incipient microstylolites and dissolution seams; sparse possible compacted burrows

Compaction: Moderate to high (based on the presence of possibly compacted burrows, dissolution seams, and stylolites)

Detrital Grains / Allochems:

Major: Peloids

Minor: Quartz silt; quartz sand; undifferentiated bioclastic material

Accessory: Plagioclase feldspar; potassium feldspar; muscovite; echinoderm fragments; brachiopod fragments; algal fragments

Matrix: The matrix has been mostly replaced to fine sparry calcite; organic material and undifferentiated detrital clays are associated with the microstylolites and dissolution seams.

Cement / Replacement: Calcite is the primary authigenic mineral in this sample and occurs in a variety of ways: replacement/recrystallization of allochems, micritization of allochems, and fine spar replacement of the matrix. Many allochems have been micritized making complete identification impossible. Pyrite is sparse and occurs as a replacement of calcite and organic material.

Porosity Types: Sparse pores are associated with the partially healed fractures. Some of the fracture porosity may be an artifact of the sampling process. Sparse possible intercrystalline micropores are present within the matrix.

Magnification: A: 50X B: 200X

A) Photomicrograph 5A depicts a contact between a bioclastic wackestone (AG1-A11) and a mudstone-wackestone (K3-BK15). A dissolution seam occurs as a contact (HK1 to A11-15). Detrital grains include muscovite (HJ4.3, JK6.3), quartz (AB5, FG7, H1), and feldspars (EF5.2, DE6, DE5.6). Detrital grains are much more common in association with dissolution seams and stylolites. Undifferentiated detrital clays and organic material are also associated with the dissolution seam. Allochems include possible algal fragments (BC3-5, J5.3-H8.3) and undifferentiated bioclastic material (E2.3, BC5.8, BC8.2). Calcite (stained pink) is the primary authigenic mineral in this sample.

B) High magnification view of Photomicrograph 5A at C8 depicts the dissolution seam (K1-A15). An undifferentiated allochem occurs at AB6-7. Detrital grains include quartz (CD13, EF8, JK10-11) and altered feldspar (E14, D9.5). Organic material and undifferentiated detrital clays are common within the dissolution seam. Authigenic pyrite (AB13.5, EF8.7, A11.7) partially replaces calcite (stained pink) and organic material and is disseminated throughout the matrix.

7408.60' - 7408.70'
Plate 6

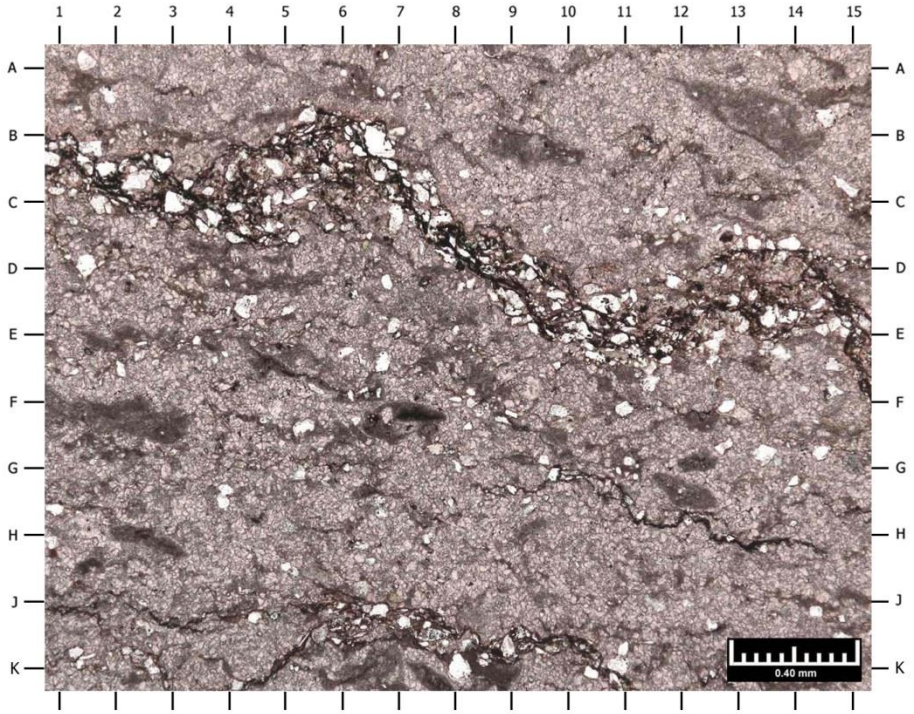

A

50X

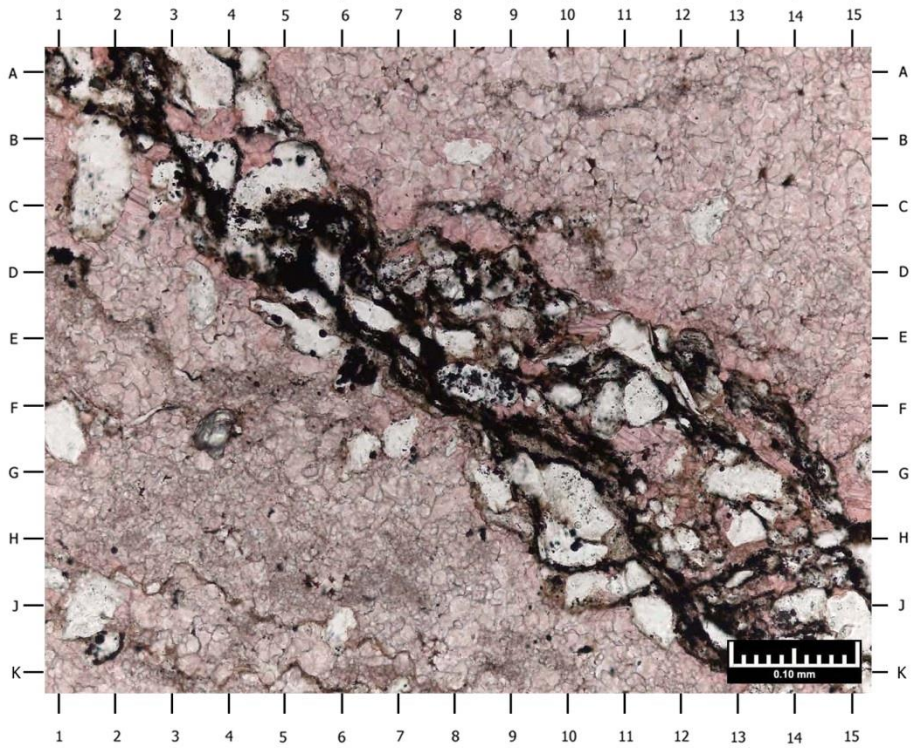

B

200X

SAMPLE DEPTH: 7408.60 – 7408.70 FEET
PLATE 6

Lithology: Variably silty/sandy, bioclastic limestone

Sedimentary Fabric: Limestone texture ranges from a crystalline limestone to a wackestone; several variably oriented, thin fractures are partially to completely healed by organic material; sparse incipient microstylolites; possible bioturbation

Compaction: Moderate to high (based on the presence of stylolites)

Detrital Grains / Allochems:

Major: Peloids

Minor: Quartz silt; quartz sand

Accessory: Muscovite; possible algal fragments; brachiopod fragments; foraminifera; plagioclase feldspar; potassium feldspar; undifferentiated heavy minerals

Matrix: The matrix has been mostly replaced to fine sparry calcite; organic material and undifferentiated detrital clays are associated with the microstylolites and dissolution seams.

Cement / Replacement: Calcite is the primary authigenic mineral in this sample and occurs in a variety of ways: replacement/recrystallization of allochems, micritization of allochems, and fine spar replacement of the matrix. Many allochems have been micritized making complete identification impossible. Pyrite is sparse and occurs as a replacement of calcite and organic material. Dolomite, baroque dolomite, and anhydrite are sparse and occur as a pore- and vug-filling cement.

Porosity Types: Sparse pores are associated with the partially healed fractures. Some of the fracture porosity may be an artifact of the sampling process. Sparse possible intercrystalline micropores are present within the matrix.

Magnification: A: 50X B: 200X

A) Photomicrograph 6A depicts a variably silty/sandy, bioclastic limestone. The texture ranges from crystalline limestone to a wackestone. This sample has been recrystallized extensively by neomorphic calcite spar (AB11, A4, HJ3.8) making identification of allochems difficult. Allochems include peloids (GH12, G12.3, FG12.3) and foraminifera (FG7.3). Several organic-rich stylolites are present (BC1-EF15, J1-K11). Some of the fabric in this sample is possibly due to bioturbation (AB12-14, BC9-10, F1-3). Detrital grains include quartz (K8.2, B6.6, C3), muscovite (JK5.3, BC5.6), and plagioclase feldspar (F10.8, E12.6). Detrital grains are much more common in association with stylolites.

B) High magnification view of Photomicrograph 6A at D8 depicts a stylolite extending from A1-HK15. Detrital grains include quartz (FG1, FG7, J11.5), feldspar (EF8-9, D7-8), undifferentiated heavy minerals (FG3.8), and muscovite (F2-3, F12). Undifferentiated detrital clays, organic material, and detrital grains are much more common in association with stylolites. Pyrite (CD1, A2, EF6.3) partially replaces calcite (stained pink) and organic material and is disseminated throughout the matrix. The matrix has been mostly replaced to fine sparry calcite.

7412.00' - 7412.10'
Plate 7

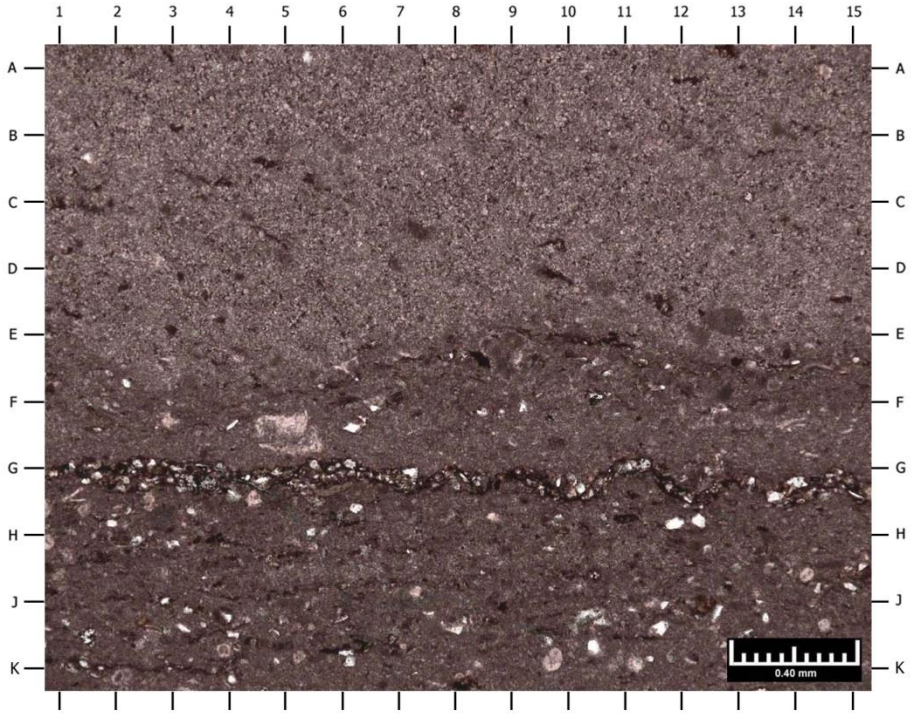

A

50X

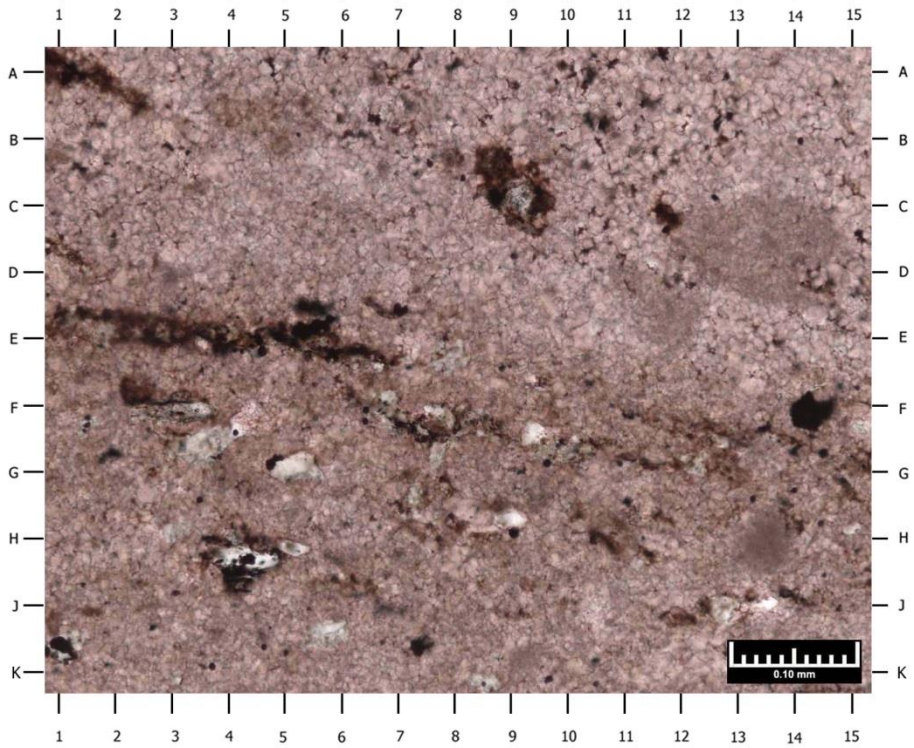

B

200X

SAMPLE DEPTH: 7412.00 – 7412.10 FEET
PLATE 7

Lithology: Slightly silty limestone

Sedimentary Fabric: The limestone texture of this sample is a mudstone to wackestone; several sandy, peloidal wackestone to packstone laminations are also present; incipient microstylolites are moderately common giving an impression of laminations

Compaction: Moderate to high (based on the presence of microstylolites)

Detrital Grains / Allochems:

Major: Peloids; quartz silt

Minor: Quartz sand

Accessory: Muscovite; calcareous foraminifera; mudstone lithoclasts; plagioclase feldspar; spherules; phosphatic fragments

Matrix: The matrix has been mostly replaced to fine sparry calcite; organic material and undifferentiated detrital clays are associated with the microstylolites.

Cement / Replacement: Calcite is the primary authigenic mineral in this sample and occurs in a variety of ways: replacement/recrystallization of allochems, pore-filling cement, micritization of allochems, and fine spar replacement of the matrix. Many allochems have been micritized fully making identification impossible. Dolomite and baroque dolomite are sparse and occur as a cement. Pyrite is sparse and occurs as a replacement of calcite and organic material.

Porosity Types: Rare sampling-induced cracks

Magnification: A: 50X B: 200X

A) Photomicrograph 7A depicts a slightly silty lime mudstone to wackestone. An incipient microstylolite extends from G1 to GH15. Organic material, detrital clays, and detrital grains are commonly associated with the microstylolites. Detrital grains include quartz silt (FG6.2, GH11.8, GH12.3) and muscovite (FG4, GH14.9). Peloids are the primary allochem in this sample (E12-13, CD7.3, F12.9). Spherules are also present (H1, K2.2, JK9.8). Some allochems have been replaced by sparry calcite (stained pink; FG5) but most have been replaced by micrite, making identification difficult. Pyrite (EF13.8, GH4.6, GH8.8) partially replaces organic material and calcite and is disseminated throughout the matrix.

B) High magnification view of Photomicrograph 7A at E11 depicts peloids (CD12-13, DE11-12, H13-14). These allochems have been micritized, making identification difficult. The matrix contains fine calcite spar (stained pink). Quartz silt (J13.5, FG9.3, FG5) is the primary detrital grain in this sample. Pyrite (F14.2, JK1, JK7.3) partially replaces calcite and organic material and is disseminated throughout the matrix.

7413.30' - 7413.40'
Plate 8

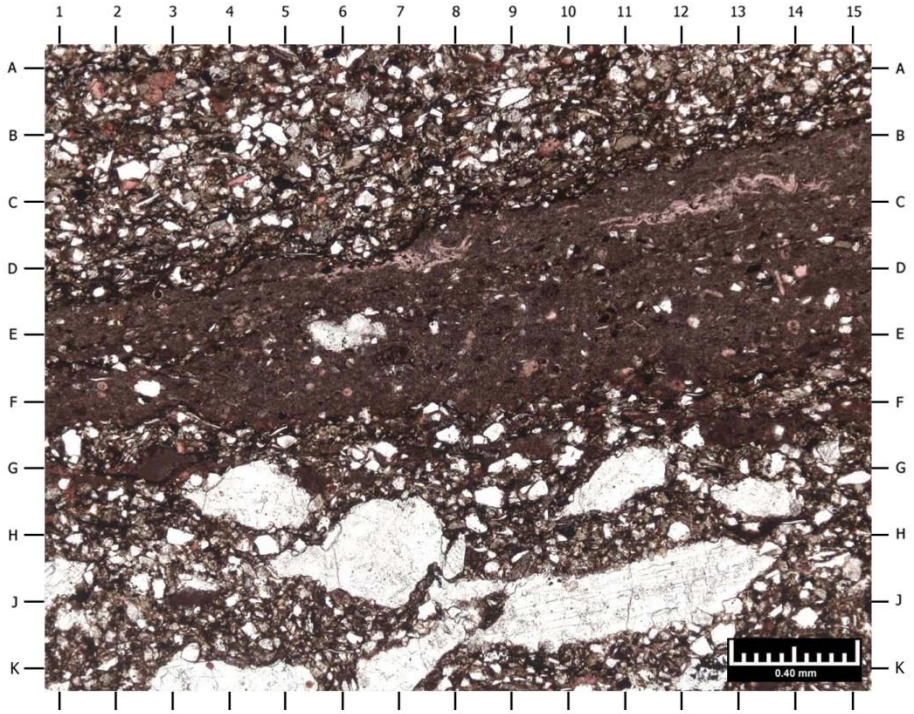

A

50X

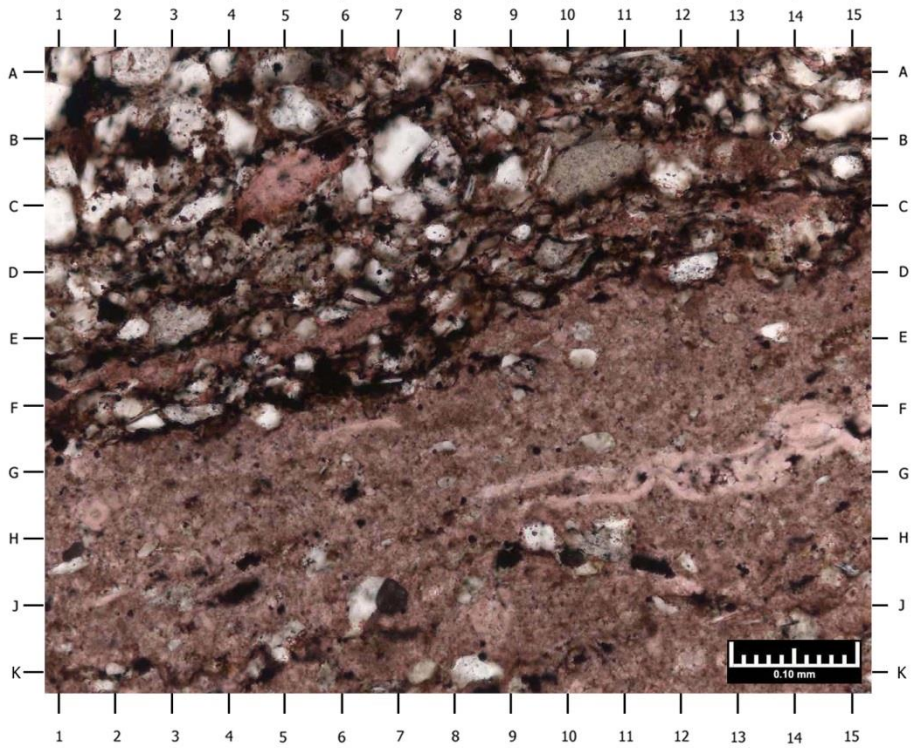

B

200X

7413.30' - 7413.40'
Plate 8

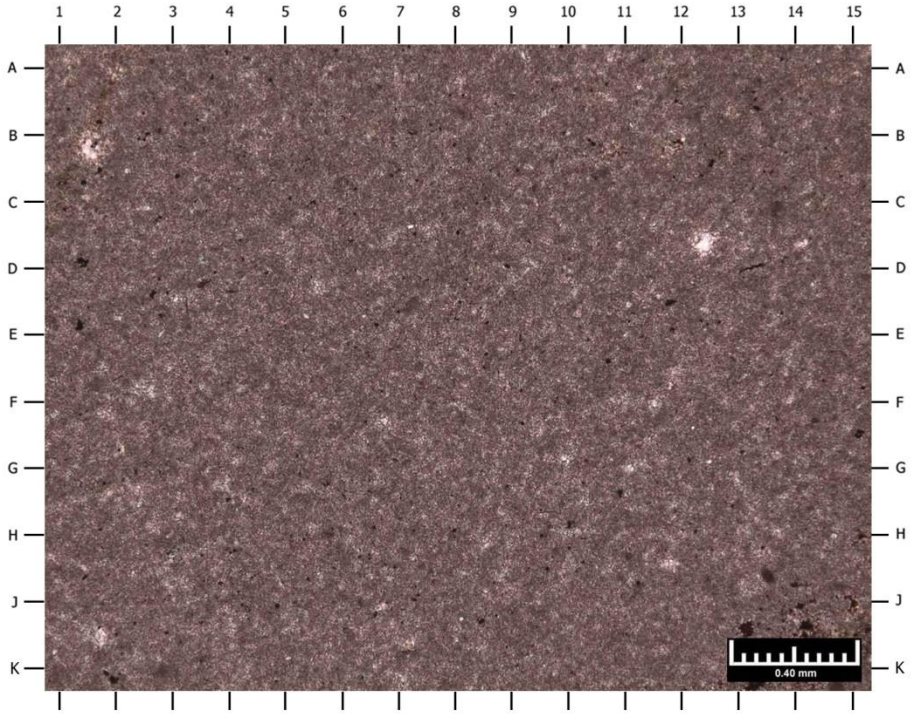

C

50X

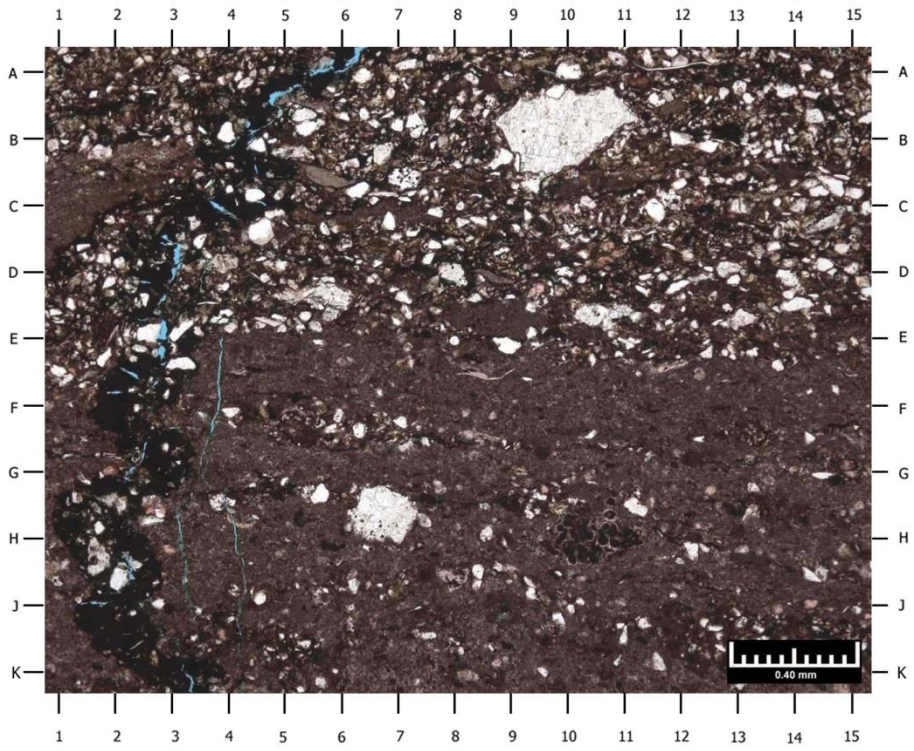

D

200X

SAMPLE DEPTH: 7413.30 – 7413.40 FEET
PLATE 8

Lithology: Lithologies include limestone, silty limestone, siltstone, and sandstone

Sedimentary Fabric: Limestone texture ranges from a crystalline limestone to a wackestone; several variably oriented, thin fractures partially to completely healed by organic material with rare calcite and quartz; sparse incipient microstylolites

Compaction: Moderate to high (based on the presence of stylolites)

Detrital Grains / Allochems:

Major: Quartz silt; anhydrite sand; quartz sand

Minor: Peloids; plagioclase feldspar; potassium feldspar; undifferentiated bioclastic material

Accessory: Muscovite; foraminifera; brachiopod fragments; undifferentiated heavy minerals

Matrix: In the limestone portions of this sample the matrix has been mostly replaced to fine sparry calcite; organic material and undifferentiated detrital clays are associated with the microstylolites and dissolution seams; the matrix contains mostly undifferentiated detrital clays with less common micrite and organic material in the siltstone and sandstone portions of this sample.

Cement / Replacement: Calcite is the primary authigenic mineral in this sample and occurs in a variety of ways: replacement/recrystallization of allochems, rare healing of fractures, micritization of allochems, and fine spar replacement of the matrix. Many allochems have been micritized fully making identification impossible. Pyrite is sparse and occurs as a replacement of calcite and organic material. Dolomite only occurs within the siltstone and sandstone portions of this sample as a cement.

Porosity Types: Sparse pores are associated with the partially healed fractures. Some of the fracture porosity may be an artifact of the sampling process. Sparse possible intercrystalline micropores are present within the matrix.

Magnification: A: 50X B: 200X C: 50X D: 200X

A) Photomicrograph 8A shows many of the lithologies present in the sample, including siltstone (AD1-A15), limestone (EF1-BE15), and sandstone (GK1-FK15). Detrital grains include quartz (AB9, GH8.4, H3.3), muscovite (GH14, EF1.7, FG4.8), anhydrite clasts (GH3-5, H5-8, J9-HJ13.5), and feldspar (J4.3, AB6.3). Undifferentiated detrital clays are much more common in association with the siliciclastic lithologies than the carbonate lithologies. Calcite (stained pink) is the primary authigenic mineral in this sample. Allochems include possible brachiopod fragments (D6-8, CD11-BC14) and undifferentiated bioclastic material (AB1.7, AB2.7, BC9.7).

B) Photomicrograph 8B depicts a high magnification view of Photomicrograph 8A at C10 depicts the contact between a siltstone (AF1-AC15) and a limestone (GK1-CK15). Undifferentiated bioclastic material (BC4-6, EF2-DE7) and possible brachiopod fragments are sparse (G8-FG15).

Pyrite (BC5.8, AB1.5, HJ10) partially replaces calcite (stained pink) and organic material and is disseminated throughout the matrix. Detrital grains include quartz (B7, AB14-15, C1, FG2.7), muscovite (EF6.8, BC8.3, A11-12), undifferentiated heavy minerals (HJ6.9), and altered feldspar (BC10-11, DE3).

C) Photomicrograph 8C depicts the miciritic limestone portion of this sample.

D) Photomicrograph 8D depicts an organic-filled fracture extending from A6-K3.5.

7413.45’ - 7413.55’
Plate 9

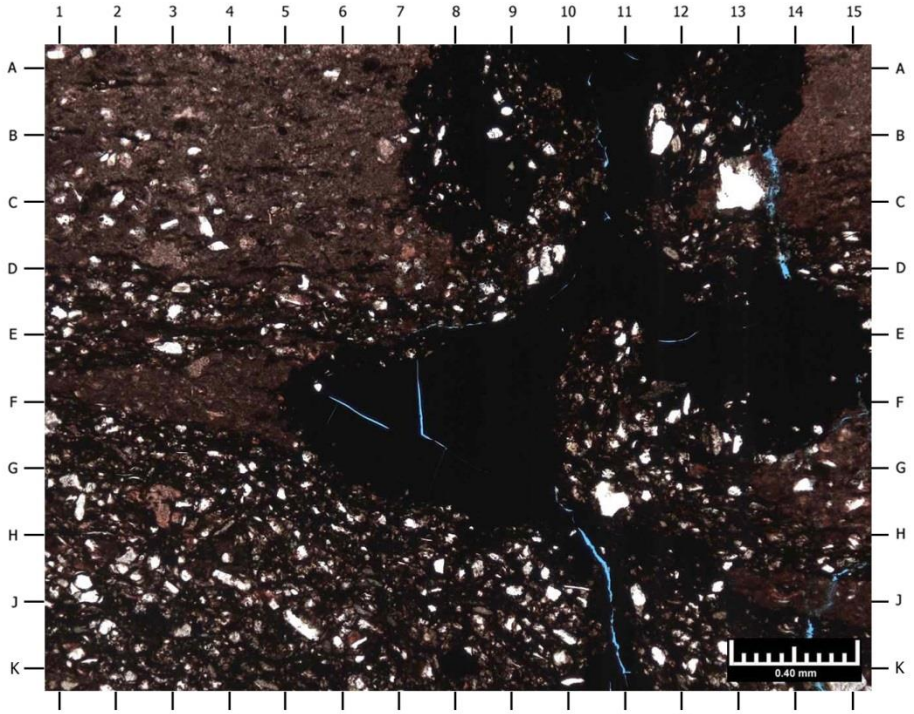

A

50X

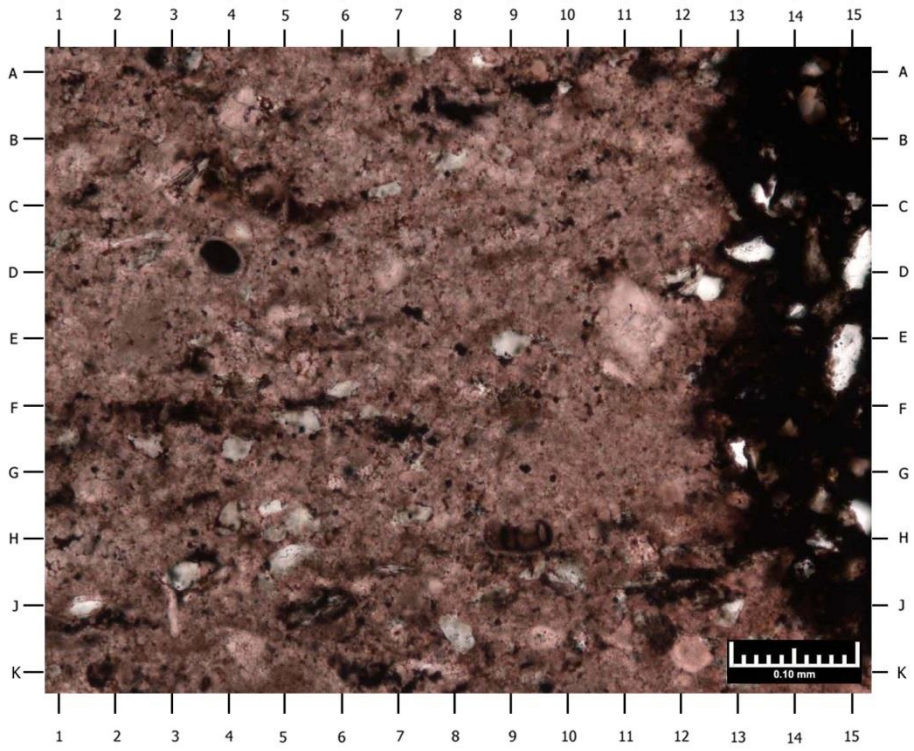

B

200X

SAMPLE DEPTH: 7413.45 – 7413.55 FEET
PLATE 9

Lithology: Limestone

Sedimentary Fabric: The limestone texture is a mudstone; an organic-filled fracture is present; several sandy, argillaceous mudstone laminations; several incipient microstylolites are present

Compaction: Moderate to high (based on the presence of incipient microstylolites)

Detrital Grains / Allochems:

Major: Quartz silt

Minor: Quartz sand

Accessory: Muscovite; plagioclase feldspar; phosphatic fragments; foraminifera; spherules; mudstone lithoclasts

Matrix: The matrix has been mostly replaced to fine sparry calcite; organic material and undifferentiated detrital clays are associated with the microstylolites and mudstone laminations.

Cement / Replacement: Calcite is the primary authigenic mineral in this sample and occurs in a variety of ways: replacement/recrystallization of allochems, micritization of allochems, and fine spar replacement of the matrix. Many allochems have been micritized making complete identification impossible. Dolomite replacement of calcite is rare. Pyrite is sparse and occurs as a replacement of calcite and organic material.

Porosity Types: The only pore types present are sampling-induced cracks, and desiccation cracks within organic material

Magnification: A: 50X B: 200X

A) Photomicrograph 9A depicts the large organic-filled fracture (A8-14 to K11). Sandy, argillaceous mudstone laminations are visible (FK1-GK15). Detrital grains include quartz sand (B11.6, BC13, GH10.7), quartz silt (J4.8, GH11.3, A1.4), and muscovite (HJ10.2, FG3.2, H1.7). Undifferentiated allochems (CD2.7, GH2.8, EF3.3) have been replaced by sparry calcite (stained pink). Pores within organic material (FG5-7, EF7-8, HK10-11) and extending from BD13.7 possibly occur as a result of the sampling process.

B) High magnification view of Photomicrograph 9A at B6 depicts the organic-filled fracture (AK13-15). Quartz silt (D15, CD13.2, FG13) is the primary detrital grain in this sample. Undifferentiated allochems (DE11, J3, JK4.3) and spherules (JK12.2) have been replaced/recrystallized by calcite (stained pink). Foraminifera are also present (CD3.8). Pyrite (AB9.5, K7.8, FG9.3) partially replaces calcite and organic material and is disseminated throughout the matrix.

7414.90' - 7415.00'
Plate 10

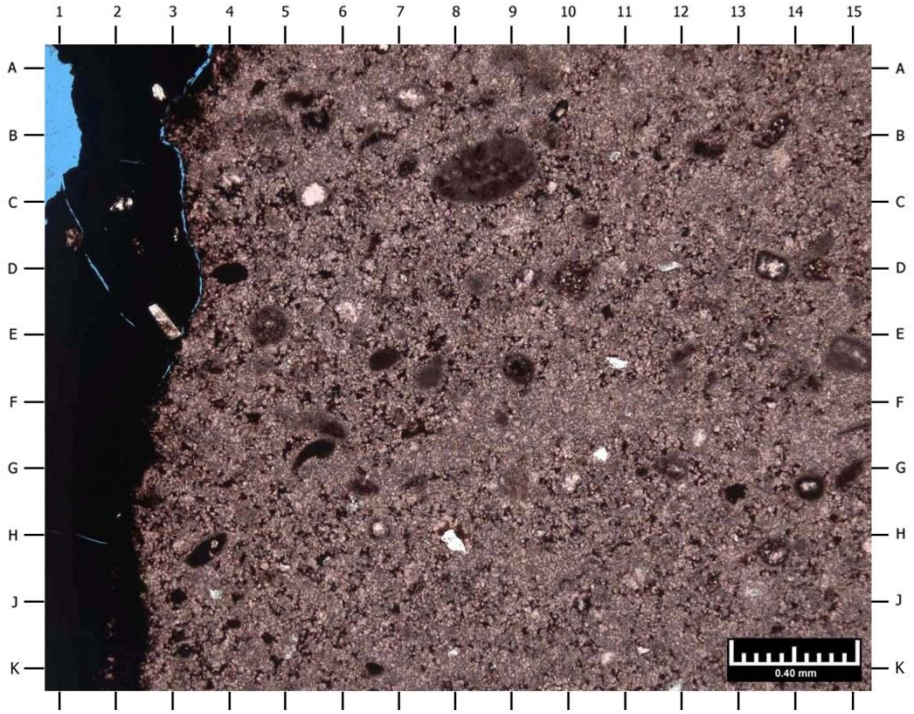

A

50X

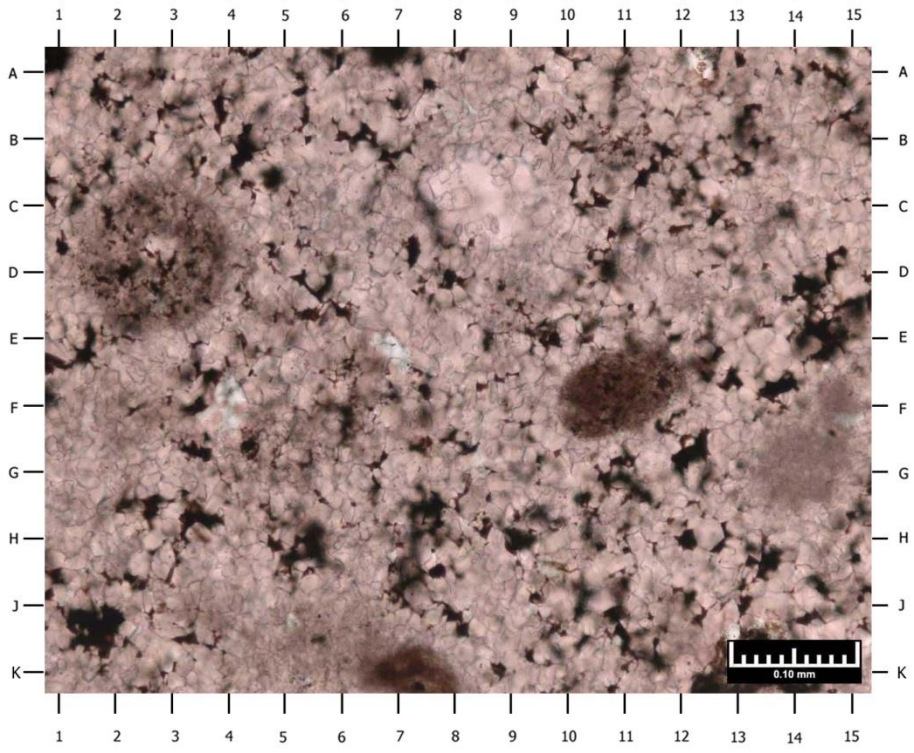

B

200X

SAMPLE DEPTH: 7414.90 – 7415.00 FEET
PLATE 10

Lithology: Bioclastic limestone

Sedimentary Fabric: Limestone texture ranges from a crystalline limestone to a wackestone; a 0.60mm thick fracture extends the length of the thin section; rare dissolution seams and stylolites

Compaction: Moderate to high (based on the presence of stylolites)

Detrital Grains / Allochems:

Major: Peloids

Minor: Foraminifera

Accessory: Quartz silt; quartz sand; muscovite; brachiopods; echinoderm fragments; algal fragments (?)

Matrix: The matrix has been mostly replaced to fine sparry calcite; organic material and undifferentiated detrital clays are associated with the microstylolites and dissolution seams; organic material is also moderately common and occluding pores.

Cement / Replacement: Calcite is the primary authigenic mineral in this sample and occurs in a variety of ways: replacement/recrystallization of allochems, micritization of allochems, and fine spar replacement of the matrix. Many allochems have been micritized making complete identification impossible. Pyrite is sparse and occurs as a replacement of calcite and organic material. Sparse anhydrite occurs as a pore-filling cement. Dolomite is rare and occurs as a cement

Porosity Types: Sparse pores are associated with the partially healed fractures. Some of the fracture porosity may be an artifact of the sampling process. Sparse possible intercrystalline micropores are present within the matrix.

Magnification: A: 50X B: 200X

A) Photomicrograph 10A depicts a bioclastic wackestone. An organic-filled fracture extends from A2 to K2. Most of the allochems (EF15, G14.8, D4, EF9.3) in this sample have been almost completely micritized making identification difficult. A possible algal fragment occurs at BC8-9. Detrital quartz is sparse (EF10.8, FG10.7, H7.9). The matrix of this sample has been recrystallized to neomorphic calcite spar (stained pink; A6, A11.5, A15).

B) High magnification view of Photomicrograph 10A at E6 depicts several peloids (CE2-3, EF10-12, K7-8). These allochems have been micritized, making identification difficult. The characteristics of the neomorphic calcite spar are shown in detail in this high magnification photograph (AB4.8, A9, HJ8.5). Organic material is moderately common within the matrix (A6.8, A1, JK1.8) and has been partially pyritized.

7417.60' - 7417.70'
Plate 11

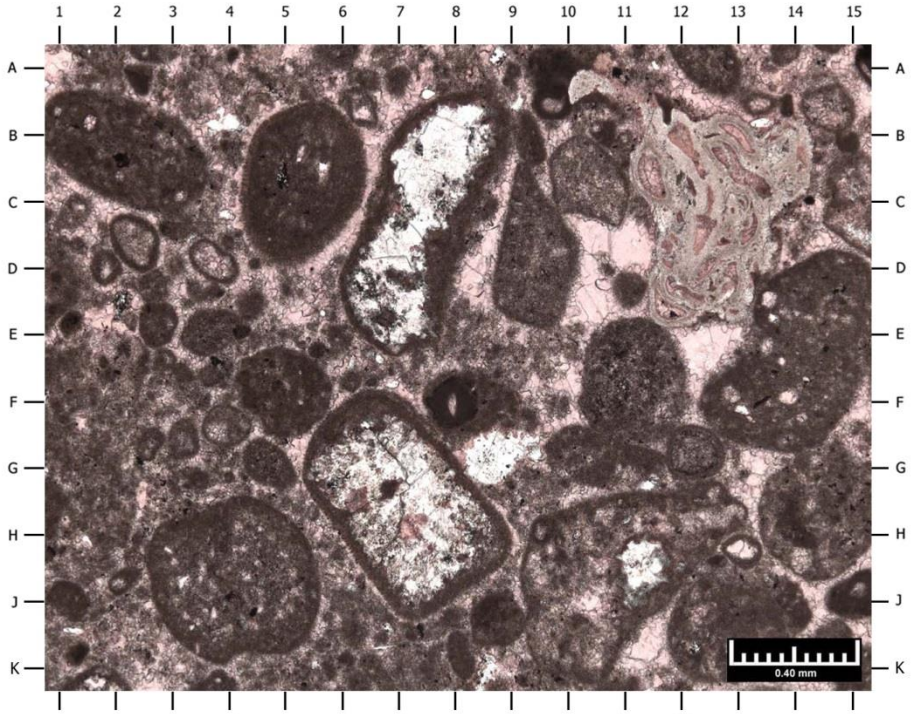

A

50X

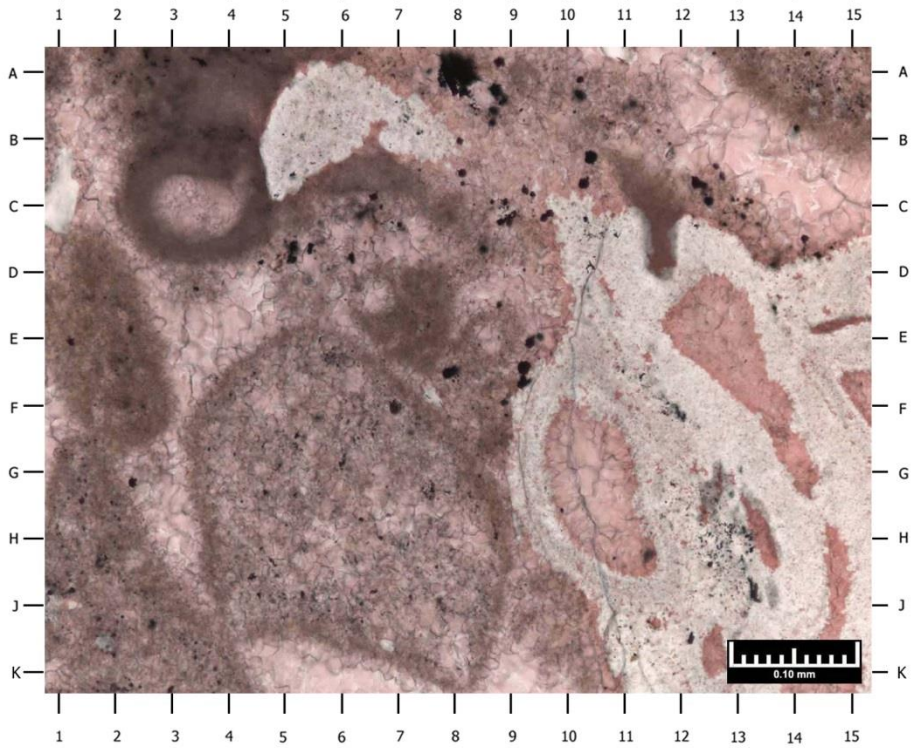

B

200X

SAMPLE DEPTH: 7417.60 – 7417.70 FEET
PLATE 11

Lithology: Bioclastic limestone
Sedimentary Fabric: The limestone texture ranges from a wackestone to packstone
Compaction: Moderate

Detrital Grains / Allochems:

Major: Peloids
Minor: Foraminifera
Accessory: Possible algal fragments; quartz silt; quartz sand; muscovite

Matrix: The matrix has been mostly replaced to fine sparry calcite

Cement / Replacement: Calcite is the primary authigenic mineral in this sample and occurs in a variety of ways: replacement/recrystallization of allochems, pore and vug-filling cement, micritization of allochems, and fine spar replacement of the matrix. Many allochems have been micritized fully making identification impossible. Dolomite and baroque dolomite are sparse and occur as a cement. Anhydrite is sparse and occurs as a cement and a replacement of allochems. Pyrite is sparse and occurs as a replacement of calcite and organic material. Possible quartz cement is rare.

Porosity Types: Pore types include rare intraparticle pores, rare sampling-induced pores, and rare possible intercrystalline micropores present within the matrix.

Magnification: A: 50X B: 200X

A) Photomicrograph 11A depicts a bioclastic packstone. Allochems include possible algal fragments (HK3-5, B1-3, BD4-6), possible compacted foraminifera (BE11-14), and peloids (E1, E2.8, J1). Many of these allochems have been micritized or have been replaced by chert (BE11-13), calcite (stained pink), and/or baroque dolomite (B7.8, CD6.8, G6.5), making identification of some allochems almost impossible. Calcite also occurs as a pore-filling cement (A1, AB6.8, CD11.2). Detrital quartz is sparse (AB3.8, AB7.4, A8.8). Possible authigenic quartz is also present, but not common (DE13.4, F13, BC5.7).

B) High magnification view of Photomicrograph 11A at B11 depicts a possible compacted foraminifera (AB5-6, CK10-15). The test of the foraminifera has been recrystallized to chert (white). Calcite cement occludes intraparticle pores (G11, E12.5, H13.5) as well as interparticle pores (AB1.2, DE3.5, GH3, K6). Isopachous calcite cement occurring on the edge of many grains is indicative of phreatic zone cementation (JK8.6, HJ9, FG3.4). A detrital quartz grain is rare (C1). Allochems (DF1-2, G1-K4, G6) have been almost completely micritized, making identification difficult to impossible. Authigenic pyrite is sparse (A8, EF9.2, EF7.9). A thin fracture possibly occurs as a result of the sampling process (CD10.8-K11).

7419.65' - 7419.75'
Plate 12

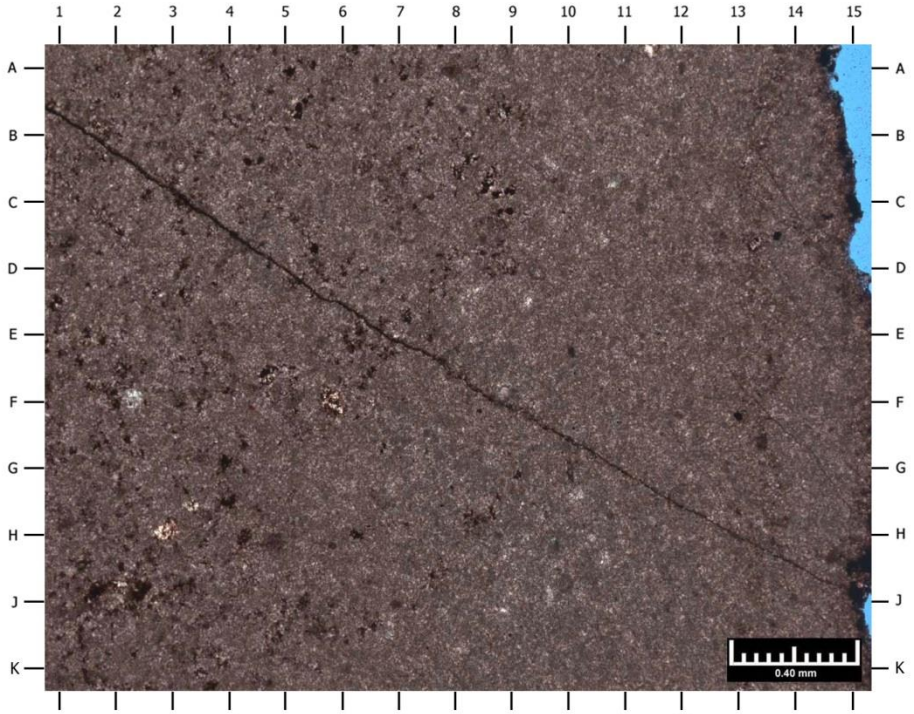

A

50X

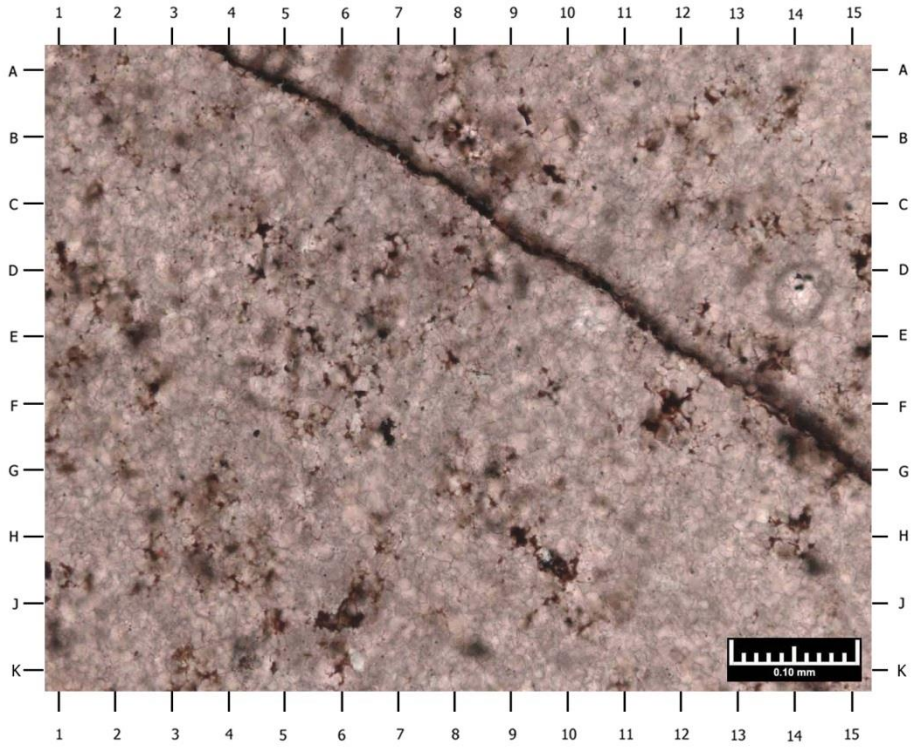

B

200X

SAMPLE DEPTH: 7419.65 – 7419.75 FEET
PLATE 12

Lithology: Limestone
Sedimentary Fabric: The limestone texture is a mudstone to wackestone; organic-filled fractures are rare
Compaction: Moderate

Detrital Grains / Allochems:
Major: N/A
Minor: Peloids
Accessory: Calcareous foraminifera; quartz silt; quartz sand

Matrix: The matrix has been mostly replaced to fine sparry calcite

Cement / Replacement: Calcite is the primary authigenic mineral in this sample and occurs in a variety of ways: replacement/recrystallization of allochems, pore and vug-filling cement, micritization of allochems, and fine spar replacement of the matrix. Some allochems have been micritized fully making identification impossible. Dolomite is rare and occurs as a cement. Rare authigenic kaolinite. Pyrite is sparse and occurs as a replacement of calcite and organic material.

Porosity Types: Rare sampling-induced racks; rare matrix micropores

Magnification: A: 50X B: 200X

A) Photomicrograph 12A depicts a lime mudstone to wackestone. Peloids (BC10.4, A7.9, H4.9) are the primary allochem in this sample. Organic material (AB5.2, G3.9, K3.6) occurs within the matrix and fills a fracture (AB1-J15). Pyrite partially replaces organic material and is disseminated throughout the matrix.

B) High magnification view of Photomicrograph 12A at C2 depicts an organic-filled fracture (A4-G15). The matrix contains fine calcite spar (A12, A15, F10.5). A possible foraminifer (DE14) has been micritized. Pyrite (JK6.3, FG4.4, E11.2) partially replaces calcite and organic material.

7437.10' - 7437.20'
Plate 13

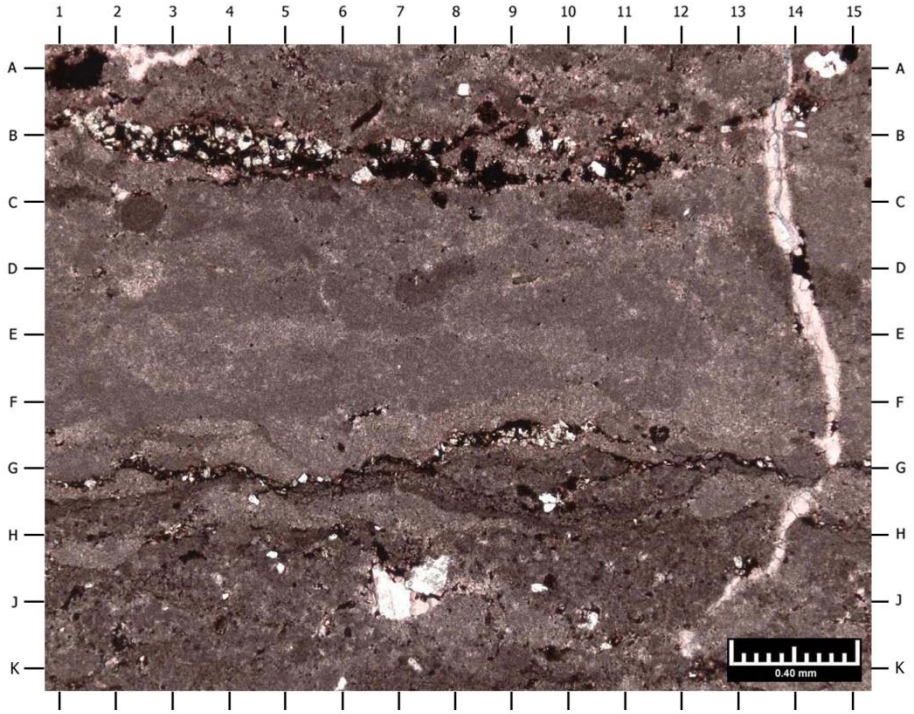

A

50X

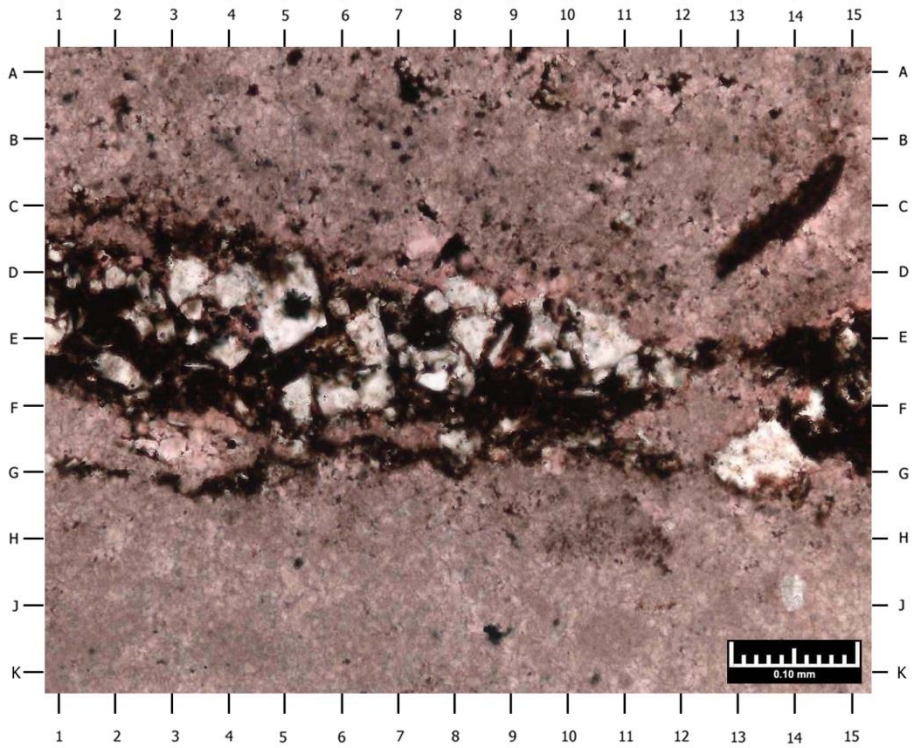

B

200X

SAMPLE DEPTH: 7437.10 – 7437.20 FEET
PLATE 13

Lithology: Slightly silty limestone

Sedimentary Fabric: The limestone texture is an algal boundstone; moderately common dissolution seams and microstylolites between many algal laminations; sparse sub-vertical calcite, and organic-filled fractures

Compaction: Moderate to high (based on the presence of stylolites)

Detrital Grains / Allochems:

Major: Algal laminites

Minor: Quartz silt

Accessory: Quartz sand; plagioclase feldspar; muscovite

Matrix: The matrix has been mostly replaced to fine sparry calcite; organic material and undifferentiated detrital clays are associated with the microstylolites and dissolution seams.

Cement / Replacement: Calcite is the primary authigenic mineral in this sample and occurs in a variety of ways: replacement/recrystallization of allochems, micritization of allochems, and fine spar replacement of the matrix. Dolomite and baroque dolomite are sparse and occur as a cement. Pyrite is sparse and occurs as a replacement of calcite, dolomite, and organic material.

Porosity Types: Pore types include rare sampling-induced pores, rare pores associated with fractures, and rare possible intercrystalline micropores present within the matrix.

Magnification: A: 50X B: 200X

A) Photomicrograph 13A depicts a slightly silty limestone. This sample is likely a series of interlaminated stylolites and/or argillaceous laminations (B1-BC11.7, GH1-G15) and algal laminations (AB1-15, CG1-15, HK1-GK15). Detrital grains are more commonly associated with the stylolites and include quartz silt (AB14.3, GH5.3, HJ4.7), quartz sand (BC10.6, GH9.7), and muscovite (BC2.5, BC3.8). A fracture extends from B13.8 to J12.6 and has been healed by calcite (stained pink) and organic material (D14). Organic material (AB8.6, FG11.4, B3.4) has been partially replaced by pyrite. It is difficult to determine whether peloids are present (CD2-3, DE7-8, C10-11) or if it is just part of the clotted texture of the algal laminites.

B) High magnification view of Photomicrograph 13A at B5 depicts an incipient microstylolite (CF1-EG15) between two algal laminations (AC1-AD15, FK1-GK15). Dolomite (D3.3, FG13-14, E10.7) cement is common within this incipient microstylolite. Detrital grains include quartz silt (EF7.6, F14.2) and muscovite (EF3.3). The matrix contains fine calcite spar. Pyrite (DE5.2, HJ5.3, JK8.8) partially replaces calcite (stained pink), organic material, and dolomite and is disseminated throughout the matrix.

7438.55' - 7438.70'
Plate 14

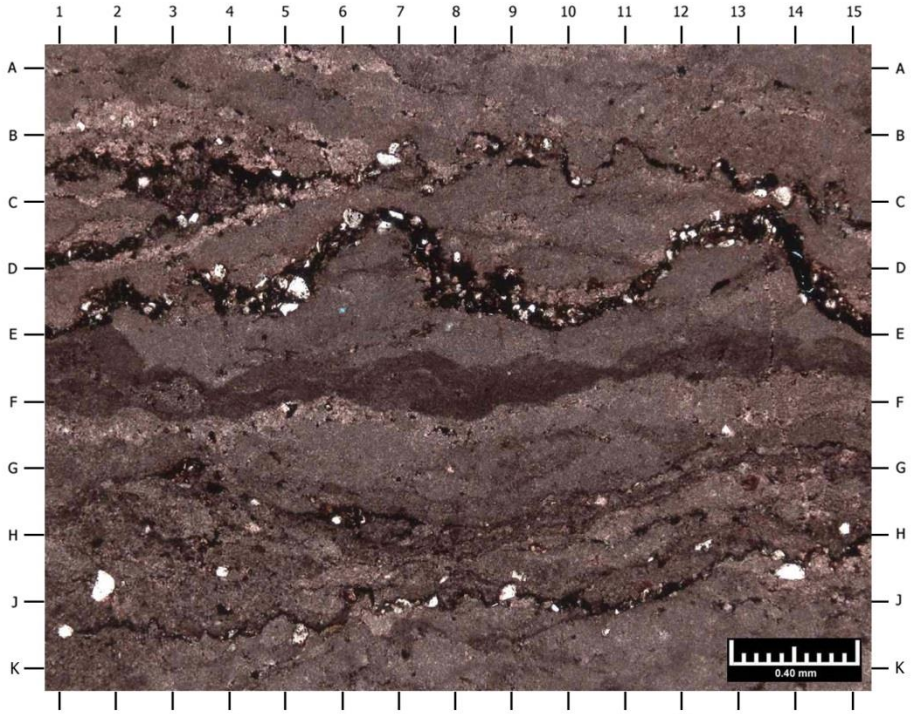

A

50X

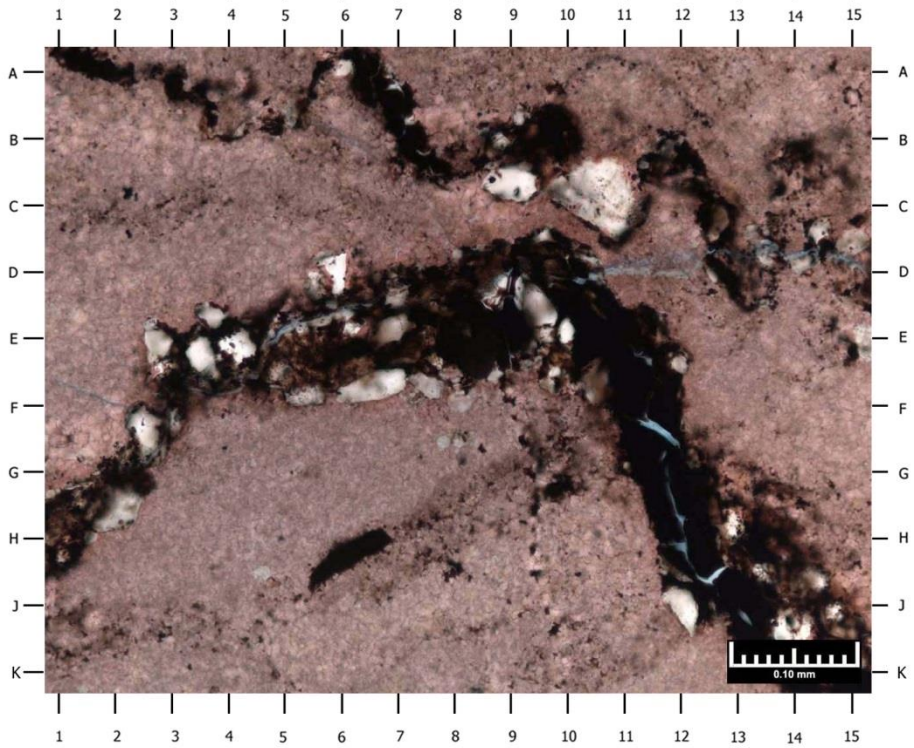

B

200X

SAMPLE DEPTH: 7438.55 – 7438.70 FEET
PLATE 14

Lithology: Slightly silty limestone

Sedimentary Fabric: The limestone texture is an algal boundstone; moderately common dissolution seams and microstylolites between many algal laminations; sparse sub-vertical calcite, and organic-filled fractures

Compaction: Moderate to high (based on the presence of stylolites)

Detrital Grains / Allochems:

Major: Algal laminites

Minor: Quartz silt

Accessory: Quartz sand; plagioclase feldspar; muscovite; spherules

Matrix: The matrix has been mostly replaced to fine sparry calcite; organic material and undifferentiated detrital clays are associated with the microstylolites and dissolution seams.

Cement / Replacement: Calcite is the primary authigenic mineral in this sample and occurs in a variety of ways: replacement/recrystallization of allochems, micritization of allochems, and fine spar replacement of the matrix. Dolomite and baroque dolomite are sparse and occur as a cement. Pyrite is sparse and occurs as a replacement of calcite and organic material. Rare authigenic kaolinite occludes a vug.

Porosity Types: Pore types include rare sampling-induced pores, rare pores associated with fractures, and rare possible intercrystalline micropores present within the matrix.

Magnification: A: 50X B: 200X

A) Photomicrograph 14A depicts a slightly silty carbonate. This sample is likely a series of interlaminated stylolites and/or argillaceous laminations (E1-15, BC1-CD15, JK1-H15) and algal laminations (A1-AC15, DE1-D15, EF1-15). Detrital grains, which include quartz (HJ1.8, HJ13.9, H14.8), muscovite (J8.7, CD5.5), and plagioclase feldspar (DE4.9), are more common in association with stylolites. Calcite (stained pink) is the primary authigenic mineral in this sample. The matrix has been mostly replaced to fine sparry calcite.

B) High magnification view of Photomicrograph 14A at D13 depicts several stylolites (A1-DE15, H1-K15). Quartz (D5.8, FG2.7, J12) is the primary detrital grain in this sample. Organic material is common in association with the stylolites and has been partially replaced by pyrite. Pyrite also partially replaces calcite (stained pink). Pores are rare within this fracture (FG11-12, GH12, HJ12.6). Another pore might occur as a result of the sampling process (D10.5-D15).

7452.15’ - 7452.30’
Plate 15

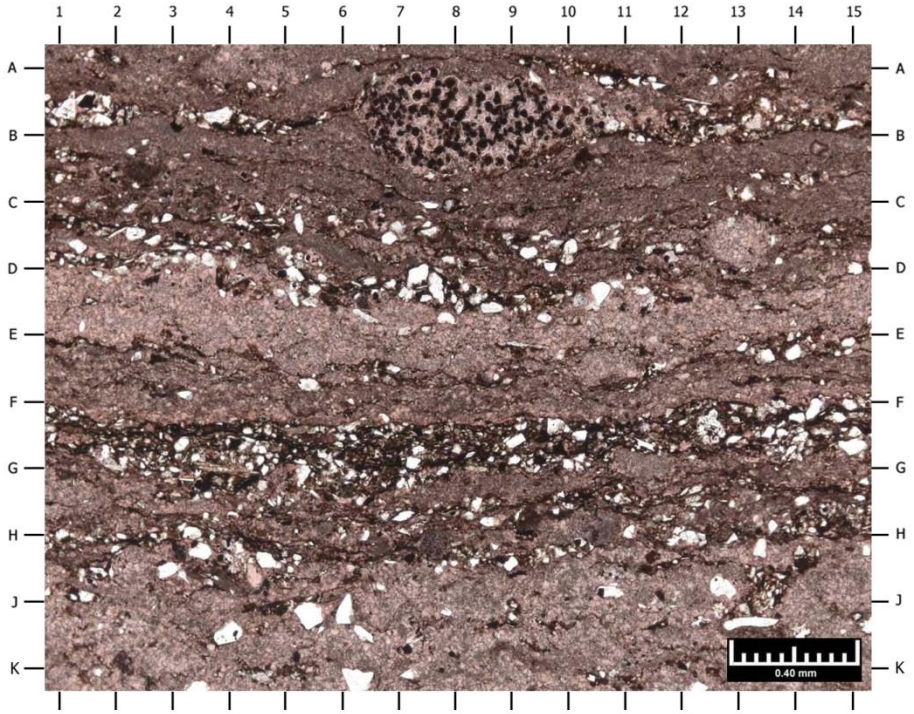

A

50X

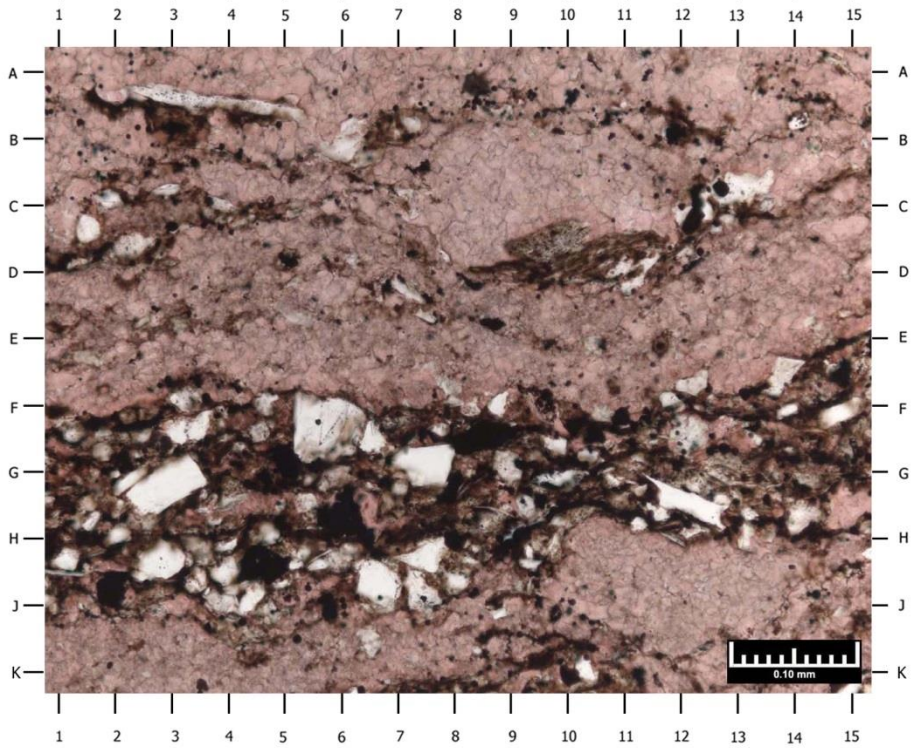

B

200X

SAMPLE DEPTH: 7452.15 – 7452.30 FEET
PLATE 15

Lithology: Slightly silty limestone

Sedimentary Fabric: The limestone texture is a mudstone to wackestone; moderately common incipient microstylolites giving an impression of a laminated texture; rare possible burrows

Compaction: Moderate to high (based on the presence of incipient microstylolites)

Detrital Grains / Allochems:

Major: Quartz silt

Minor: Peloids

Accessory: Quartz sand; muscovite; plagioclase feldspar; spherules; mudstone lithoclasts (?); calcareous foraminifera; pellets

Matrix: The matrix has been mostly replaced to fine sparry calcite; organic material and undifferentiated detrital clays are associated with the microstylolites.

Cement / Replacement: Calcite is the primary authigenic mineral in this sample and occurs in a variety of ways: replacement/recrystallization of allochems, pore- and vug-filling cement, micritization of allochems, and fine spar replacement of the matrix. Many allochems have been micritized making complete identification impossible. Pyrite is sparse and occurs as a replacement of calcite and organic material. Rare quartz overgrowth cement.

Porosity Types: Rare sampling-induced cracks

Magnification: A: 50X B: 200X

A) Photomicrograph 15A depicts a slightly silty lime mudstone to wackestone. Numerous incipient microstylolites are present in this field of view (E1-15, FG1-15, HJ1-GH15). Detrital grains, organic material, and undifferentiated detrital clays are more commonly associated with the stylolites. Detrital grains include quartz silt (CD2.8, A13.6, K10.6), muscovite (AB12.3, CD4.8, CD2), and quartz sand (AB3.8, D7.3, K6.2). A possible pellet (AB6-10.5) is filled with spherules. Peloids are also present (BC2.4, GH9.3, CD10.3). These allochems have been replaced by calcite (stained pink) or have been micritized, making identification difficult. Pyrite (DE7.3, C11.7, HJ10.6) partially replaces calcite and organic material and is disseminated throughout the matrix.

B) High magnification view of Photomicrograph 15A at F10 depicts incipient microstylolites (FJ1-EH15). Detrital grains, which include quartz sand (G3, GH11-13, FG7-8), muscovite (HJ1, HJ5.6, H11.8), and quartz silt (H2.1, K10.3, J8.8), are more common within the microstylolite. The matrix contains fine calcite spar (A6, A12.8, D14). Authigenic pyrite is also present (AB11.3, HJ2, K10).

7457.15' - 7457.25'
Plate 16

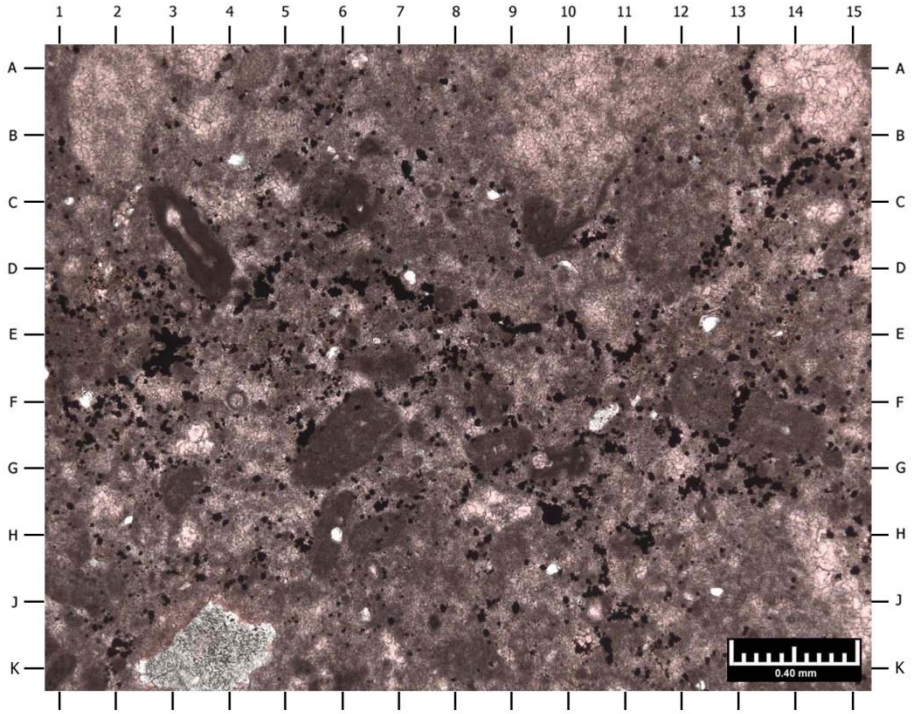

A

50X

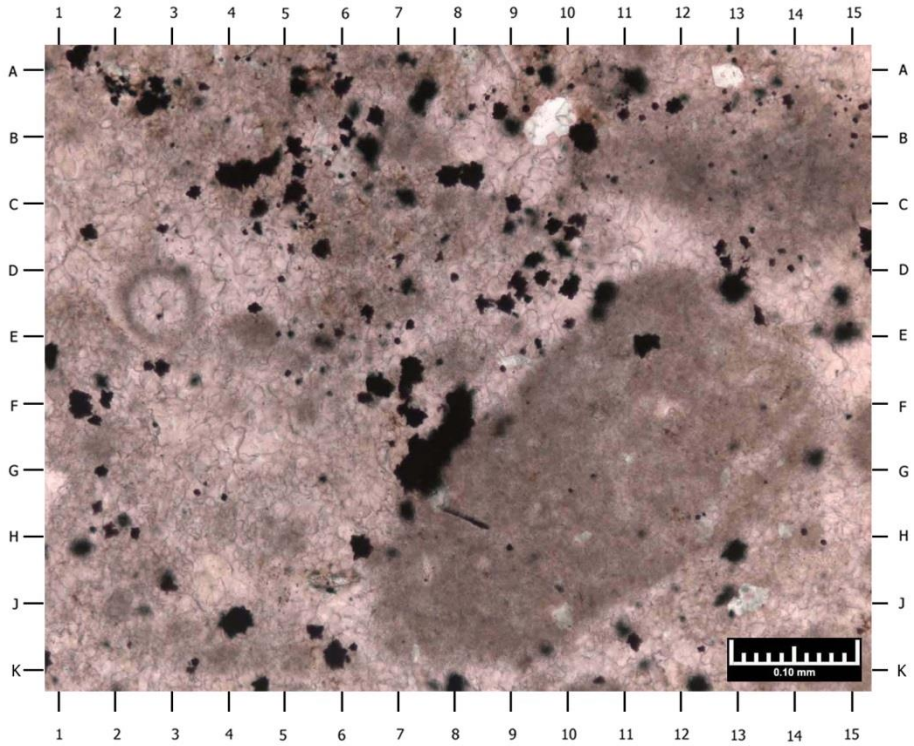

B

200X

SAMPLE DEPTH: 7457.15 – 7457.25 FEET
PLATE 16

Lithology: Slightly silty, bioclastic limestone
Sedimentary Fabric: The limestone texture is a wackestone to packstone
Compaction: Moderate

Detrital Grains / Allochems:

Major: Peloids
Minor: Quartz silt; calcareous foraminifera
Accessory: Brachiopod fragments; plagioclase feldspar; algal fragments (?); quartz sand

Matrix: The matrix has been mostly replaced to fine sparry calcite

Cement / Replacement: Calcite is the primary authigenic mineral in this sample and occurs in a variety of ways: replacement/recrystallization of allochems, pore and vug-filling cement, micritization of allochems, and fine spar replacement of the matrix. Many allochems have been micritized making complete identification impossible. Dolomite and baroque dolomite are sparse and occur as a cement. Pyrite is sparse and occurs as a replacement of calcite and organic material.

Porosity Types: Rare sampling-induced cracks

Magnification: A: 50X B: 200X

A) Photomicrograph 16A depicts a slightly silty packstone. Peloids (CD3-4, FG5-7, GH3, FG8-9) are the primary allochem in this sample. Most of the allochems in this sample have been micritized making identification difficult. Other undifferentiated allochems have been replaced by sparry calcite (stained pink; AB14-15). Baroque dolomite cement (JK3-4) is sparse. Pyrite (B1, BC7.2, JK10.3) partially replaces calcite and organic material. Detrital grains include quartz silt (C1.3, C8.7, J12.8) and chert fragments (FG10.6).

B) High magnification view of Photomicrograph 16A at F5 depicts common peloids (BC11-15, D12-J7, DE4-5). These allochems have been micritized making identification impossible. A possible calcareous foraminifera is also present (DE2-3) and has been replaced by calcite (stained pink). The matrix contains fine calcite spar (C2, F4, K12). Pyrite (B10.3, FG7-8, H13) partially replaces calcite and organic material. Quartz silt (A12.8, B9-10) is the primary detrital grain in this sample.

7460.85' - 7460.95'
Plate 17

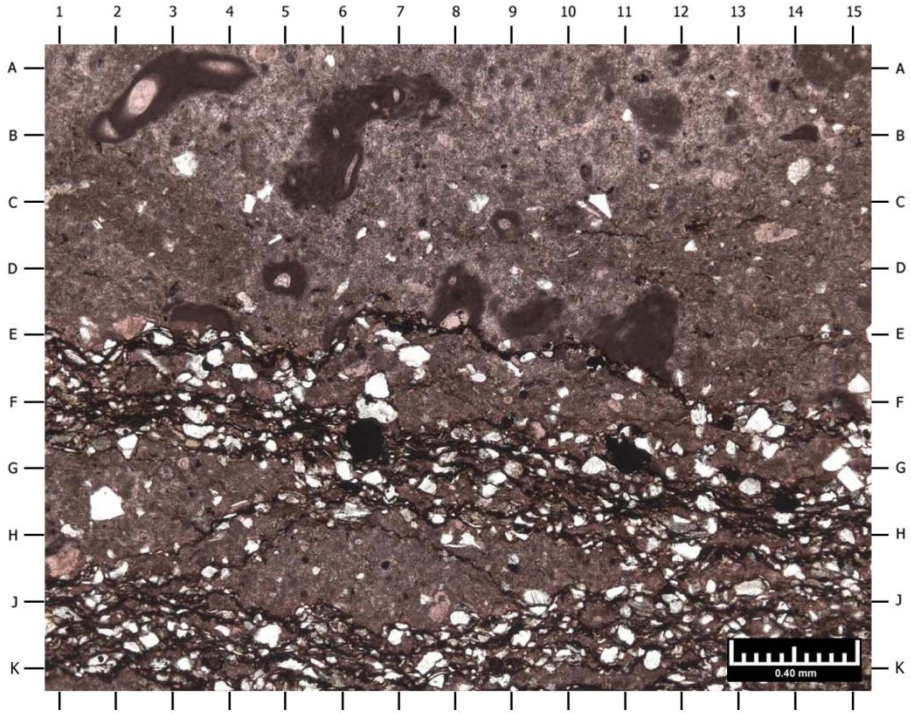

A

50X

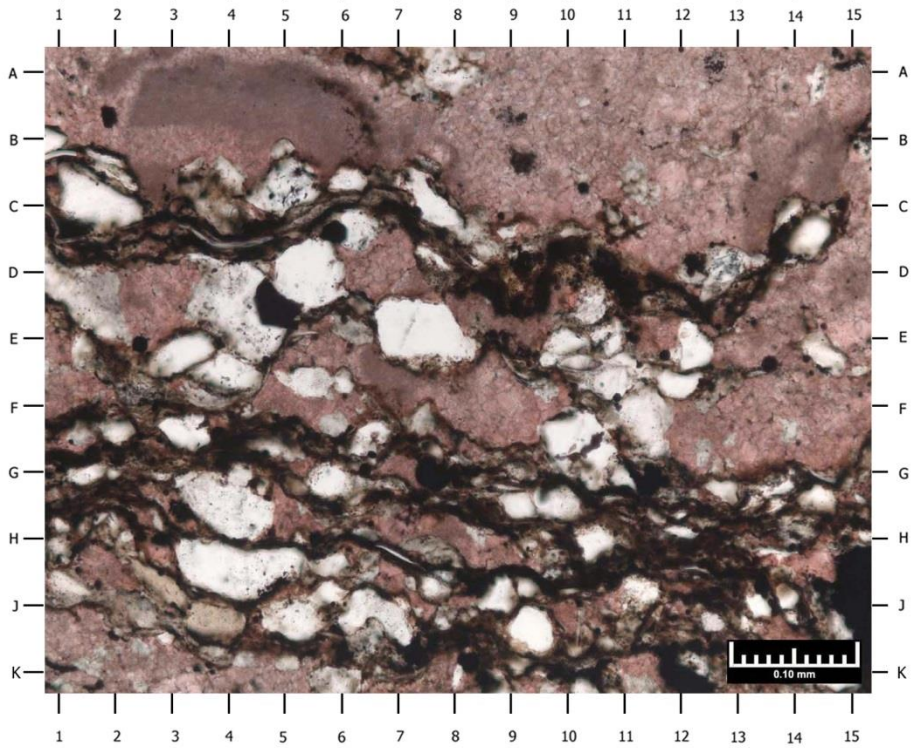

B

200X

SAMPLE DEPTH: 7460.85 – 7460.95 FEET
PLATE 17

Lithology: Slightly sandy limestone

Sedimentary Fabric: The limestone texture is a wackestone; numerous incipient microstylolites are present

Compaction: Moderate to high (based on the presence of microstylolites)

Detrital Grains / Allochems:

Major: Peloids

Minor: Quartz sand; quartz silt

Accessory: Calcareous foraminifera; muscovite; plagioclase feldspar; spherules

Matrix: The matrix has been mostly replaced to fine sparry calcite; organic material and undifferentiated detrital clays are associated with the microstylolites.

Cement / Replacement: Calcite is the primary authigenic mineral in this sample and occurs in a variety of ways: replacement/recrystallization of allochems, pore and vug-filling cement, micritization of allochems, and fine spar replacement of the matrix. Many allochems have been micritized making complete identification impossible. Pyrite is sparse and occurs as a replacement of calcite and organic material.

Porosity Types: Rare sampling-induced cracks

Magnification: A: 50X B: 200X

A) Photomicrograph 17A depicts a slightly sandy wackestone (AE1-AF15). Several incipient microstylolites (E1-F12, FG1-GH15, JK1-15) are present. Detrital grains, organic material, and undifferentiated detrital clays are more common within the stylolites. Detrital grains include quartz sand (GH1.8, EF7.2, C10.6), quartz silt (B14.8, A5.8, K3.2), and muscovite (JK3.7, H8.3, GH4.2). Allochems include calcareous foraminifera (AB2-4, C5-AB8, DE8) and peloids (AB11-12, A10.7, AB8.9). These allochems have been micritized and/or replaced by calcite cement (stained pink). Pyrite (DE7.2, G11, FG15) partially replaces organic material and calcite and is disseminated throughout the matrix.

B) High magnification view of Photomicrograph 17A at F4 depicts several incipient microstylolites (CD1-C15, FH1-GH15). Detrital grains include quartz silt (JK9.3, FG3.2, J13.3), quartz sand (D5.3, DE7-8, HJ3-5), and muscovite (H7, HJ12.2, BC1). A peloid (AB2-6) has been micritized making identification of the allochem impossible. The matrix contains fine calcite spar (A10, C15, F15). Pyrite (AB1.8, CD5.8, G7.7) partially replaces calcite (stained pink) and organic material and is disseminated throughout the matrix.

7466.30' - 7466.40'
Plate 18

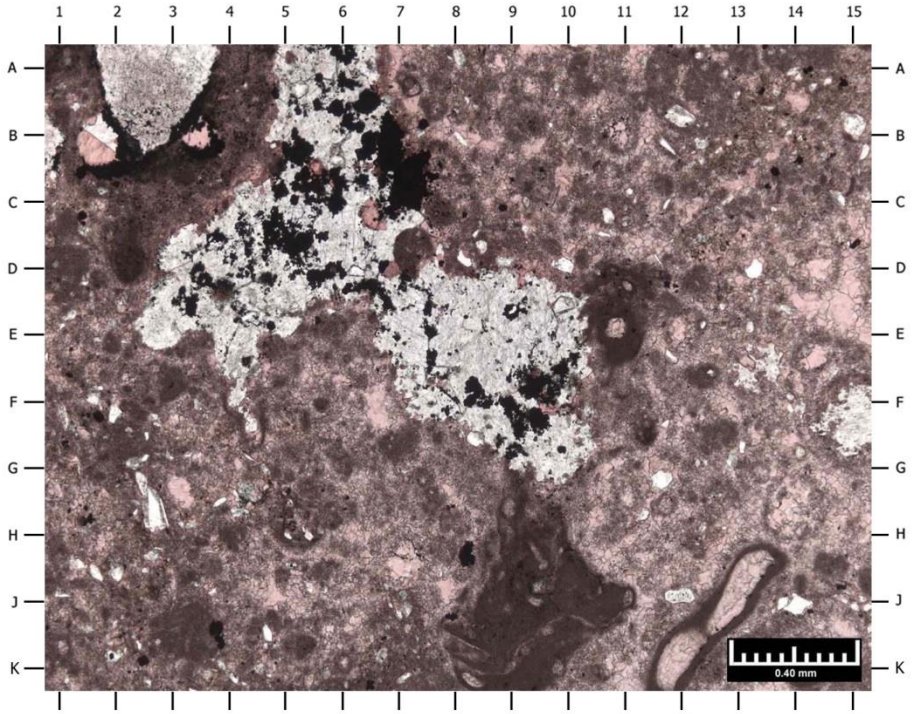

A

50X

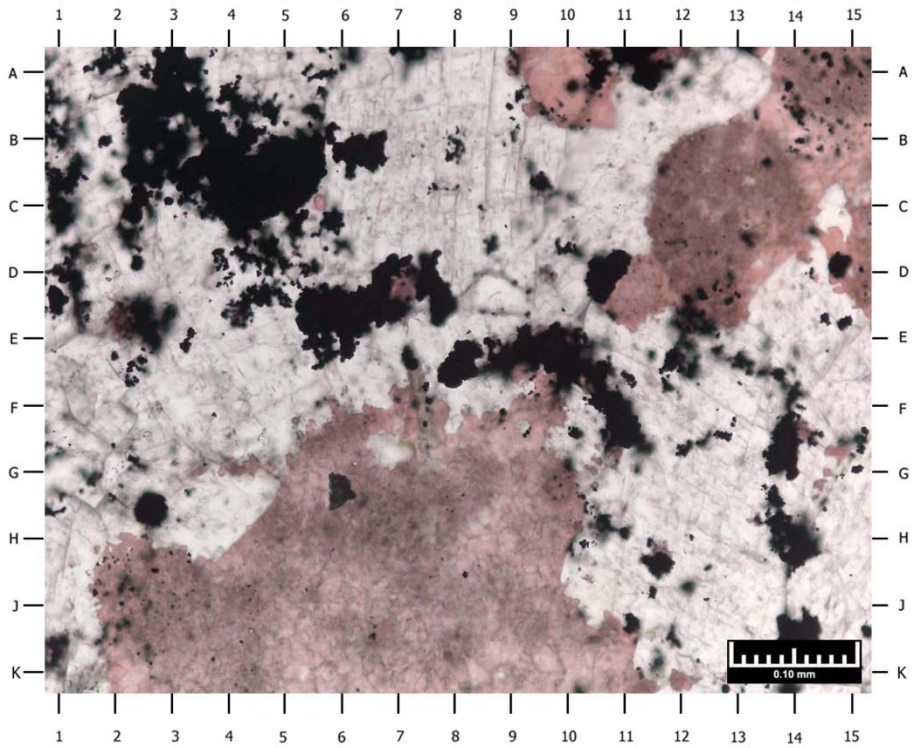

B

200X

SAMPLE DEPTH: 7466.30 – 7466.40 FEET
PLATE 18

Lithology: Bioclastic limestone
Sedimentary Fabric: The limestone texture ranges from a wackestone to a packstone
Compaction: Moderate

Detrital Grains / Allochems:

Major: Peloids
Minor: Foraminifera; quartz silt
Accessory: Quartz sand; muscovite; echinoderm fragments; plagioclase feldspar; potassium feldspar

Matrix: The matrix has been mostly replaced to fine-medium sparry calcite

Cement / Replacement: Calcite is the primary authigenic mineral in this sample and occurs in a variety of ways: replacement/recrystallization of allochems, pore and vug-filling cement, micritization of allochems, and fine spar replacement of the matrix. Many allochems have been micritized fully making identification impossible. Dolomite and baroque dolomite are moderately common and occur as a cement and a replacement of allochems. Pyrite is sparse and occurs as a replacement of calcite and organic material. Rare authigenic quartz replaces calcite, more likely in association with altered allochems.

Porosity Types: Pore types include rare intercrystalline matrix pores, rare intraparticle pores, and rare sampling-induced pores

Magnification: A: 50X B: 200X

A) Photomicrograph 18A depicts a bioclastic packstone. Peloids (F5.7, FG7, EF12.3) are the primary allochem. Most of the allochems in this sample have been recrystallized by micrite making identification difficult. Baroque dolomite cement (AB2-3, FG15, E8.5) occurs as a vug-filling cement and as a replacement of allochems. Detrital grains include quartz (D9.9, D13.4, J14) and muscovite (FG4.4). Calcite (stained pink) replaces many allochems and occurs as a cement (B1.4, B3.4, DE14.8). Organic material (BC2.3, BC7, HJ8.3) has been partially replaced by calcite.

B) High magnification view of Photomicrograph 18A at D6 depicts common baroque dolomite cement (F3, A8, H13). Pyrite (D14.8, GH2.7, DE1) partially replaces calcite (stained pink) and organic material. Peloids are the primary allochem in this sample (BD12-14, A14-15, GH6-8). The matrix contains fine spar calcite to micrite (G5.2, B15, K6).

Core Descriptions

Introduction

The detailed sedimentological log, conducted by the Weatherford Laboratories for all recovered cores, includes information on lithologies, textures, fossil assemblages, sedimentary structures, and depositional environments. The lithology column is drawn based on visual estimates and binocular microscope examination of slabbed core with applications of 10% HCl. Color designations are based on the *Geological Rock-Color Chart* published by Munsell (2009) and are assessed on unwet core.

Core # 1 (7375.00 - 7419.80 ft)

7375.00 – 7380.00 ft: Interval consists of brownish gray to dark gray (5YR 4/1 – N3) limestone ranging from mudstone to wackestone layers. A packstone layer occurs from 7378.60 – 7378.80 ft. Allochems include echinoderms, lithoclasts, foraminifera, and undifferentiated bioclastic debris. Fractures are generally thinner than 1 millimeter and are healed mostly by calcite as well as bitumen, dolomite, and anhydrite. Laminations are sparse. Stylolites are also present and occur with thin layers of silty mudstone. Possible fenestral pores are sparse. There is a sharp lower contact. The depositional environment of this section is interpreted as middle to inner ramp.

7380.00 – 7391.45 ft: Interval consists of brownish gray to dark gray (5YR 4/1 – N3) limestone ranging from mostly lime mudstone with less common wackestone. Laminations are fairly common. The laminated portions contain common laminations of silty mudstone. Undifferentiated bioclastic material is the primary allochem with less common foraminifera and lithoclasts. A stromatactis texture is present at 7386.30 ft. A fracture-induced microfault occurs at 7389.60 ft. Fractures are generally thinner than 1 millimeter and are healed mostly by calcite as well as bitumen, dolomite, and anhydrite. Vugs or grain-moldic pores have been occluded mostly by calcite. The lower contact is missing. The depositional environment of this section is interpreted as middle to outer ramp.

7391.45 – 7391.60 ft: Spacer inserted

7391.60 – 7392.35 ft: Interval consists of an oolitic limestone (7391.60 – 7392.15 ft) and a bioclastic limestone (7392.15 – 7392.35 ft). The oolitic limestone has a grainstone texture and is dark yellowish brown (10YR 2/2). The bioclastic limestone has a wackestone to packstone texture and is medium dark gray (N4). The allochems in these two layers have been commonly recrystallized and have been identified as peloids. Ooids are abundant in the grainstone. The grainstone portion has oil staining that is strongest at the top becoming sparse within the wackestone to packstone layer. A

stylolitic contact separates the two layers. Vugs in the grainstone have been occluded by gypsum/anhydrite as well as calcite and dolomite. Calcite- and bitumen-filled fractures are present in the wackestone to packstone unit. Lower contact is sharp. The depositional environment of this section is interpreted as ooid shoal.

7392.35 – 7403.50 ft: Interval consists of brownish gray to medium gray (5YR 4/1 – N5) limestone. A silty limestone layer occurs from 7398.30 – 7398.80 ft. The texture of these limestones generally ranges from mudstone to wackestone. Several packstone (7398.60 ft) and grainstone (7397.80 – 7398.00 ft) layers are also present. A dolopackstone unit occurs at 7397.30 ft. Laminations are fairly common. The laminated portions contain common laminations of silty mudstone. Stromatactis texture occurs at 7392.70 ft and is abundant from 7400.70 – 7402.00 ft. Bioturbation occurs at 7393.40 ft, 7396.25 ft, 7396.60 ft, 7396.80 ft, and 7397.00 ft, and generally occurs as undifferentiated horizontal or vertical, elliptical burrows. Allochems include undifferentiated bioclastic material, algal or bryozoan fragments, peloids, and lithoclasts. Vugs or allochem-molds are sparse and have been mostly occluded by calcite with less common anhydrite/gypsum and dolomite. Possible mudcracks occur at 7394.25 ft. Oil stain is moderately common from 7403.20 – 7403.40 ft. Fractures occur throughout and are typically filled by calcite as well as bitumen, anhydrite, and dolomite. Stylolites are also present throughout and occur as contacts between many layers. The lower contact is sharp. The depositional environment of this section is interpreted as middle to outer ramp.

7403.50 – 7407.65 ft: Interval consists of brownish gray to medium dark gray (5YR 4/1 – N4) limestone. The oil stained portion of this interval 7405.10 ft is olive black (5Y 2/1). A silty mudstone layer occurs at 7403.95 – 7404.00 ft. The limestone texture ranges from mostly wackestone to packstone. Allochems include peloids, undifferentiated bioclastic material, possible bivalves, gastropod fragments. Stromatactis texture is moderately common throughout. An *Arenicolites*-like burrow occurs at 7404.65 – 7404.75 ft. An anhydrite vug occurs at 7404.80 ft with a dolomite vug occurring at 7405.75 ft. The darker portions of this interval contain more bitumen and clay while the lighter portions are cleaner limestones. Fractures are present throughout and are healed by calcite, bitumen, dolomite, and gypsum/anhydrite. The lower contact is sharp. The depositional environment of this section is interpreted as inner ramp.

7407.65 – 7419.80 ft: Interval consists of brownish gray to dark gray (5YR 4/1 – N3) limestone to silty limestone. This interval consists mostly of wackestone. The interval from 7413.20 – 7413.55 ft consists of interlaminated limestone (mudstone-wackestone), argillaceous, calcareous siltstone, and a silty mudstone. This interval contains common gypsum/anhydrite clasts. The limestone lamination at 7413.25 ft has been broken up

possibly by the fractures, which are common from 7413.50 – 7416.65 ft. The previously mentioned fracture interval has been healed by abundant bitumen. The laminated portions contain common laminations of silty mudstone. A possible hardground occurs at 7410.80 ft. Stromatactics texture is common from 7413.80 – 7415.00 ft. Allochems include undifferentiated bioclastic material, peloids, foraminifera, and lithoclasts. Stylolites are moderately common throughout. Vugs or allochem molds are occluded by calcite, dolomite, and gypsum/anhydrite. The lower contact is sharp. The depositional environment of this section is interpreted as middle to inner ramp.

Core #2 (7435 - 7466.70 ft)

7435.00 – 7435.75 ft: Interval consists of a brownish gray to dark gray (5YR 4/1 – N3) limestone (7435.00 – 7435.40 ft) to silty limestone (7435.40 – 7435.75 ft). These layers are both wackestones with undifferentiated bioclastic material. Silty mudstone laminations are present. Fractures have been healed by calcite with some bitumen. The lower contact is irregular. The depositional environment of this section is interpreted as middle to outer ramp.

7435.75 – 7440.40 ft: Interval consists of medium gray to brownish black (N5 – 5YR 2/1) limestone. This interval consists of planar algal limestone. Algal laminations are abundant throughout and are interlaminated with silty mudstone layers. Stylolites are commonly present throughout the unit and often occur as contacts. Fractures are healed with bitumen and calcite. Possible desiccation cracks occur as well. Vugs are possible associated with fractures. Rare possible fenestral pores are also present. The lower contact is sharp. The depositional environment of this section is interpreted as basin.

7440.40 – 7445.00 ft: Interval consists of interlaminated silty limestone and limestone. These layers range between wackestone a packstone textures. Several algal limestones are also present (7440.70 – 7440.90 ft and 7441.35 – 7441.55 ft). Silty mudstone laminations are common. The silty laminations are brownish black (5YR 2/1) while the limestones are brownish gray to medium dark gray (5YR 4/1 – N4). Stylolitic contacts are present within the algal limestones but are rare elsewhere in the interval. A possible algal limestone clast occurs at 7441.20 ft. Undifferentiated bioclastic material is sparse throughout. Fractures are more common within the less argillaceous portions of the interval and are healed by calcite and contain bitumen. The lower contact is irregular. The depositional environment of this section is interpreted as basin to outer ramp.

7445.00 – 7453.90 ft: Interval consists of interlaminated limestone and silty limestone. The limestone portion of this interval occurs exclusively as algal limestones. The silty limestone texture is a mudstone to wackestone. Silty mudstone laminations are common. The silty laminations are brownish black (5YR 2/1) while the limestones are

brownish gray to medium dark gray (5YR 4/1 – N4). Stylolitic contacts are present within the algal limestones but are rare elsewhere in the interval. Possible fenestral pores are also present within the algal laminations. Pinched out laminations occur sparsely (7450.70 ft, 7451.50 ft, 7452.10 ft, 7453.10 ft). Undifferentiated bioclastic material is rare. Fractures have been healed by calcite, dolomite, and/or gypsum/anhydrite and also may contain bitumen. The lower contact is sharp. The depositional environment of this section is interpreted as basin to outer ramp.

7453.90 – 7466.70 ft: Interval consists of brownish gray to dark gray (5YR 4/1 – N3) limestone ranging from mudstone to wackestone layers. Silty mudstone laminations are rare and only occur in association with stylolites. Allochems include brachiopods, benthic foraminifera, undifferentiated bioclastic material, and lithoclasts. Fractures are moderately common and have been healed by calcite, dolomite, and gypsum/anhydrite. Bitumen is also present within many fractures. Grain-moldic pores or vugs are sparse. A geopetal structure is present within a brachiopod fragment at 7466.60 ft. The lower contact is missing. The depositional environment of this section is interpreted as middle to inner ramp.

Reference

Munsell Color, 2009, Geological rock-color chart, Grand Rapids, Michigan, Munsell Color.

Geochemical Analysis

Introduction

Geochemical analysis of rock samples can provide insights into the characteristics of a source rock as well as resource assessment. Total organic carbon (TOC) and Rock-Eval pyrolysis were used to evaluate the organic richness, kerogen type, and thermal maturity of the Brown Dense interval at twenty-two (22) selected depths in the Sessions #1 well. Vitrinite reflectance data was not available for this study.

TOC and Rock-Eval Pyrolysis

Organic Richness

The quantity of organic matter or organic richness of the sampled interval is determined from TOC in weight percent.

TOC

Typically, TOC values under 0.5% are considered to have poor potential (Jarvie, 1991), and most unconventional shale resource plays have TOC values greater than 2% (Jarvie et al., 2007; Jarvie, 2012). TOC values in excess of 1.0% are highlighted in Table 1. The median and average TOC values are 0.54% and 1.07%, respectively, which represent minimal source rock potential given the thickness of the interval; the interval with more than 1% TOC is less than 40 ft (Figure 2). TOC varies greatly throughout the interval with a high of 5.33% at 7,419.8 ft and a low of 0.03% at a depth of 7,457 ft.

S2

S2 indicates remaining petroleum generation potential. Values of 2.00-5.00 mg/g indicate fair source potential and values greater than 5.00 mg/g are indicative of good source potential (Espitalié, 1982), although these values are diminished with increasing thermal maturity. Like TOC, S2 shows high variability within the sampled interval (Table 1 and Figure 2). A high value of 31.36 mg/g occurs at 7,419.8 ft and a low of 0.02 mg/g at 7,457 ft, which are the same depths with the highest and lowest TOC values. The median and average S2 values are 2.23 and 5.42 mg/g, respectively. Six organic-rich intervals have average S2 values of 16.04 mg/g and these values represent the best source potential in the section analyzed. Most samples have indications of low temperature shoulders or peaks on the kerogen pyrolysate, which is typically heavier oil fractions carried over to the pyrolysis peak. Upon extraction these are usually removed, thereby decreasing S2 values, but increasing the total oil yield and T_{max} values. Overall, the organic-rich interval is interpreted as having good to excellent petroleum generation potential, albeit over only about 40 ft.

Kerogen Type

Visual kerogen analysis was not available for this study, so interpretation of the kerogen type is based on Rock-Eval pyrolysis and TOC data in the form of hydrogen index (HI) and oxygen index (OI). Hydrogen indices are the pyrolysis (S2) yield normalized by TOC with conversion to yield of petroleum in milligrams per gram of TOC. Similarly, oxygen indices are the yield of organic carbon dioxide from kerogen normalized by TOC in milligrams of carbon dioxide per gram of TOC.

HI and OI

HI values over the sampled interval range from 53 mg/g at 7,462 ft, to 600 mg/g at 7,408.55 ft, with a median of 384 mg/g and an average of 352 mg/g (Table 1 and Figures 2 and 3). The average HI for the six organic-rich intervals is 565 mg/g TOC. All organic-rich values indicate Type II, oil prone kerogen (usually marine) (Jones, 1984). Due to the variability in source potential, organofacies, and depositional setting, lower values (< 350 mg/g TOC) are indicative of Mixed (Type II and III) or Type III kerogen (Jones, 1984). The high HI values are consistent with a low to modest level of thermal maturity.

S2/S3

This ratio can be evaluated for remaining petroleum generation potential using the following range of values: 0-2.5 = Type III (gas prone); 2.5-5 = Type III (gas/oil prone); > 5.00 = Type I or II (oil prone) (Clementz, 1979). The sampled interval has a median S2/S3 ratio of 6.22 and an average of 15.14. Both of these values point to Type I or II oil prone kerogen types. There is variability in the interval, however, with values as low as 0.1 at 7,457 ft and as high as 65.0 at 7,414.65 ft.

Thermal Maturity

The thermal maturity of the sampled interval has been interpreted primarily based on T_{max} values.

T_{max}

T_{max} values can be interpreted in multiple ways (Espitalié et al., 1977, 1984, 1985). Using the S2/S3 and HI averages above to indicate kerogen type, the T_{max} interpretation can be narrowed into the Type II kerogen category. The available data is non-specific for Type II-S kerogen, which is sulfur-rich organic matter, but higher sulfur contents are known to be found in many Smackover sourced oils. All of the values in the sampled interval have a T_{max} between 425°C and 450°C (Table 1). However, the organic-rich samples average 441^{o}C or an equivalent vitrinite reflectance value of 0.78% R_{oe}. This temperature range is indicative of the main phase of oil generation for Type II kerogens (Figure 4). A Type II-S kerogen, i.e., a high sulfur kerogen, may actually be more highly converted than indicated by this T_{max} and equivalent R_o value. However, the HI values are indicative of less than peak oil generation. T_{max} values can be unreliable due to low

S2 values. Depths of 7,384, 7,388, 7,403, 7,417, 7,457, 7,462, and 7,466.7 ft have questionable T_{max} readings.

Production Index (PI)

PI is the yield of oil (S1) as a ratio of the oil and remaining kerogen potential (S2) (S1/(S1+S2)). It reflects thermal maturity as kerogen is converted to petroleum through maturation. However, it is affected by expulsion and thus can show higher or lower values depending on whether oil has been expelled from a source rock or emplaced in a non-source interval. Samples under 0.08 are typically a good indication of immature organic matter, over 0.50 are in the gas window, and in between are in the oil window (Espitalié, 1982). PI values in samples with greater than 1% TOC fall into the immature and oil window ranges (Figure 5). The median and average values, 0.11 and 0.15, respectively, both indicate oil window maturity. The low PI, 0.01, occurs at 7,414.65 ft, while the high, 0.50, occurs at 7,457 ft (Table 1).

S1x100/TOC

S1x100/TOC is indicative of thermal maturity and relative oil saturation. It shows considerable variability over the sampled interval, which is not unusual (Table 1 and Figure 2). Depths 7,398 and 7,405.85 ft have much higher values than any other depths. Those two depths have values of 166 and 267 mg/g TOC, respectively. Such high values can indicate potentially productive petroleum intervals or contamination. The median is 28 mg/g TOC, which indicates an interval that is lean in organics. The average, however, is 51 mg/g TOC, which falls just into the low end of the mature, tight source rock interpretation (Jarvie and Baker, 1984).

Conclusions

Rock-Eval pyrolysis results indicate that the majority of source rock organic matter (>1.00% TOC) of the sampled cores in the Sessions #1 well is Type II, oil-prone kerogen. The averaged TOC value suggests that the Brown Dense has fair to good source potential. The thermal maturity assessed from T_{max} indicates that the organic matter is in the oil window, which is consistent with the observations from biomarker data. There is high oil saturation indicated in two intervals. Most of the intervals have indications of carry-over of oil into the pyrolysis (S2) peak, which means oil contents are higher than indicated and pyrolysis yields are lower than reported.

References

Clementz, D.M., 1979, Effect of oil and bitumen saturation on source-rock pyrolysis: AAPG Bulletin v. 63, p. 2227–2232.

Espitalié, J., M. Madec, B. Tissot, and P. Leplat, 1977, Source rock characterization method for petroleum exploration, *in* Proceedings of the Offshore Technology Conference, Houston, TX.

Espitalié, J., 1982, Institut Français du Pétrole, Syntheses Géologiques et Géochimie 7020, April 28.

Espitalié, J., F. Marquis, and I. Barsony, 1984, Geochemical logging, *in* Voorhees, K.J., *ed*., Analytical pyrolysis techniques and applications: Butterworth, Boston, p. 276-304.

Espitalié, J., G. Deroo, and F. Marquis, 1985, Rock-Eval Pyrolysis and its applications: Institut Français du Pétrole 40, p. 563-578.

Jarvie, D.M. and D.R. Baker, 1984, Application of the Rock-Eval III oil show analyzer to the study of gaseous hydrocarbons in an Oklahoma gas well, 187th ACS National Meeting, St. Louis, Missouri, April 8-13.

Jarvie, D.M., 1991, Total Organic Carbon (TOC) analysis, *in* R.K. Merrill, *ed.,* Treatise of Petroleum Geology, Handbook of Petroleum Geology, Source and Migration Processes and Evaluation Techniques, AAPG Press, Tulsa, OK, p. 113-118.

Jarvie, D.M., R.J. Hill, T.E. Ruble, and R.M. Pollastro, 2007, Unconventional shale-gas systems: The Mississippian Barnett Shale of north-central Texas as one model for thermogenic shale-gas assessment: AAPG Bulletin, v. 91, p. 475-499, doi:10.1306/12190606068.

Jarvie, D.M., 2012, Shale resource systems for oil and gas: Part 1—Shale-gas resource systems, *in* J.A. Breyer, ed., Shale Reservoirs—Giant resources for the 21st century: AAPG Memoir 97, p. 69-87, doi:10.1306/13321446M973489.

Jones, R.W., 1984, Comparison of carbonate and shale source rocks, *in* J.G. Palacas, *ed.*, Petroleum geochemistry and source rock potential of carbonate rocks: AAPG Studies in Geology 18, p. 163-180.

Table 1. Total organic carbon and Rock-Eval pyrolysis data of the Brown Dense, Sessions #1 well.

Depth (ft)	TOC (%)	S_1 (mg/g)	S_2 (mg/g)	S_3 (mg/g)	T_{max} (°C)	HI	OI	S_2/S_3	S_1/TOC x 100	PI	Note
7379	0.27	0.13	0.97	0.31	436	366	117	3.1	50	0.12	
7384	0.24	0.05	0.39	0.26	438	165	110	1.5	21	0.11	*
7388	0.09	0.03	0.07	0.21	436	80	239	0.3	35	0.30	*
7393	0.73	0.14	2.14	0.32	437	293	44	6.7	19	0.06	
7398	0.53	0.87	1.42	0.49	429	270	93	2.9	166	0.38	
7403	0.25	0.21	0.47	0.43	434	187	171	1.1	83	0.31	*
7405.85	1.13	3.02	4.68	0.63	435	413	56	7.4	267	0.39	
7408.55	3.66	0.32	21.96	0.39	443	600	11	56.3	9	0.01	
7409.7	0.56	0.05	2.32	0.17	437	418	31	13.6	9	0.02	
7411.2	1.41	0.28	7.98	0.33	441	565	23	24.2	20	0.03	
7412	0.48	0.05	2.14	0.20	443	451	42	10.7	11	0.02	
7414.15	4.26	0.82	23.33	0.52	443	548	12	44.9	19	0.03	
7414.65	1.26	0.04	7.15	0.11	440	570	9	65.0	3	0.01	
7417	0.17	0.05	0.45	0.29	440	269	174	1.6	31	0.10	*
7419.8	5.33	1.14	31.36	0.50	442	589	9	62.7	21	0.04	
7436	0.56	0.25	2.44	0.34	439	433	60	7.2	44	0.09	
7441.75	1.11	0.96	4.48	0.38	436	402	34	11.8	86	0.18	
7447	0.83	0.56	2.96	0.52	433	355	62	5.7	67	0.16	
7452	0.45	0.29	2.53	0.44	433	558	97	5.8	65	0.10	
7457	0.03	0.02	0.02	0.20	431	69	690	0.1	70	0.50	*
7462	0.09	0.01	0.05	0.17	432	53	181	0.3	10	0.16	*
7466.7	0.04	0.01	0.03	0.24	427	81	649	0.1	26	0.25	*

* low S_2, T_{max} is unreliable

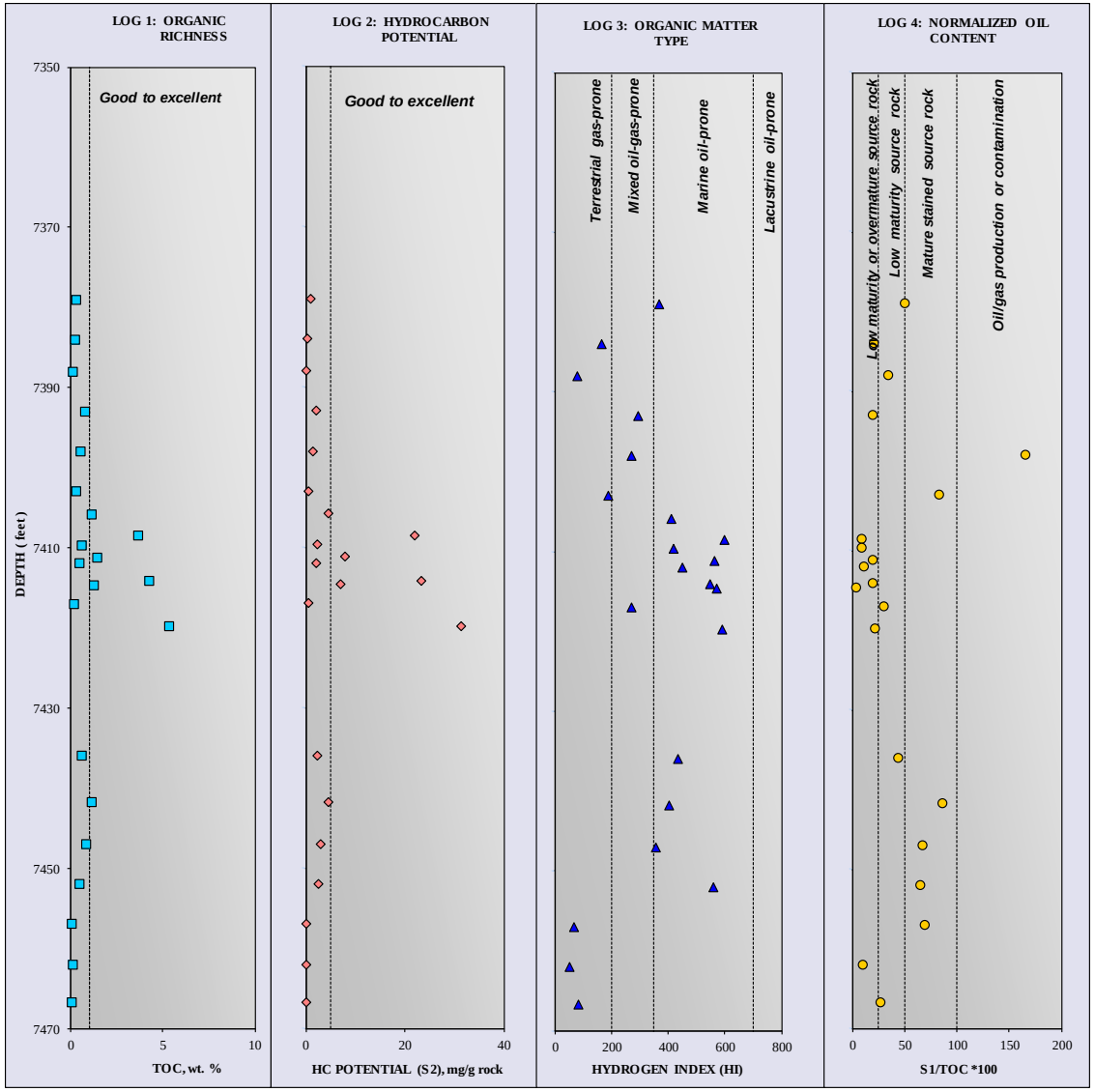

Figure 2. Parameters of organic matter richness and kerogen type of the Brown Dense, Sessions #1 well.

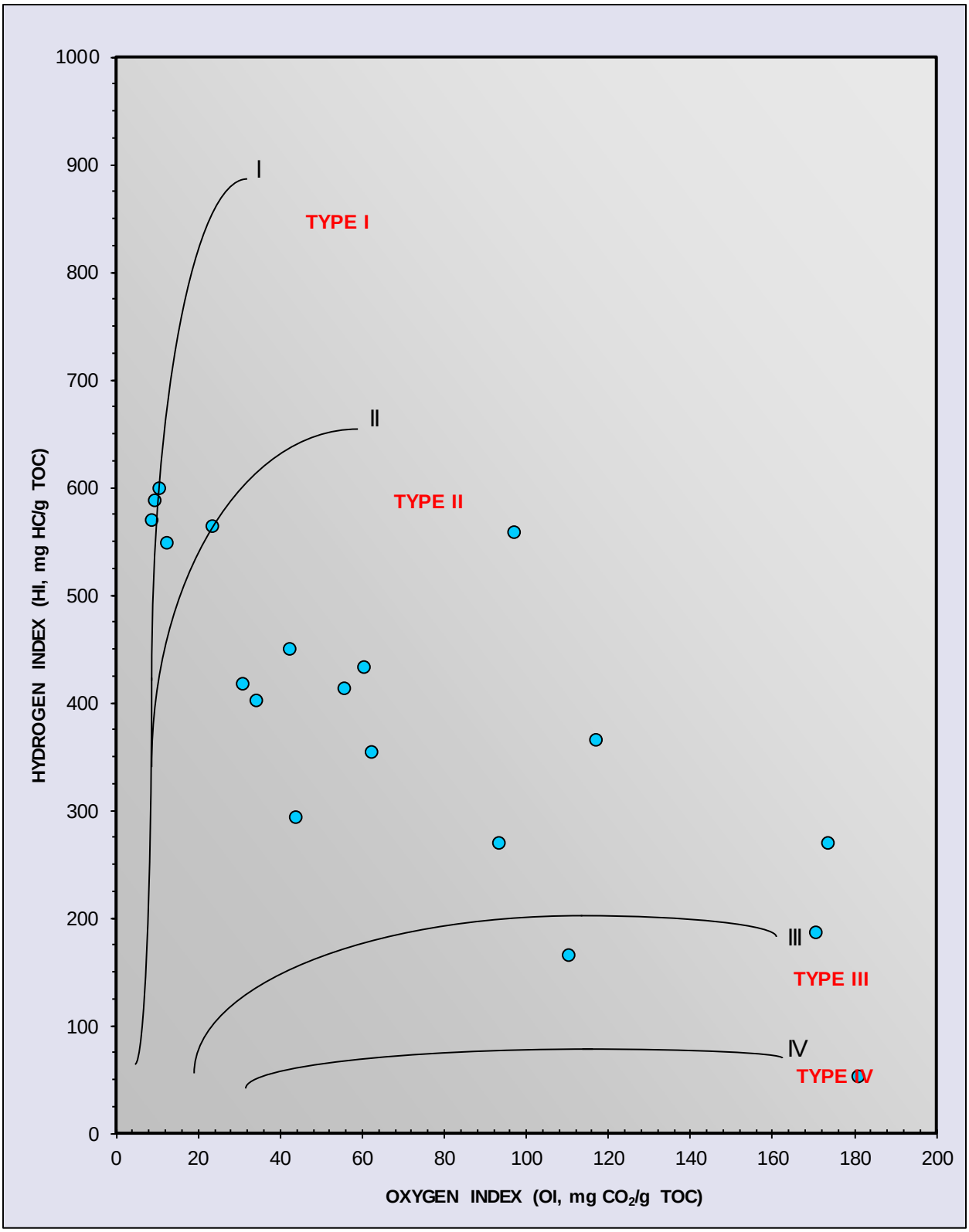

Figure 3. Kerogen types of the Brown Dense based on HI and OI data, Sessions #1 well.

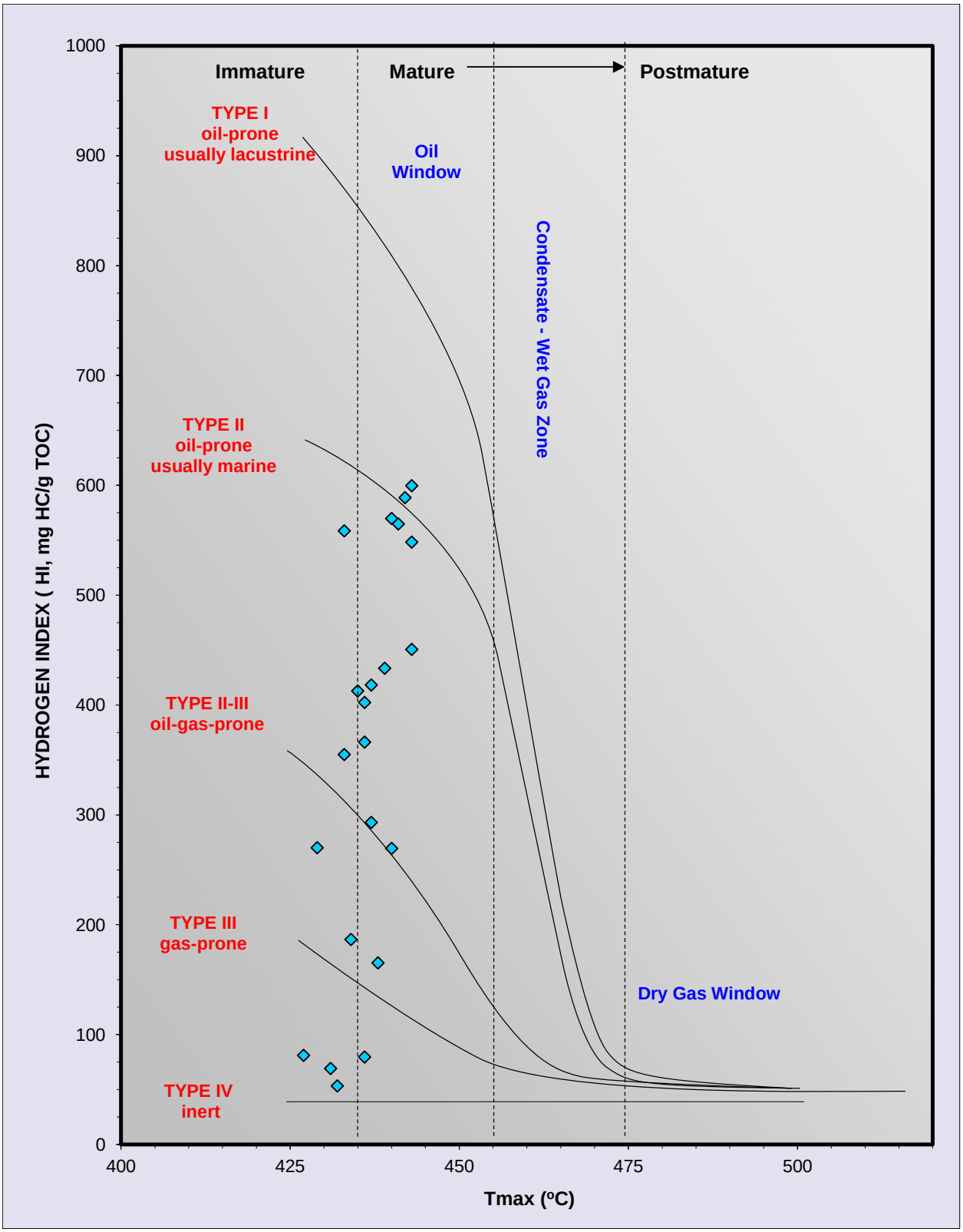

Figure 4. Thermal maturity (T_{max}) associated with kerogen types (HI) of the Brown Dense, Session #1 well.

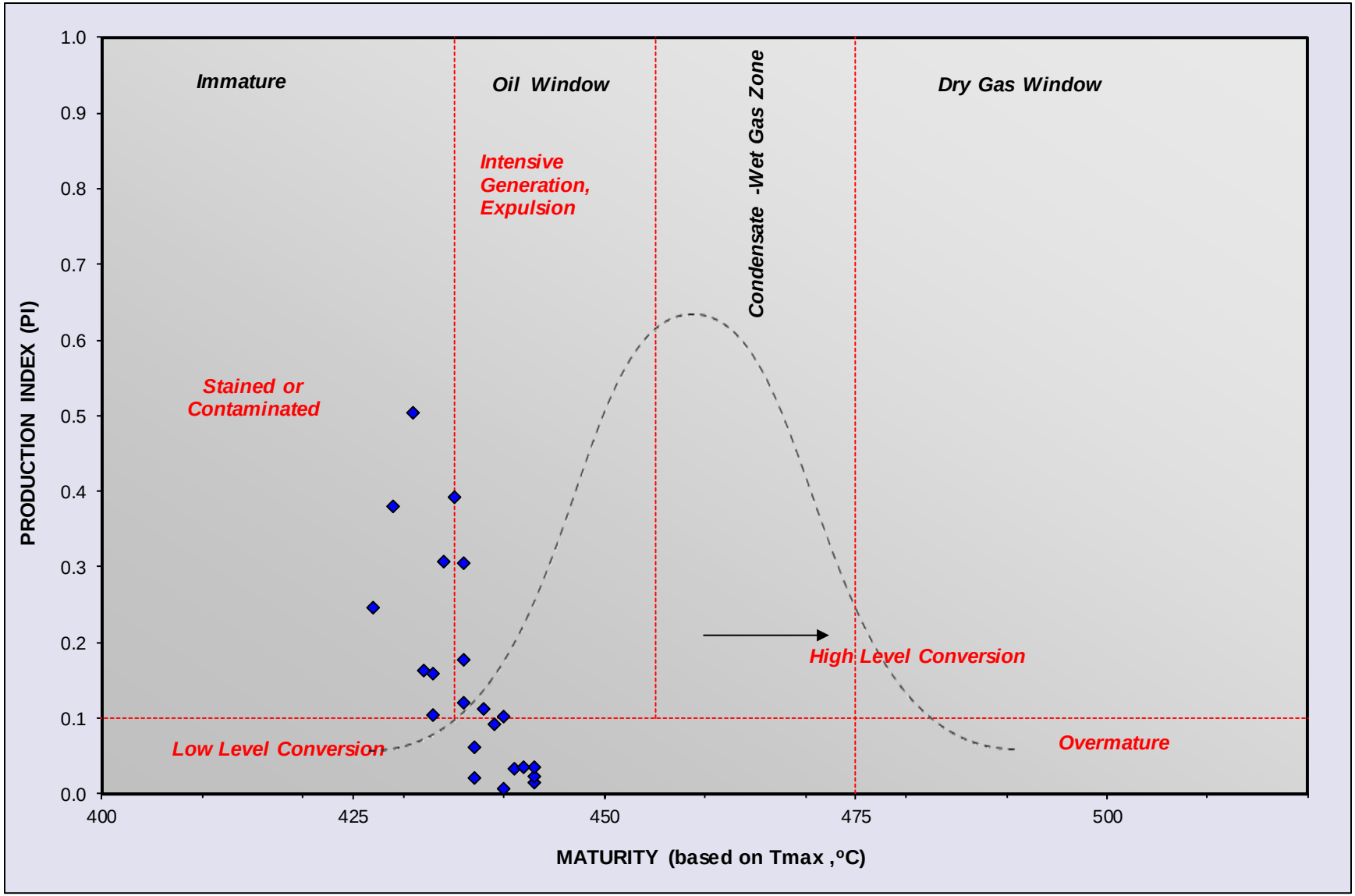

Figure 5. Thermal maturity of the Brown Dense based on T_{max} and PI data, Sessions #1 well.

Field Emission Scanning Electron Microscopy Analysis with Argon Ion Milling Preparation

Introduction

Field Emission Scanning Electron Microscopy (FE-SEM) analysis provides high resolution, high magnification SEM imaging capabilities, which is especially beneficial for characterizing micro- to nano-sized pores in shale/mudstone samples. Three samples were examined for this study by Weatherford Laboratories in Houston, Texas. Sample depths are at 7408.45-7408.65 ft, 7419.80 ft, and 7441.30-7441.60 ft. Twelve photomicrographs range in magnification from 400X to 20,000X including six (6) secondary electron (SE) images and six (6) backscattered electron (BSE) images for each sample.

Procedures for AIM and FE-SEM Analysis

Samples are first milled for 8 hours with a focused argon ion beam using a JOEL model SM-09-010 cross section polisher. This provides a flat, polished surface with minimal debris or other artifacts typically associated with mechanical polishing. The milled samples are then analyzed in an FEI model Quanta FEG 650 FE-SEM with simultaneous energy dispersive spectroscopy (EDS) analysis using a Bruker Quantax EDS system. Analysis with EDS aids in identification of minerals. The FE-SEM system used has environmental/low-vacuum mode capabilities, which allows samples to be viewed uncleaned and either uncoated or with only a minimal gold coating applied with a sputter coater, depending on the objectives of each individual study.

For each sample submitted for Argon Ion Milling FE-SEM analysis, a series of images are acquired at increasing magnifications. Both SE imaging and BSE imaging are utilized during FE-SEM analysis, because each provides unique information about the sample. BSE imagery aids in mineral identification by providing gray scale atomic number contrast. Low density material, such as bitumen or kerogen, will appear very dark gray to black and high density minerals, such as pyrite, will appear bright white in a BSE image. Although some gray-scale mineral density contrast is also visible in the SE image, only the SE image allows for the examination of topographical features, such as nanopores that may occur within organic material. Through the use of SE imaging, these nano-scale pores can be viewed for spatial relationships and pore-diameter measurements directly collected using annotative SEM imaging software. Comparisons

between the image pairs assist in evaluating characteristics of the fabric and pore system.

FE-SEM Plates and Descriptions

PLATE 1 (7419.80 FEET)

The surface of these argon-ion milled samples were photographed using secondary electron (SE images; Photographs A and C) and backscattered electron (BSE images; Photographs B and D) images to reveal detailed compositional and textural characteristics. Secondary electron (SE) images illustrate sample topography and allow for visual identification of micropores and/or nanopores. Backscattered electron (BSE) images, such as shown in photos B and D, display gray-scale atomic number contrast, which aids in the differentiation of minerals. Backscatter electron intensity (gray scale brightness) increases with mean atomic number (and density). Minerals with high atomic number are typically easily distinguished when present in grayscale images. Pyrite for example, has a high mean atomic number and is shown in the grayscale image as white. Comparisons between the image pairs assist in evaluating characteristics of the fabric and pore system. Analysis with energy dispersive spectroscopy (EDS) aids in identification of minerals. Vertical streaks, or “curtaining” across the sample surface is a common artifact of the milling process.

Low magnification photomicrographs (Photographs A and B) provide an overview of the fabric of the argon-ion milled (AIM) surface. This sample consists of a limestone (based on the core description).

Photographs C and D depict a high magnification view of the area around F8 in Photographs A and B. These photographs consist almost entirely of euhedral to subhedral calcite cement (B3, A10, CD5.8, K12, E12.8). Organic material (JK3, H9, K5.9, KL8.3, L9.7) is present within intercrystalline pores.

The presence of pores can be evaluated by using the SE image (Photograph C) to identify the white “edge effect” that commonly occurs around sharp edges of pore boundaries. Both pores and organic material appear black in BSE images; however, organics lack the white “edge effect” associated with pores in the SE images. The primary pore type in this sample appears to be intercrystalline micropores (Photograph C: C8.5, EF12.4, H2.3, M7) between calcite crystals. Possible micropores are present within the organic material as well (Photograph C: KL3.3, GH8.7, CD6.1, FG8.5). Possible organic material with micropores occurs within the intercrystalline micropore at C8.5.

Magnification: A: 400X B: 400X C: 1500X D: 1500X

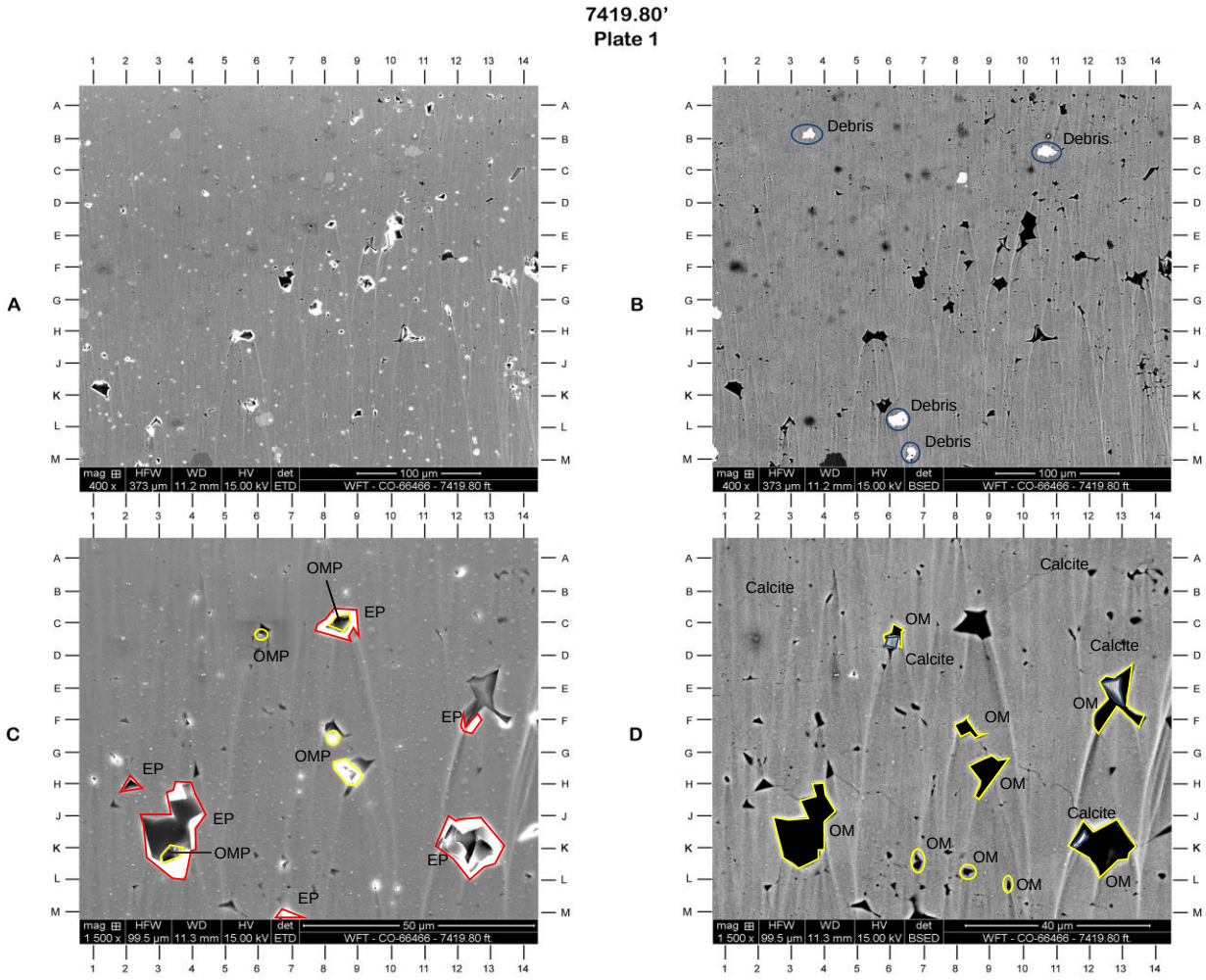

EP	**Intercrystalline Pore**	**OM/OMP**	**Organic Matter / Organic Matter Pore**
RP	**Intracrystalline Pore**		**Minerals**

PLATE 2 (7419.80 FEET)

Additional features of this limestone are shown in Photographs E-H. Secondary images (SE) are shown in Photographs E and G, and backscattered electron images (BSE) are shown in Photographs F and H. Euhedral to subhedral authigenic calcite is the dominant constituent in this sample (Photographs E and F: B8, D2, C13, J11, K2-3, M11-13; Photographs G and H: B9, A13, L2, HJ13). Other constituents include authigenic quartz (Photographs E and F: L10.9) and possible pyrite (Photographs G and H: HJ13.8). Organic material in Photographs G and H at GH12-13 appears to completely occlude an intercrystalline pore. Organic material is present in numerous other places in these photographs (Photographs E and F: C5.5-H4.7, KL3-5, KL10-11; Photographs G and H: AD11-13, GH3-4, K7-8, HK14).

Even though organic material and pores both appear black in BSE images, pores present within the organic material can generally be identified in the SE images based on the white “edge effect.” Pore types consist of intercrystalline micropores (Photograph E: A8; Photograph G: CD1.3) and intracrystalline micropores (Photograph E: CD7.7, AB5.7, F13, K6.8; Photograph G: EF10.2, FG10.7, KL8.2). Micropores are also present within possible organic material (Photograph E: KL3; Photograph G: GH3.2, JK6.9). It is difficult to determine whether some of the micropores in Photograph E are intercrystalline micropores or micropores within organic material (CD5-6, FG4-6, KL4.8). Pore diameters were measured at 2.097 microns (Photograph E: K7-9) and 332.3 nanometers (Photograph G: JK6.9).

Magnification: E: 6000X F: 6000X G: 10000X H: 10000X

7419.80'
Plate 2

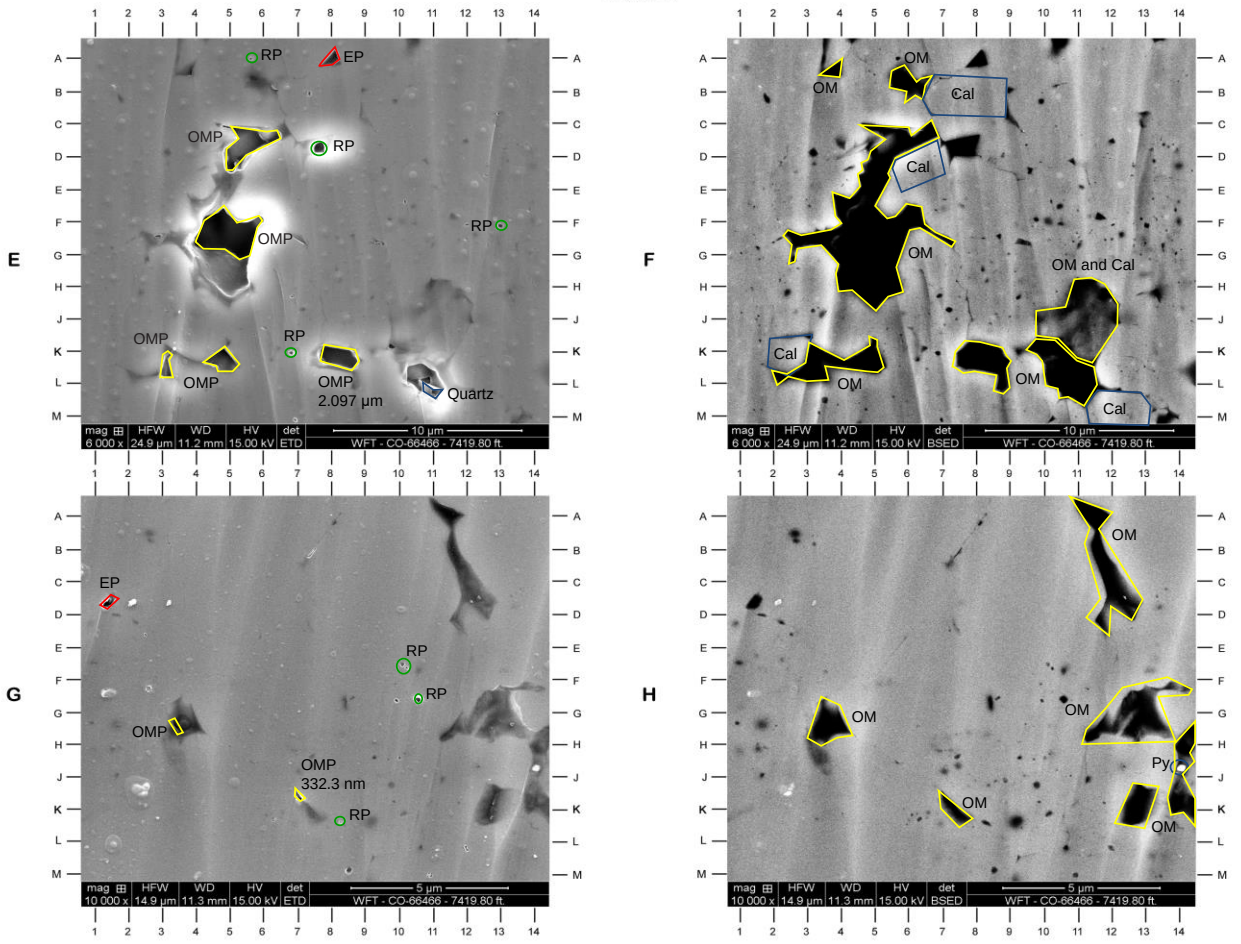

EP	**Intercrystalline Pore**	**OM/OMP**	**Organic Matter / Organic Matter Pore**
RP	**Intracrystalline Pore**		**Minerals**

PLATE 3 (7419.80 FEET)

Euhedral to subhedral calcite cement is common in these plates (Photographs I and J: B4, J1, A13, JK5.5, L10; Photographs K and L: C3, B12, GH11, L10). Pyrite (Photographs I and J: E3, B8.5, E7, GH13, J3) partially replaces organic material. Organic material occurs between calcite crystals (Photographs I and J: AB7-8, FG2, KL3-5, HJ2-3; Photographs K and L: DF8-9, HJ12-13, GJ8-9).The majority of the nanopores and micropores in these photographs appear to be within the organic material (Photograph I: AB7.7, KL4, FG4.4, J11-12, JK6.8; Photograph K: E8.5, GH8-9, JK3). Intracrystalline nanopores (Photograph K: KL4.3, L5.3, A13) are also present between the calcite crystals. Pore diameters were measured at 990.6 nanometers (Photograph I: KL4) and 331.1 nanometers (Photograph K: JK3).

The lithology of this sample is a limestone. The vast majority of this sample is dominated by fine crystalline, euhedral to subhedral calcite cement. Authigenic quartz and pyrite are rare. Pyrite appears to partially replace organic material while the authigenic quartz occurs as a pore-filling cement. Organic material occurs primarily as an intercrystalline micropore to nanopore fill. Micro- to nanopores are also present within the organic material in many places. In fact, most of the micro- and nanopores seem to be associated with organic material. However, some micro- and nanopores occur within/between calcite cement without organic material.

Magnification: I: 15000X J: 15000X K: 20000X L: 20000X

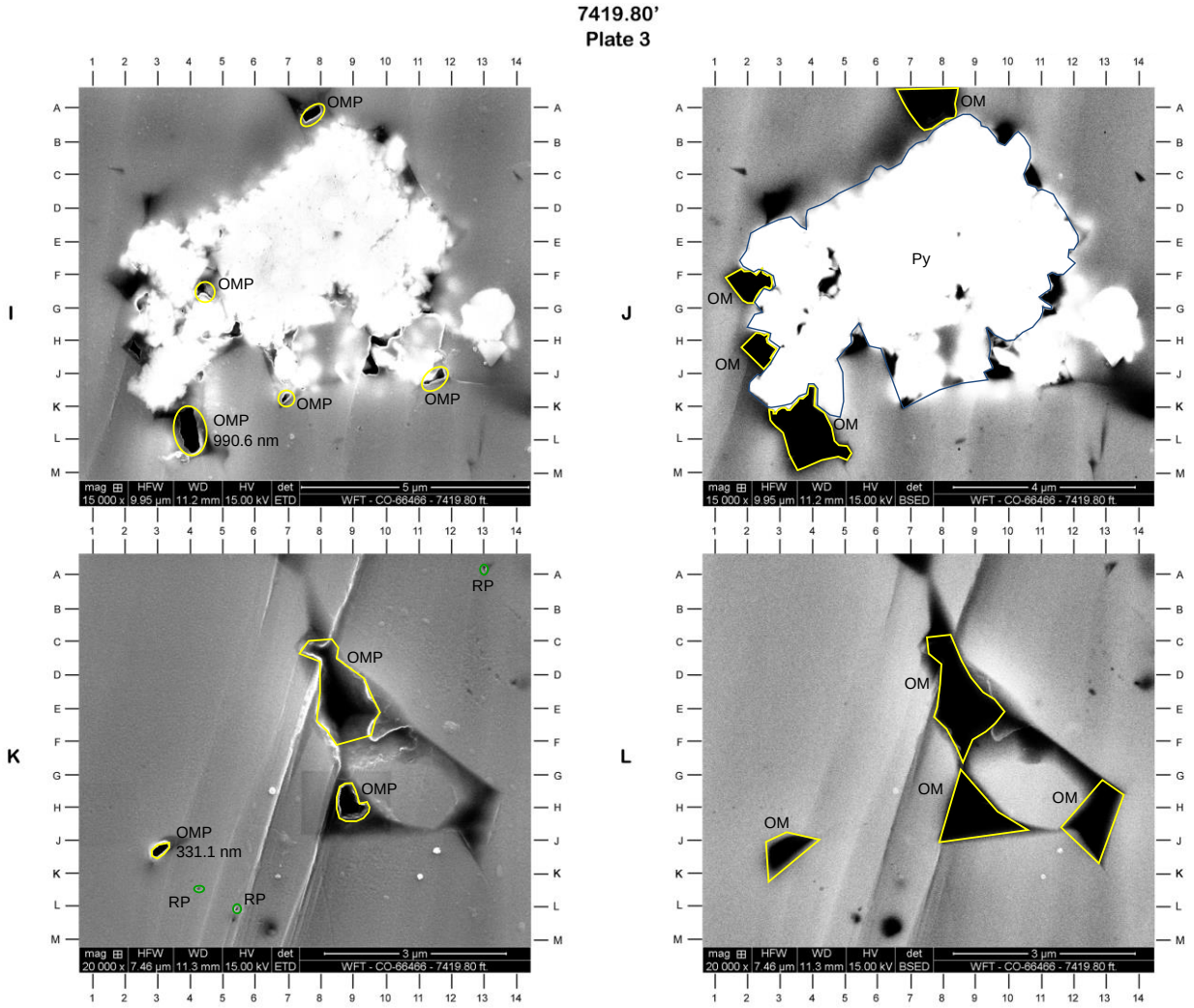

EP	Intercrystalline Pore	OM/OMP	Organic Matter / Organic Matter Pore
RP	Intracrystalline Pore		Minerals

PLATE 4 (7408.45 – 7408.65 FEET)

Low magnification photomicrographs (Photographs A and B) provide an overview of the fabric of the argon-ion milled (AIM) surface. This sample consists of a silty/sandy limestone (based on the core description). Quartz grains (CD6, DE7.7, HJ2, JK4.5) are the primary detrital grain identified by EDS. Pyrite is identified by the white color (CD9, DE3.9, LM4.9, FG14.9). A possible incipient microstylolite extends from FG1.7 to FG14.

Photographs C and D represent a high magnification view of Photographs A and B at F8. Pyrite framboids are easily identified by the framboidal crystal growth and white color (CD7.2, CD13, FG7.7, FG8). Detrital grains identified in these photographs include quartz (A7, B14, DE9-13, H2, FG5, J9, K4) and mica (EF1-3, DE4-5, GH14-JK10). A titanium bearing mineral occurs at A11 to A12. Illite and chlorite are associated with a possible incipient microstylolite extending from DE1 to FG13. Authigenic kaolinite (F3.4, F7.8) is not common. The fine crystalline nature of the calcite is visible in these photographs (AC1-3, BD9-11, KM7-13). Most of the black color in these photographs is likely organic material (A3.8, GH3.8, CD12.7, HJ11.8, M9.3).

The presence of pores can be evaluated by using the SE image (Photograph C) to identify the white “edge effect” that commonly occurs around sharp edges of pore boundaries. Both pores and organic material appear black in BSE images; however, organics lack the white “edge effect” associated with pores in the SE images. Pores are sparse in this field of view and include intraparticle micro to nanopores within detrital grains (BC7.7, GH10, H9, HJ9.8, KL5.2), microfracture porosity (sampling induced?; M11.7-K13), intercrystalline micro to nanopores (LM6.8), and possible nanopores within organic material (GH4.0, HJ11.7, J11.6, JK11.3).

Magnification: A: 400X B: 400X C: 1500X D: 1500X

7408.45' - 7408.65'
Plate 4

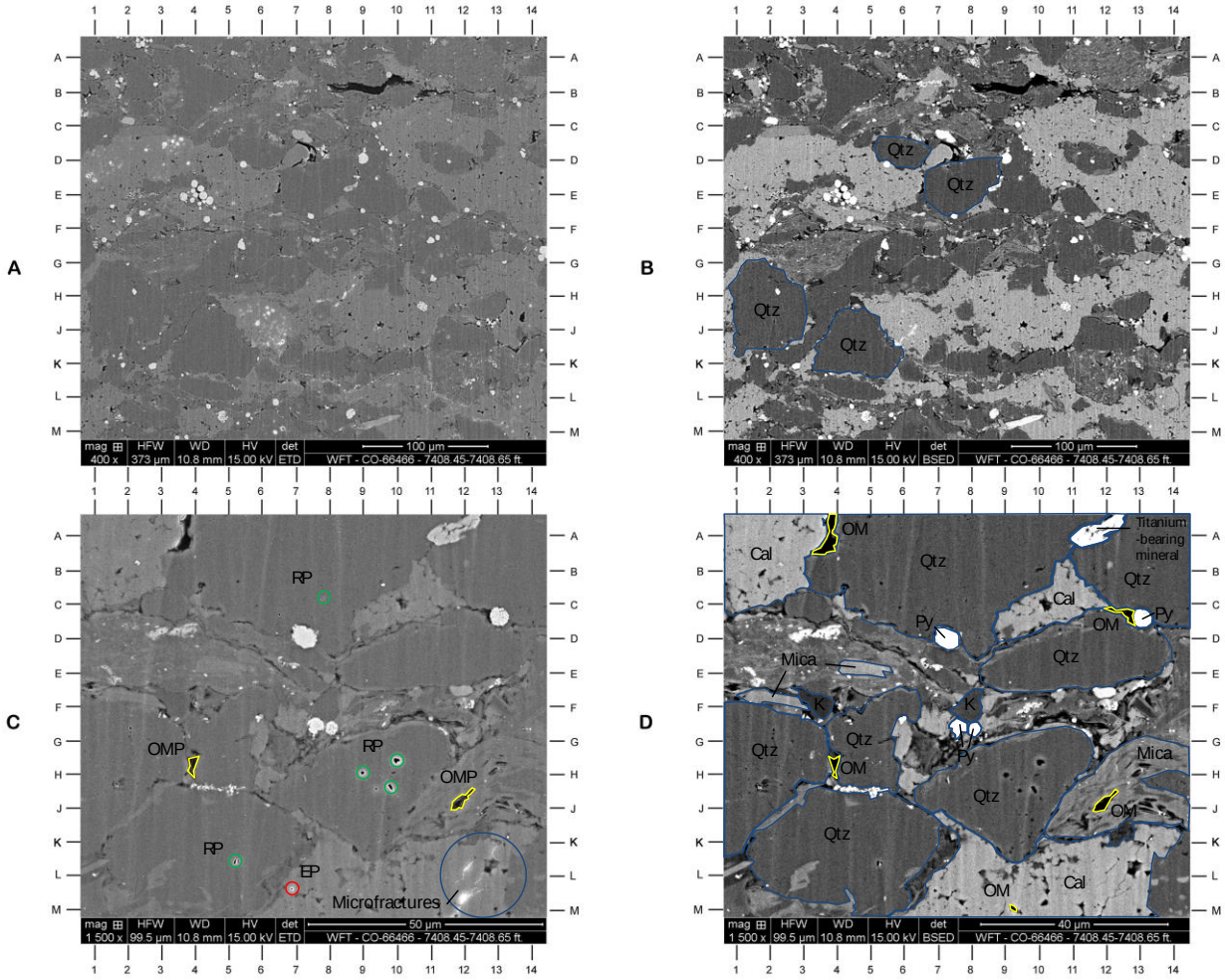

EP	**Intercrystalline Pore**	**OM/OMP**	**Organic Matter / Organic Matter Pore**
RP	**Intracrystalline Pore**		**Minerals**

PLATE 5 (7408.45 – 7408.65 FEET)

Additional features of this limestone are shown in Photographs E-H. Secondary images (SE) are shown in Photographs E and G, and backscattered electron images (BSE) are shown in Photographs F and H. Detrital grains include quartz (Photographs E and F: A1-GH6, HM1-M14, FK7-GK14, DE6-10; Photographs G and H: BC7-8, DF7-8, FG3-5, LM1-7, LM9-11, KM12-14), sodium rich plagioclase feldspar (Photographs G and H: A13-14, BD12-13), and mica (Photographs E and F: A7-D7.5, B11-A14; Photographs G and H: CD6-9, JK11-14, E13). Authigenic kaolinite (Photographs E and F: BD13-14, B9), calcite (Photographs E and F: A10-12; Photographs G and H: AD5-6), dolomite (Photographs G and H: AF1-4), and pyrite (Photographs E and F: C5, KL12-13, CD9.7; Photographs G and H: HK8-10) are also present. Debris caused by sampling is rare (Photographs E and F: BC2.9, C10.2, AB14). Organic material is common between detrital grains in these photographs (Photographs E and F: A9, AB3.5, FG2.3, F14). Organic material intermixed with illite and chlorite in the matrix in Photographs G and H (B9, F5.5, F11, H6.5). The darkest portions of Photograph G likely represent the organic material mixed with little to no clays within the matrix (KL1.5, F9, KL2, GH12).

Even though organic material and pores both appear black in BSE images, pores present within the organic material can generally be identified in the SE images based on the white “edge effect.” Micro to nanopores are predominantly associated with organic material and/or the matrix (Photograph E: GH3.5, GH4.2, EF8.6; Photograph G: EF13.7, GH4.7, EF12.9). Many of these micro to nanopores occur at the contact between a grain and organics (Photograph E: E1-FG1.6, G1.7, E12-13; Photograph G: FG1-2, DE5, GH8.2). It is difficult to determine whether the nanopores at GH13.6 in Photograph E occur within organic material that occluded a pore within a quartz grain or if that space represents a grain boundary between two quartz grains. Pore diameters were measured at 1.142 microns (Photograph E: GH3.3) and 628.0 nanometers (Photograph G: H1.2).

Magnification: E: 6000X F: 6000X G: 8000X H: 8000X

7408.45' - 7408.65'
Plate 5

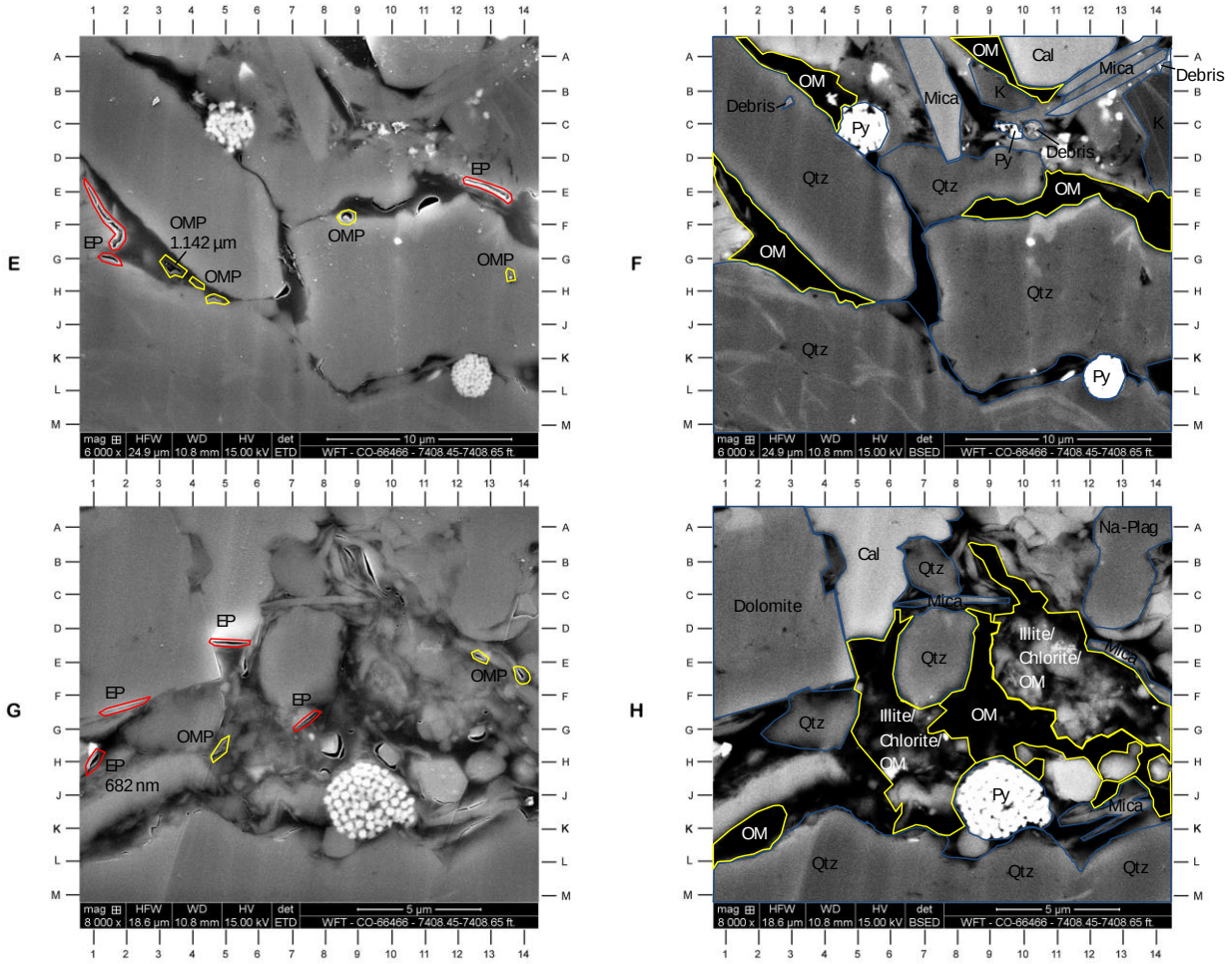

EP	**Intercrystalline Pore**	**OM/OMP**	**Organic Matter / Organic Matter Pore**
RP	**Intracrystalline Pore**		**Minerals**

PLATE 6 (7408.45 – 7408.65 FEET)

Detrital grains in these photographs include mica (Photographs I and J: A5-AB14, DE10-14, FG8-E12; Photographs K and L: HJ1-M4) and quartz (Photographs I and J: F2-3, C13-14, FH12-14, KM9-11; Photographs K and L: LM7-9). Authigenic minerals include pyrite (Photographs I and J: BE1-3, JM4-9, L12-13, CD7-9; Photographs K and L: AB10.4, K14) and kaolinite (Photographs I and J: LM1-3; Photographs K and L: AB1-A10, AD12-13, DH4-FH13). Microcrystalline crystal growths (Photographs K and L: GH4.9, GH5.1, H11.8) occur after the sample has been milled. According to EDS, illite and chlorite (Photographs I and J: BC4-6, G2-3, KL3-4; Photographs K and L: CD3-4, EG1-JK7, KL10-14) are the dominant clays within the matrix. The darker portions of the matrix likely represent organic material with little to no intermixed clays (Photographs I and J: AB2, B11.2, GH6-7, KL1; Photographs K and L: B9-E14). Nanopores are more commonly associated with organic material (Photograph I: A1.5, EF5, FG5, GH5.7, HJ3; Photograph K: LM10.8, M11.8, D1.7, CD2.8). Several nanopores are associated with grain boundaries (Photograph I: BC12, AB6.5-7.5, C7.4; Photograph K: BC1, EF2.6-H4, J7-8). A rare possible intercrystalline nanopore is present at LM5.9 in Photograph K. Pore diameters were measured at 639.1 nanometers (Photograph I: FG4.2) and 148.2 nanometers (Photograph K: CD2.6).

Magnification: I: 10000X J: 10000X K: 12000X L: 12000X

7408.45' - 7408.65'
Plate 6

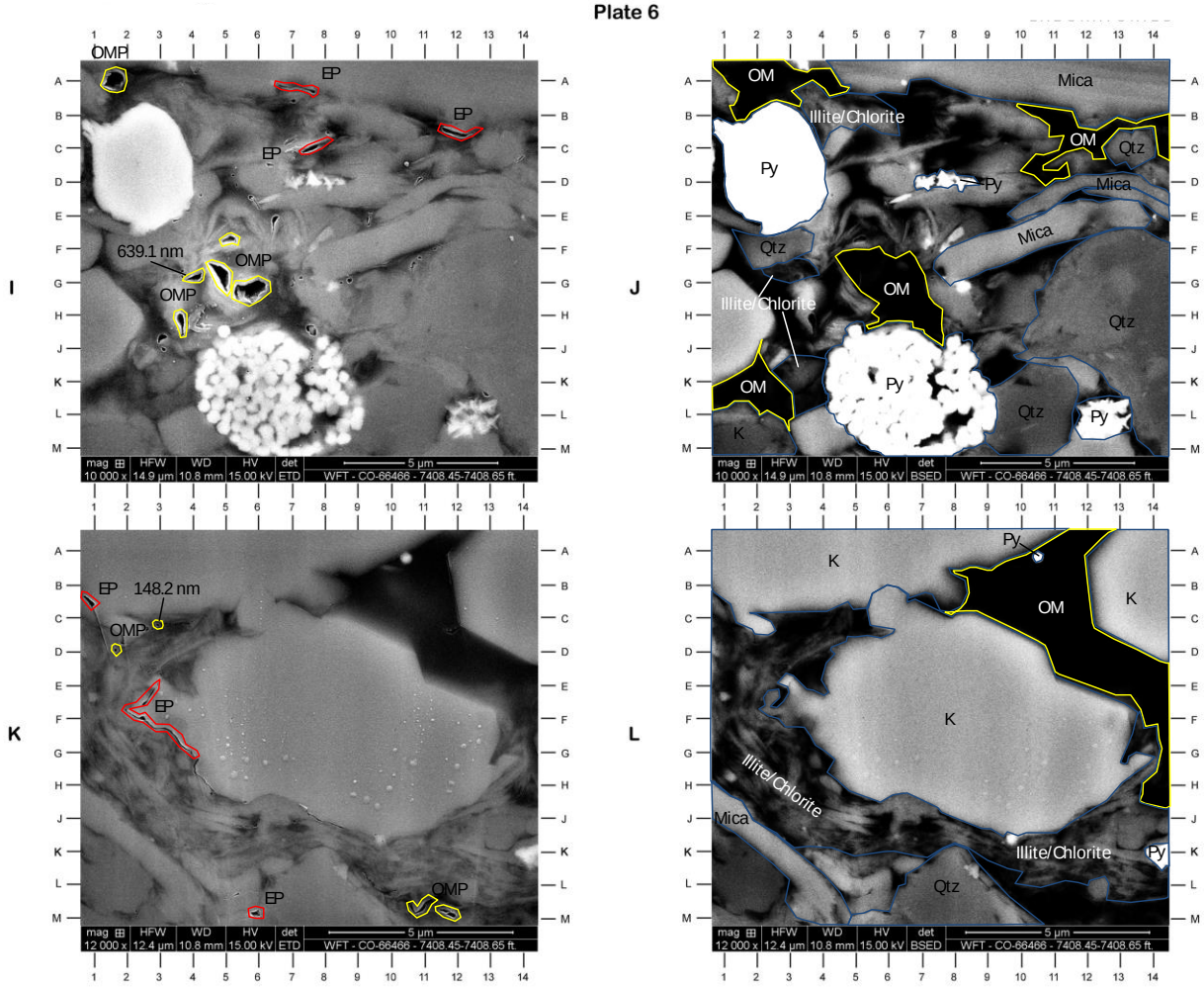

EP	**Intercrystalline Pore**	**OM/OMP**	**Organic Matter / Organic Matter Pore**
RP	**Intracrystalline Pore**		**Minerals**

PLATE 7 (7441.30 – 7441.60 FEET)

Low magnification photomicrographs (Photographs A and B) provide an overview of the fabric of the argon-ion milled (AIM) surface. This sample consists of a silty limestone (based on the core description). Quartz grains (DE7, GH9, FG6.5. AB13) are the primary detrital grain identified by EDS. Pyrite is identified by the white color (FG2.8, KL2.9, JK8.4, L5.8). Organic material is somewhat common (K1.2-4, M1-3.5, J12-JK13.6).

Photographs C and D represent a high magnification view of Photographs A and B at F7. Detrital grains include quartz (AB5-8, HM12-14, KL1, KM2-3, LM3-7), sodium rich plagioclase feldspar (FG3-6, GH2-3), and mica (GH5-8, KL3.4-JK6.4). Micrite has likely been replaced to very fine sparry calcite (AB9-12, C1-2, C6-8, LM9-12) as the primary authigenic mineral in this sample. Authigenic kaolinite is also present (HJ5). Kaolinite has been identified at DE1.5 to DE7.7 by EDS; it is possible that this is a dissolved feldspar that is being altered to kaolinite. Pyrite (G3.2, GH4.6, BC12.2, D11) partially replaces organic material (CD2, D10, EF12.5, L8.3-M9). A dolomite rhomb (GH9-10) shows a variable shade of gray due to the higher amount of iron in the outer rim. The matrix (FG1-2, FG12-14, EF10) contains intermixed illite and chlorite as well as organic material. Debris occurs as a result of sampling (LM2.4, M4.4, LM5.5).

The presence of pores can be evaluated by using the SE image (Photograph C) to identify the white “edge effect” that commonly occurs around sharp edges of pore boundaries. Both pores and organic material appear black in BSE images; however, organics lack the white “edge effect” associated with pores in the SE images. The micro to nanopores in these photographs appear to be associated with organic material (E12.6, EF11.8, FG9.4, GH9.2, KL8.3-M8.8). Intracrystalline micro to nanopores are not common (A10.7, HJ10.7).

Magnification: A: 400X B: 400X C: 1500X D: 1500X

7441.30' - 7441.60'
Plate 7

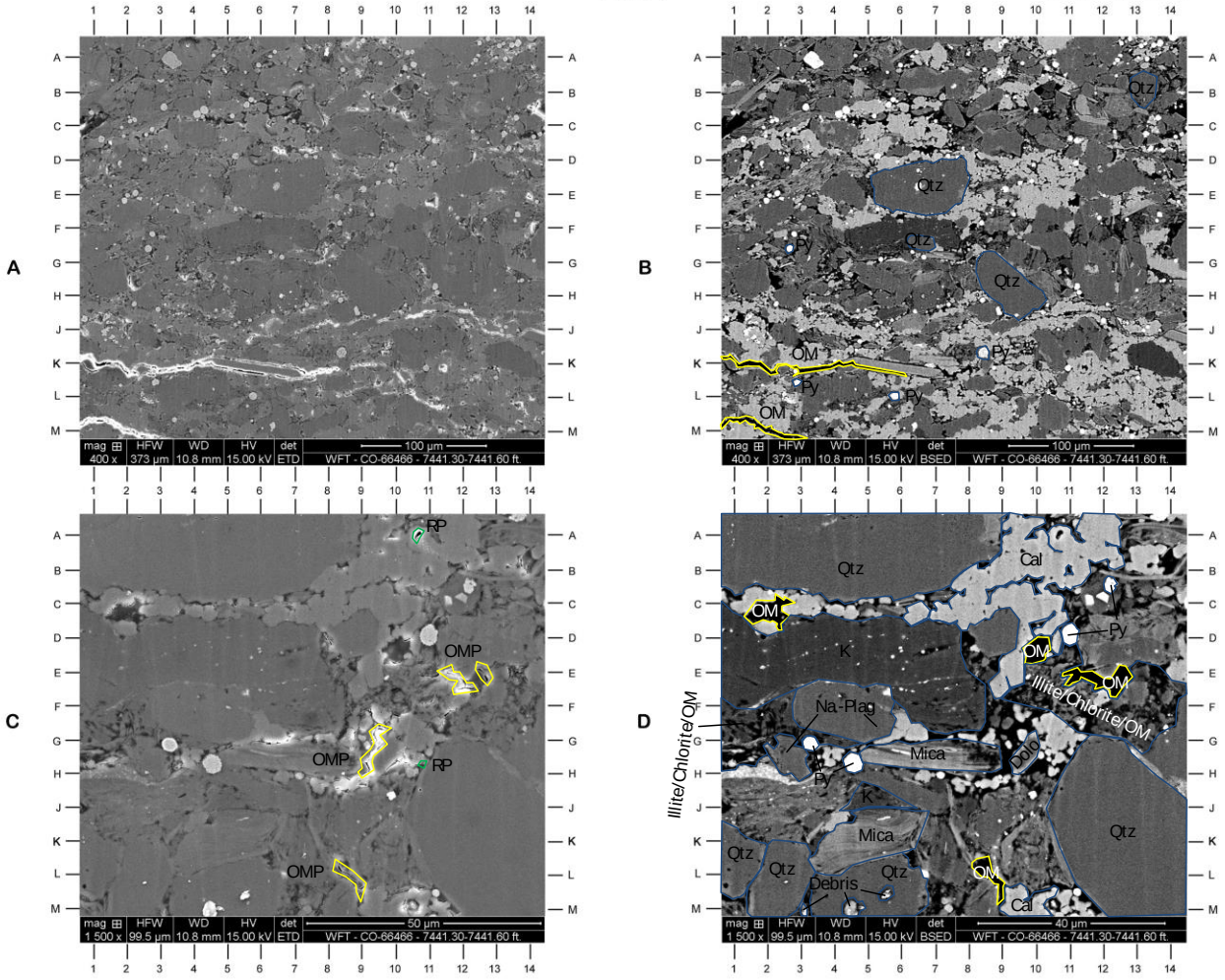

EP	**Intercrystalline Pore**	**OM/OMP**	**Organic Matter / Organic Matter Pore**
RP	**Intracrystalline Pore**		**Minerals**

PLATE 8 (7441.30 – 7441.60 FEET)

Additional features of this limestone are shown in Photographs E-H. Secondary images (SE) are shown in Photographs E and G, and backscattered electron images (BSE) are shown in Photographs F and H. Quartz is the primary detrital grain in this sample (Photographs E and F: EG10-12, KL5-8, JM1-LM5; Photographs G and H: BE1-2, EG1-2) with less common mica (Photographs E and F: F3-AB10, G14-K6). Very fine sparry calcite is common (Photographs E and F: AD1-AB14, FG5-7, GH3-4, JK4-5; Photographs G and H: GH7.7, D5-6, C13, FM13-14, HM1-M7, KM9-11). Pyrite (Photographs E and F: CD13-14, DE12-13, FG8-9, FG13.5; Photographs G and H: DE14, BC6-7, GH2-4, HK8-9, KL7) partially replaces organic material. Organic material (Photographs E and F: E2.8, AB12, CD10.2, GH10-11, KL4.8; Photographs G and H: AB1-BC3-BC9, EF2-3, LM12) is intermixed with illite and chlorite clay (Photographs E and F: EF2.7, J3-5, G9-10; Photographs G and H: A4-7, AB9-A13, G2.2) within the matrix. Authigenic kaolinite is rare (Photographs E and F: GH8). Undifferentiated surface debris (Photograph E: CD6.7, CD7.3, JK12.2; Photograph G: EF5.8) occur as a result of the sampling process.

Even though organic material and pores both appear black in BSE images, pores present within the organic material can generally be identified in the SE images based on the white “edge effect.” Micro to nanopores are predominantly associated with organic material and/or the matrix (Photograph E: B10.8, CD10, DE11.3, G5-H6, GH8-11; Photograph G: AB1-B2.7, AB3, BC3.4, BC4-6, AB7, A13.5-B10, GH2.3, JK10.3). Rare intra/intercrystalline micro to nanopores are present (Photograph E: B13.7). Pore diameters were measured at 1.152 microns (Photograph E: B10.8) and 921.7 nanometers (Photograph G: FG10.8).

Magnification: E: 6000X F: 6000X G: 8000X H: 8000X

7441.30' - 7441.60'
Plate 8

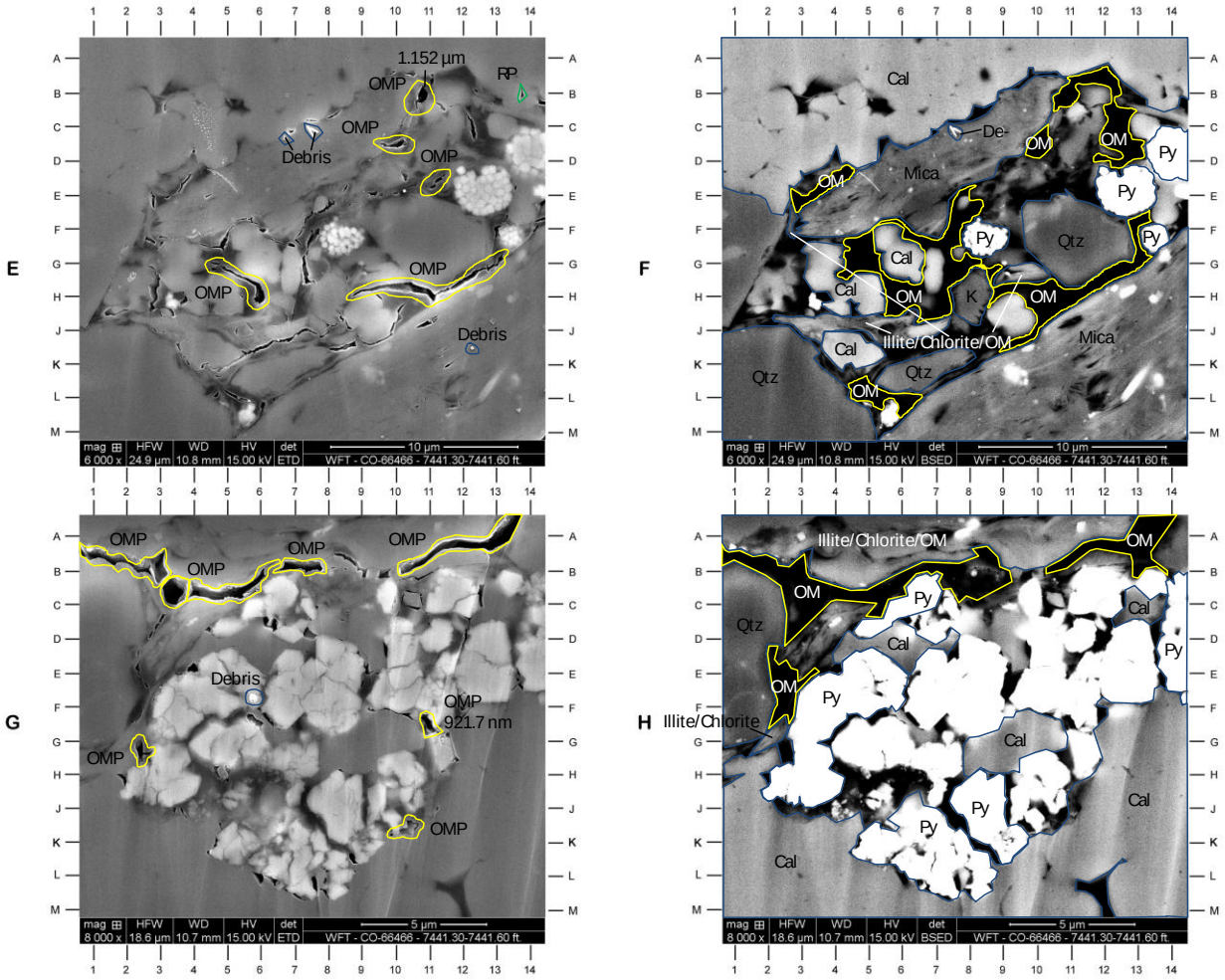

EP	**Intercrystalline Pore**	**OM/OMP**	**Organic Matter / Organic Matter Pore**
RP	**Intracrystalline Pore**		**Minerals**

PLATE 9 (7441.30 – 7441.60 FEET)

Quartz is the primary detrital grain in this sample (Photographs I and J: B1-M1, KM9-11; Photographs K and L: A4-AC8.5-A12, B13, LM1-3) with less common mica (Photographs K and L: K1-L4, JK3-GH6.3-CD10) and sodium rich plagioclase feldspar (Photographs K and L: HM8-FM14). Very fine sparry calcite is abundant in Photographs I and J (AC4-BC8, BC9-11, CE12-14, M1-JK9, GH8-9) but less common in Photographs K and L (HJ1-3, GH5, DF8-11, DE13-14). Pyrite is also present (Photographs I and J: BC11.7, KL11-12). The matrix contains intermixed organic material (Photographs I and J: A8-9, BC12-13, A3-4, K2-G8, GH11-13, DE6-9; Photographs K and L: A13-14, C11, J1-HJ7) intermixed with illite and chlorite (Photographs I and J: A1-3; Photographs K and L: BG1-2, DE4-6, CD10-11, LM5-7). The micro to nanopores in this sample seem to be almost exclusively associated with organic material (Photograph I: CD5.2, BC12-13, GH11-12, CE11.8, JK8-10, K2-H4.5, JK12.8, KL13.4; Photograph K: H3.7, A14, BC12, CD11.7, DE12.2, EF12). Intra/intercrystalline nanopores are rare (Photograph I: C5.3, BC4.9, CD13.7; Photograph K: D13.8). Pore diameters were measured at 1.233 microns (Photograph I: BC12-13) and 499.6 nanometers (Photograph K: CD11.8).

Magnification: I: 10000X J: 10000X K: 12000X L: 12000X

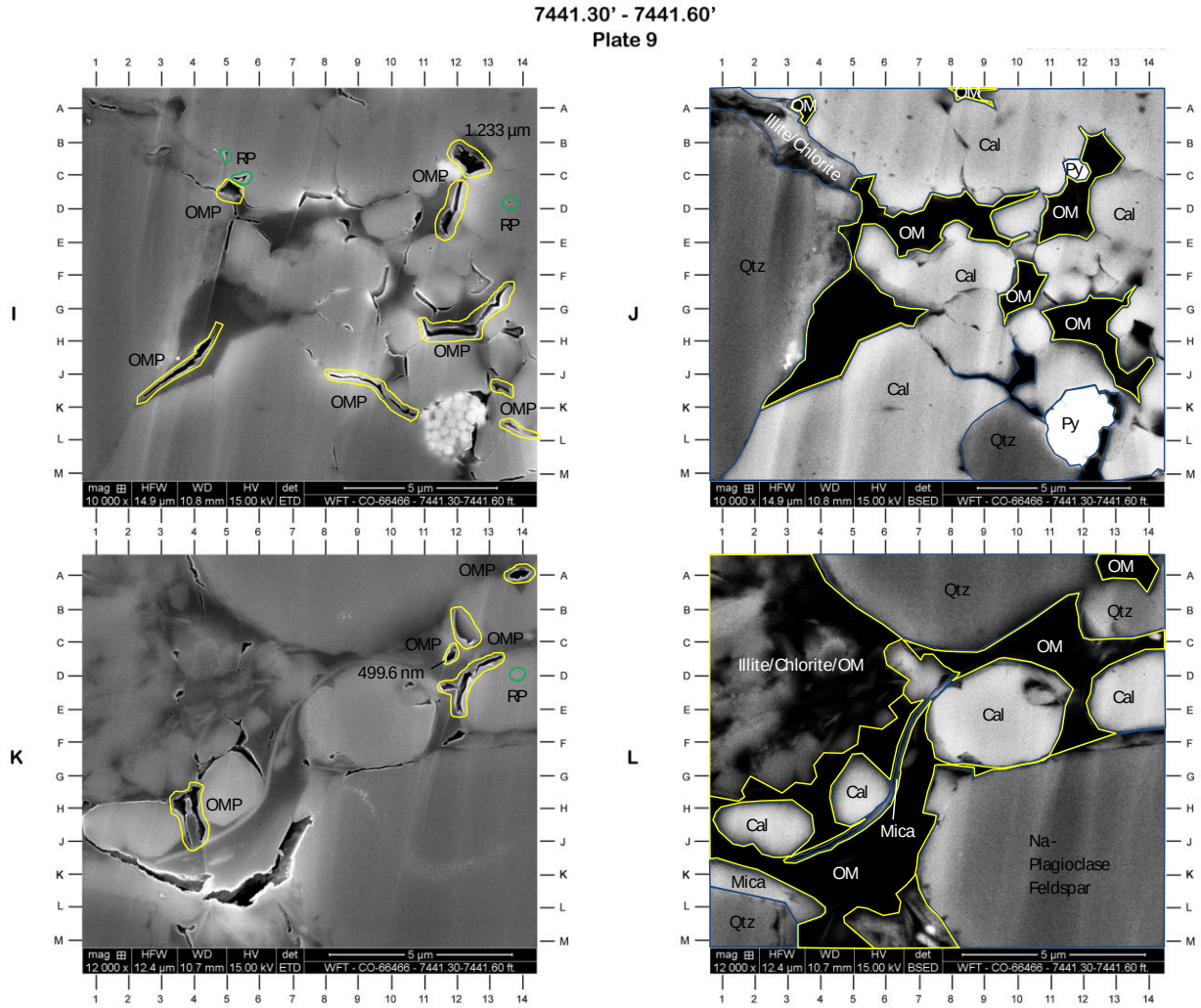

EP	Intercrystalline Pore	OM/OMP	Organic Matter / Organic Matter Pore
RP	Intracrystalline Pore		Minerals

Discussion and Conclusions

Based on the classification of Loucks et al. (2010), mudrock matrix-related pores consist of three basic types: (1) interparticle (interP) pores between grains and crystals, (2) intraparticle (intraP) pores within mineral particles, and (3) organic material (OM) pores within OM. OM pores are created during hydrocarbon maturation (Loucks et al., 2009). Loucks (2012) proposed the terms “nanopores” for pores less than 1 μm (1000 nm) and greater than or equal to 1 nanometer and “micropores” for pores ranging from 1 to less than 62.5 μm. All pore sizes observed in our samples fall into the micro to nanopore range. Most of the micro and nanopores are associated with OM. However, some intra/interparticle micro and nanopores are present.

It is extremely difficult to identify the type of OM (e.g. kerogen, bitumen, solid bitumen, and pyrobitumen) in mudrocks using a SEM. However, it is possible to distinguish original depositional associated (in place) OM (kerogen or its alteration products, solid bitumen and/or pyrobitumen) from migrated OM (solid bitumen or pyrobitumen). This identification is significant because it allows us to differentiate OM pores developed in depositional OM from OM pores developed in migrated OM. Migrated OM that fills the associated three-dimensional mineral pore network would more likely have a better three-dimensional OM pore network than would the isolated depositional OM with pores. Loucks and Reed (2014) proposed the petrographic criteria through the SEM photomicrographs to separate depositional versus migrated organic matter. Based on their criteria, OM pores in our samples appear to be associated with the migrated OM. The evidence for migrated OM found in our samples include (1) cementation formed in interP and intraP pores and crystal faces lining OM, indicating the OM entered the mineral pore after cementation, and (2) no alignment of pores in OM. Aligned elongate OM pores have been observed mainly in depositional OM.

Loucks et al. (2009) recognized that OM-pore development was related to the thermal maturation of OM. Bernard et al. (2012a, 2012b) concluded that only the pyrobitumen in gas-window-maturity samples contained OM pores. However, nanoporosity in OM has been described in the literature as developing in OM from oil-window-maturity samples (Curtis et al., 2012; Reed et al., 2014). The Rock-Eval pyrolysis and biomarker data indicate that the thermal maturity of our samples with OM pores is in the oil window, which supports that OM pores are also present in OM from oil-window-maturity samples. More analysis of OM from different mudrocks at a variety of thermal maturity levels needs to be completed as to conclude which OM produce OM pores.

References

Bernard, B., B. Horsfield, H. Schultz, R. Wirth, A. Schreiber, and N. Sherwood, 2012a, Geochemical evolution of organic-rich shales with increasing maturity: A STXM and TEM study of the Posidonia Shale (Lower Toarcian, northern Germany):

Marine and Petroleum Geology, v. 31, p. 70–89, doi:10.1016/j.marpetgeo.2011.05.010.

Bernard, B., R. Wirth, A. Schreiber, H. Schultz, and B. Horsfield, 2012b, Formation of nanoporous pyrobitumen residues during maturation of the Barnett Shale (Fort Worth Basin): International Journal of Coal Geology, v. 103, p. 3–11, doi:10.1016/j.coal.2012.04.010.

Curtis, M. E., B.J. Cardott, C.H. Sondergeld, and C.S. Rai, 2012, Development of organic porosity in the Woodford Shale with increasing thermal maturity: International Journal of Coal Geology, v. 103, p. 26–31.

Loucks, R.G., R.M. Reed, S.C. Ruppel, and D.M. Jarvie, 2009, Morphology, genesis, and distribution of nanometer-scale pores in siliceous mudstones of the Mississippian Barnett Shale: Journal of Sedimentary Research, v. 79, p. 848–861.

Loucks, R.G., R.M. Reed, S.C. Ruppel, and U. Hammes, 2010, Preliminary classification of matrix pores in mudrocks: Gulf Coast Association of Geological Societies Transactions, v. 60, p. 435–441.

Loucks, R.G., R.M. Reed, S.C. Ruppel, and U. Hammes, 2012, Spectrum of pore types and networks in mudrocks and a descriptive classification for matrix-related mudrock pores: American Association of Petroleum Geologists Bulletin, v. 96, p. 1071–1098.

Loucks, R.G. and R.M. Reed, 2014, Scanning-electron-microscope petrographic evidence for distinguishing organic-matter pores associated with depositional organic matter versus migrated organic matter in mudrocks: Gulf Coast Association of Geological Societies Journal, v. 3, p. 51-60.

Reed, R.M., R.G. Loucks, and S.C. Ruppel, 2014, Comment on “Formation of nanoporous pyrobitumen residues during maturation of the Barnett Shale (Fort Worth Basin)”: International Journal of Coal Geology, v. 127, p. 114–115, doi:10.1016/j.coal.2013.11.012.

Rock Mechanics Testing

Introduction

Brittleness and ductileness are used to describe the deformation behaviors when rocks are suffering certain stresses. A rock is considered to be ductile if it absorbs high amounts of energy before fracturing. Brittle rocks are unable to accommodate significant strain before fracturing, resulting in open microfractures after hydraulic fracturing. Therefore, brittle rocks are more likely to be naturally fractured and will usually respond well to hydraulic fracturing treatments. Brittleness is the direct measurement of a formation's ability to create an effective network that can conduct hydrocarbons to each borehole. Usually brittleness is estimated from 1) laboratory triaxial compressive tests with acoustic velocities; 2) mineral contents; and 3) elastic parameters derived from seismic inversion. We concentrate on the first two methods in this section.

Triaxial Compressive Test

The triaxial compressive test is a laboratory test method that is used to assess the mechanical properties of rocks and fine-grained soils. It provides a measure of the confined compressive strength as well as stress-strain characteristics of rock, soil or other material. Triaxial compressive tests with acoustic velocities have been conducted for interpreting the rock mechanics characteristics on three (3) samples at depths of 7379.90, 7418.05, and 7441.90 ft.

The general procedures for triaxial compressive test with acoustic velocities are summarized in the following: 1) a right cylindrical plug is cut from the sample core and its ends ground parallel each other within 0.001 inch. Physical dimensions and weight of the specimen are recorded; 2) the specimen is placed between two platens and a heat-shrink jacket is placed over the specimen; 3) axial strain and radial strain devices are mounted in the platens and on the lateral surface of the specimen, respectively. 4) the specimen assembly is placed into the pressure vessel and the pressure vessel is filled with hydraulic oil; 5) confining pressure is increased to the desired hydrostatic testing pressure; 6) measure ultrasonic velocities at the hydrostatic confining pressure; 7) specimen assembly is brought into the contact with a loading piston that allows application of axial load; 8) increase axial load at a constant displacement rate until the specimen fails or axial strain reaches a desired amount of strain while confining pressure is held constant; 9) reduce axial stress to the initial hydrostatic condition after sample fails or reaches a desired axial strain; and 10) reduce confining pressure to zero and disassemble sample.

Static moduli (Young's modulus and Poisson's ratio) are directly measured in a deformational experiment. Dynamic moduli (Young's modulus, Poisson's ratio, bulk modulus, and shear modulus) are calculated from the acoustic travel time and measured bulk density. Dynamic Young's moduli are generally higher than their static counterparts, which can be observed in all samples (Tables 2 and 3).

Sample No. 1-5RMV at 7379.90 ft contains several cracks of various angles and hence shows lower compressive strength compared to that of sample No. 1-44RMV at 7418.05 ft, although sample No. 1-5RMV has a higher Young's modulus and ultrasonic wave velocity. The stress-strain curve of sample No. 1-5RMV also suggests that this sample probably failed earlier along the pre-existing cracks within the sample (Figure 6).

Rickman et al. (2008) proposed an average brittleness equation based on the elastic parameters of Poisson's ratio and Young's modulus. These two components are combined to reflect the rock's ability to fail under stress (Poisson's ratio) and maintain a fracture (Young's modulus) once the rock fractures. Their equations to calculate brittleness, which are shown below, assume that more brittle rocks show a relatively high Young's modulus and a low Poisson's ratio while more ductile rocks exhibit a low Young's modulus and a high Poisson's ratio.

YM_BRIT = ((YMS_C – 1) / (8-1)) x 100 (1)
PR_BRIT = ((PR_C – 0.4) / (0.15-0.4)) x 100 (2)
BRIT = (YM_BRIT + PR_BRIT) / 2 (3)

Where,
YM_BRIT = Young's modulus based brittleness (%)
PR_BRIT = Poisson ratio based brittleness (%)
BRIT = average brittleness (%)
YMS_C = composite determination of Young's modulus
PR_C = composite determination of Poisson's ratio

For the three samples in the Sessions #1 well, static Young's moduli are as high as 9.43 x 10^6 psi, and static Poisson's ratio values are low, varying narrowly from 0.26 to 0.33 (Table 2). The average brittleness is very high with a range from 63.51 to 88.65 using equations (1-3) (Figure 7). This indicates that our samples are brittle from a geomechanical perspective.

Britt and Schoeffler (2009) stated that prospective shales have a dynamic-to-static Young's modulus correlation consistent with the clastic rocks. The ratio of dynamic to static Young's modulus is greater for ductile, laminated shale and less for brittle, massive shale/mudstone. They also noted that prospective shales typically have a Young's modulus in excess of 3.5 x 10^6 psi and non-prospective shales normally

contain a Young's modulus less than 3.5 x 10^6 psi. Our samples appear to fit the dynamic-to-static clastic correlation of Young's modulus, which further supports the high brittleness of the lime mudstones in the Sessions #1 well (Figure 8).

XRD Analysis

To adequately characterize the bulk and clay mineralogy, X-ray diffraction (XRD) was performed on samples from the Sessions #1 core at the same depths as the triaxial compressive test (Table 4). The minerals are grouped into three categories: quartz, carbonates, and clays. The quartz group includes quartz, feldspars, and pyrite. The carbonate group consists of calcite, dolomite, and siderite. The clay group includes the total clay. A ternary diagram is used to display the mineral contents of each sample for this study (Figure 9).

Samples at both depths of 7,379.90 and 7,418.05 ft contain similar compositions. They exhibit very high calcite content at 97%. The remaining portion consists of 2% quartz and 1% clays (primarily illite/mica). The sample from 7,441.90 ft showed a much more diverse composition with 31% calcite, 26% quartz, 18% dolomite, and 13% illite/mica. Other constituents include plagioclase, pyrite, mixed-layer illite/smectite, and kaolinite.

Jarvie et al. (2007) proposed a brittleness equation based on the amount of quartz, calcite, and clay minerals. Wang and Gale (2009) improved Jarvie et al.'s equation by considering dolomite as one of the brittle minerals and TOC as one of the ductile minerals. Note that both of the aforementioned equations were built on shale-gas systems. When applying these equations to assess the brittleness of Brown Dense limestone, all samples for the study would be regarded as ductile. However, rock mechanics tests performed on the same samples definitively classify this limestone as brittle. Therefore, the equations formulated for the shales may not yield positive results in the limestone system. A new equation structured around the mineralogy of a limestone system is needed to carry out quantitative brittle versus ductile determinations.

Conclusions

All three samples are very dense and massive as indicated by high bulk density. High static and dynamic Young's moduli and high ultrasonic velocities suggest that all samples are brittle. The brittleness calculating equations derived from the shale-gas studies are not likely to be applied to a limestone such as Brown Dense.

References

Jarvie, D.M., R.J. Hill, T.E. Ruble, and R.M. Pollastro, 2007, Unconventional shale-gas systems: The Mississippian Barnett Shale of north-central Texas as one model for thermogenic shale-gas assessment: AAPG Bulletin, 91, no. 4, 475–499.

Wang, F.P. and J.F.W. Gale, 2009, Screening criteria for shale-gas systems: Gulf Coast Association of Geological Societies Transactions, no. 59, 779–793.

Figure 6. Stress-strain curves of the Brown Dense, Sessions #1 well.

(A) Sample No. 1-5RMV at the depth of 7,379.90 ft.

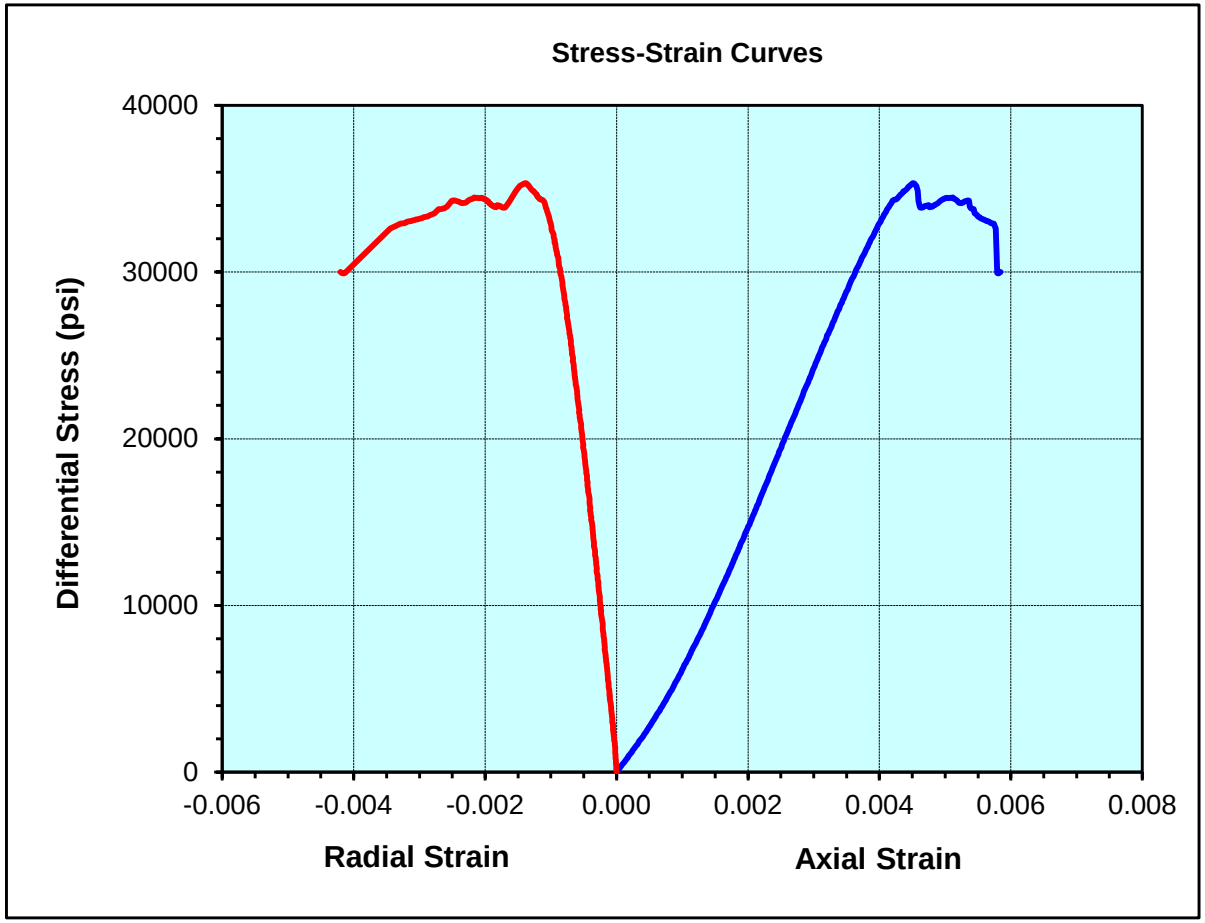

(B) Sample No. 1-44RMV at the depth of 7,418.05 ft.

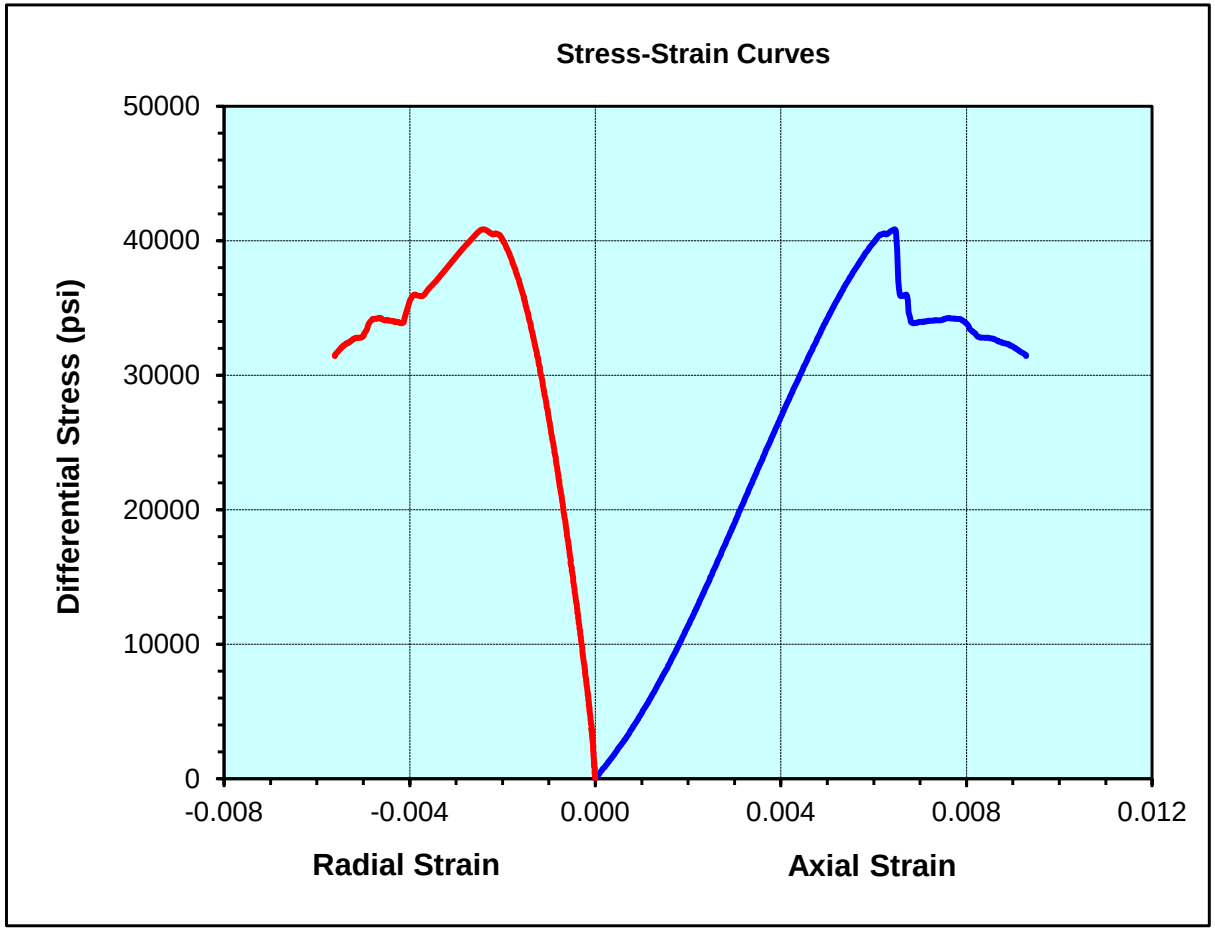

(C) Sample No. 2-7RMV at the depth of 7,441.90 ft.

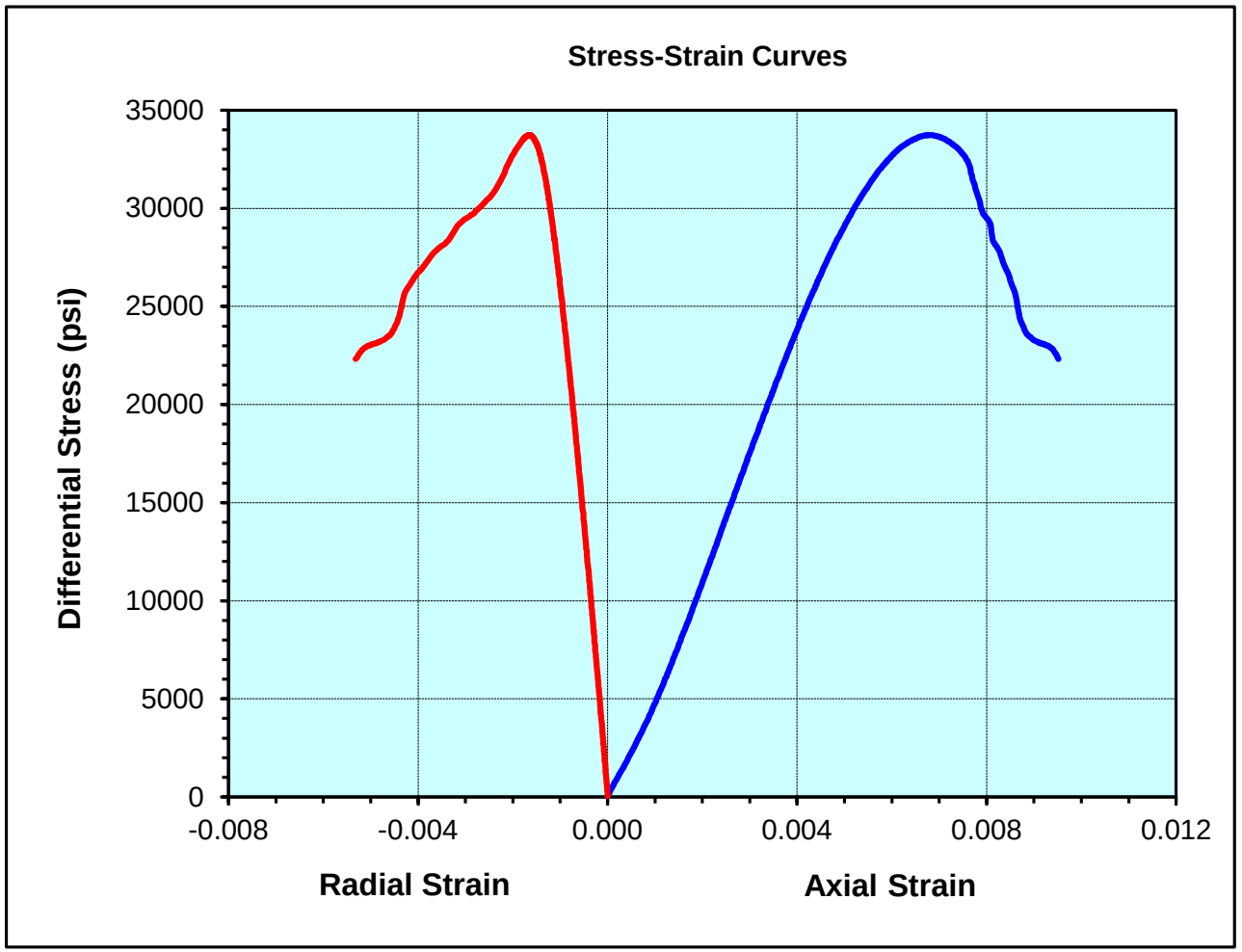

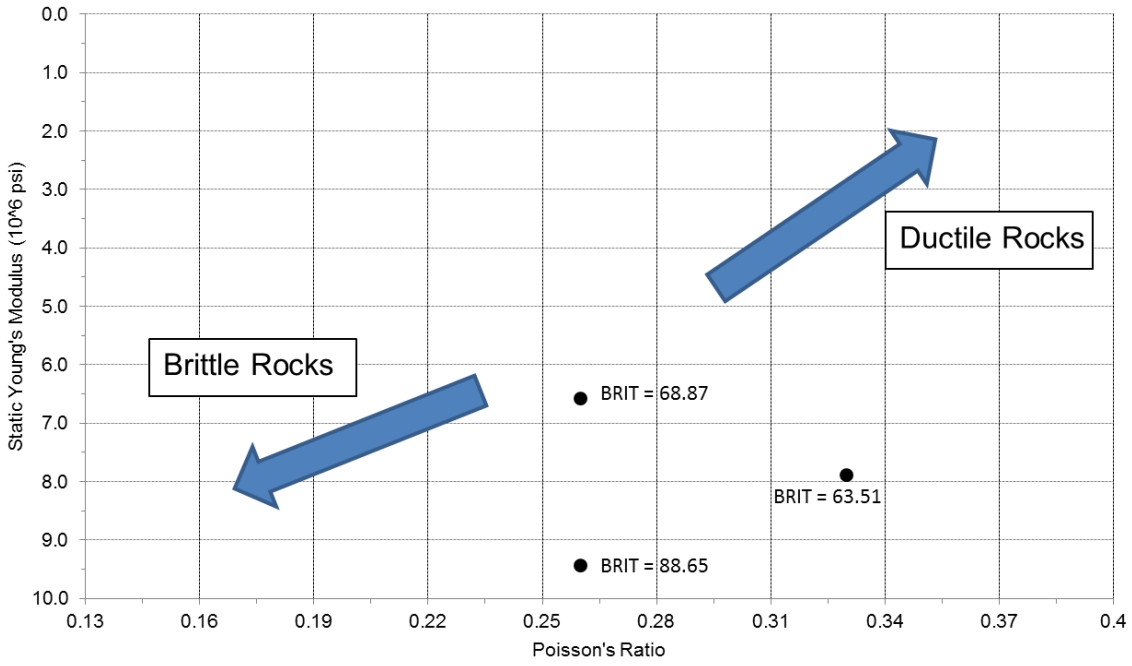

Figure 7. A cross plot of Young's modulus and Poisson's ratio of the Brown Dense, showing the brittleness percentage increasing to the lower left corner of the plot.

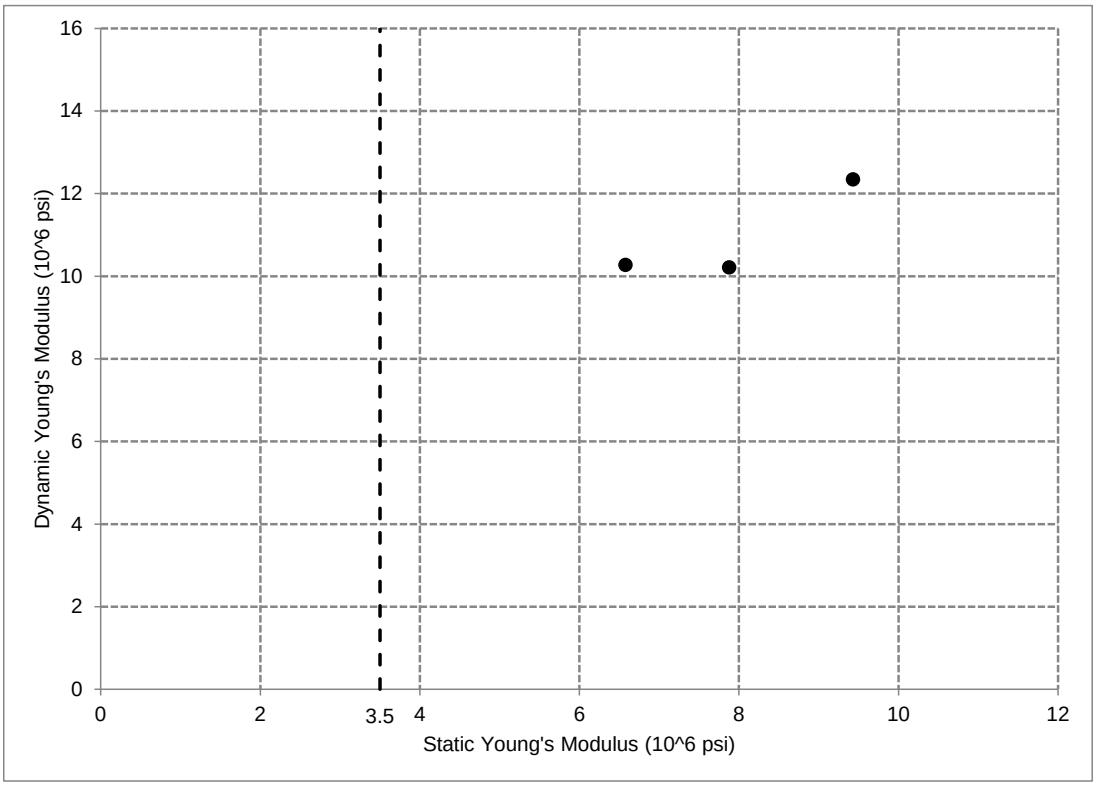

Figure 8. Dynamic to static Young's modulus correlation for the Brown Dense, Sessions #1 well.

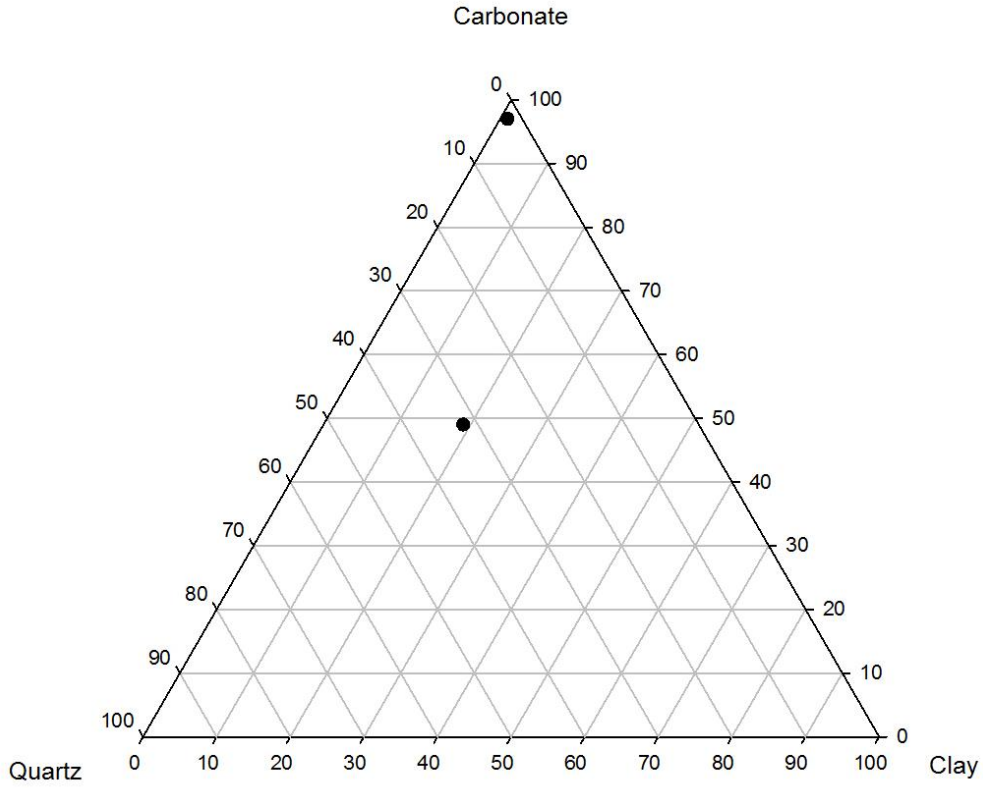

Figure 9. Ternary diagram of the mineralogy of the Brown Dense from XRD data, Sessions #1 well.

Table 2. Triaxial compressive test data and brittleness index of the Brown Dense, Sessions #1 well.

Sample No.	Depth (ft)	Confining Pressure (psi)	Compressive Strength (psi)	Static Young's Modulus ($x10^6$ psi)	Static Poisson's Ratio	YM_BRIT	PR_BRIT	BRIT
1-5RMV	7379.90	2360	37694	9.43	0.26	120.50	56.8	88.65
1-44RMV	7418.05	2360	43214	7.88	0.33	98.23	28.8	63.51
2-7RMV	7441.90	2360	36097	6.58	0.26	79.74	58	68.87

Table 3. Ultrasonic velocities and dynamic elastic parameters of the Brown Dense, Sessions #1 well.

Sample No.	Depth (ft)	Confining Pressure (psi)	Bulk Density (g/cc)	Ultrasonic Wave Velocity				Dynamic Elastic Parameter			
				Compressional		Shear		Young's Modulus ($x10^6$ psi)	Poisson's Ratio	Bulk Modulus ($x10^6$ psi)	Shear Modulus ($x10^6$ psi)
				ft/sec	µsec/ft	ft/sec	µsec/ft				
1-5RMV	7379.90	2360	2.70	21132	47.32	11452	87.32	12.34	0.29	9.90	4.78
1-44RMV	7418.05	2360	2.73	19258	51.93	10343	96.69	10.21	0.30	8.39	3.93
2-7RMV	7441.90	2360	2.66	18848	53.06	10629	94.08	10.27	0.27	7.34	4.05

Table 4. X-ray diffraction (wt. %) data of the Brown Dense, Sessions #1 well.

Sample	Sample	CLAYS				CARBONATES			OTHER MINERALS					TOTALS		
Number	Depth (ft)	Chlorite	Kaolinite	Illite/Mica	Mx I/S*	Calcite	Dolomite[1]	Siderite	Quartz	K-spar	Plag.	Pyrite	Barite	Clays	Carb.	Other
1-5RMV	7379.90	Tr	Tr	1	Tr	97	Tr	Tr	2	Tr	Tr	Tr	0	1	97	2
1-44RMV	7418.05	Tr	Tr	1	Tr	97	Tr	Tr	2	Tr	Tr	Tr	0	1	97	2
2-7RMV	7441.90	Tr	2	13	4	31	18	Tr	26	Tr	3	3	0	19	49	32
	Average	Tr	1	5	1	75	6	Tr	10	Tr	1	1	0	7	81	12

* Ordered interstratified mixed-layer illite/smectite; Approximately 10-20% expandable interlayers.

[1] Dolomite species interpretation based on the d-spacing of the highest intensity peak of dolomite group minerals; other dolomite species may be present.

Shale Rock Properties Analysis

Introduction

The fundamental properties of shales/mudstones make them virtually impossible to analyze with conventional core analysis methods. This includes permeabilities in the tens to hundreds of nanoDarcys, low effective porosities (typically less than 10 percent), and high kerogen and clay contents. The tightness of the rock and the abundance of clay minerals and kerogen generally create a number of technical challenges to core analysis. To understand reservoir properties in tight shales, it is necessary to find a new way to measure them. Shale Rock Properties (SRP) analysis was developed to evaluate cores from shale reservoirs by using crushed material to enable better access to the pore space and to eliminate the coring- and sampling-induced microfractures that increase porosity and more importantly, significantly increase permeability. In regard to permeability measurement, unconventional reservoirs are usually too tight to allow for steady-state methods. Crushed sample pressure decay systems can measure the nanoDarcy permeabilities typical of shales.

SRP analysis was conducted to measure porosity, matrix permeability, fluid saturation, and bulk/grain densities on three core plugs at depths of 7408.45, 7419.50, and 7441.30 ft, respectively. Core and thin section descriptions show that the cores at 7408.45 ft and 7419.50 ft are wackestone. The other core, at 7441.30 ft, is mudstone. Organic geochemical data indicates that the three samples contain high TOC values up to 5.33%. Organic porosity may be the most relevant porosity for hydrocarbon accumulation and production. The microstructure also suggests a biased distribution of fluids, with hydrocarbons predominantly hosted in the organic porosity and brines in nonorganic pores (Handwerger et al., 2012). These sample depths were also intentionally selected at approximately the same depths for FE-SEM analysis. Therefore, we can better benefit from the results of both analyses and provide a correlation of different unconventional reservoir properties.

Sample Preparation and SRP Analysis Procedure

The exceedingly fine-grained shale/mudstone reservoir cores provide fundamental data sets that include porosity, permeability, grain density, and core saturation. The analysis of this data set requires special sampling, analytical, and measurement techniques.

Samples are wrapped in cellophane and aluminum foil for preservation and placed in the shale chiller until ready to be processed. The sample is allowed to come to room temperature, unwrapped and weighed. The bulk volume (V_b) of the sample is measured using a mercury pump. From the weight and bulk volume determinations, an as-received (AR) bulk density is calculated for each sample. The sample is then quickly

crushed using a mechanical Marcy Cone Ball Mill to yield less than 1/8" sized material (approximately 6 to 7 mesh). The crushed material is then collected, taken into the laboratory, and re-weighed. The crushed sample is separated into two fractions: 85 grams for the permeability measurement and approximately 200 grams for other measurements. The grain volume of each AR crushed sample is measured by helium injection using the Boyle's Law method. The 85 gram fraction of AR state crushed material is subjected to a gas permeability determination using a pressure decay system derived by work pioneered by Luffel et al. (1993). This basic crushed gas permeability method was adapted as standard methodology within the Gas Research Institute (GRI) crushed shale program. Note that AR state permeability determinations are recommended for gas plays, while dry state permeability determinations are recommended for oil plays.

The AR sample is weighed to 0.01 g, placed in a pre-dried and pre-labeled extraction thimble and weighed again. The sample and thimble are then subjected to Dean-Stark extraction with toluene. Water volume in the Dean-Stark receiving tube is monitored during the toluene refluxing until a stable volume is observed over approximately 72 to 120 hours. After Dean-Stark toluene distillation-extraction, each sample is loaded into the Dean-Stark apparatus and extracted with chloroform-methanol azeotrope to complete the removal of any remaining hydrocarbons and any salts. The samples are allowed to extract in refluxing azeotrope until no visible color change is detected in the solvent for approximately 24 hours.

Each sample is then dried in a vacuum oven at 212 °F. Sample weights are monitored daily until weight stabilization (± 0.01 g) is achieved. The dried grain volume of each sample is measured by helium injection using the Boyle's Law method. The sample is separated into two (2) fractions and the dry grain volumes are measured. Dry grain density is calculated using the dry sample weight divided by dry grain volume data (V_g). With an as-received bulk volume (V_b) and the determined dried grain volume (V_g), a total gas filled dried porosity is calculated using the formula: $(V_b-V_g)/V_b$.

As-received fluid volumes are calculated as follows:

> Water = Dean-Stark extracted total water weight corrected to a brine volume using a specified brine density (1.05 g/cc is used for this study) (Note that Dean-Stark water includes free and clay bound water fractions);
>
> Oil = (AR sample weight – dry sample weight) – Dean-Stark based water weight and corrected to a volume using a specified oil density (0.85 g/cc is used in this study);
>
> Gas = Dry pore volume (V_b-V_g) – water volume – oil volume

Fluid volumes are converted to % pore volume saturations by dividing by the total dry pore volume (V_b-V_g).

Data and Preliminary Interpretation

Dry pressure decay permeability shows a linear positive relation with depth, varying from 8.43 x 10^{-5} (84.3 nanoDarcys) to 4.69 x 10^{-4} (469 nanoDarcys) with an average of 2.34 x 10^{-4} (234 nanoDarcys) (Table 5 and Figure 10). Dry helium porosity is 1.9% on average ranging from 1.3 to 2.3% (Table 5). It does not display the same linear positive relation with depth as the permeability (Figure 11). The porosity value at 7419.80 ft deviates from the trend. The lithology of the sample at 7419.80 ft is limestone based on the core description, which is markedly different from the silty/sandy limestone of the other two samples. Based on the FE-SEM analysis, the porosity of the samples is mostly associated with organic material (OM) pores. Some minor porosity occurs as matrix (interparticle/intraparticle) pores. The OM at 7419.80 ft is dominantly filled in polyhedral angular pores between fine crystalline calcite cement, while OM at 7408.45 and 7441.30 ft occurs primarily as narrow, elongate filling between the grain boundaries.

The average as-received bulk and dry bulk densities are 2.67 gm/cc and 2.66 gm/cc, respectively. Dry grain density averages 2.71 gm/cc (Table 5 and Figure 12). As-received fluid saturations indicate average water saturation is 8.3%, oil saturation is 42.9%, and gas saturation is 48.8% (Table 5 and Figure 13). Assuming that all the gas is dissolved in oil in the reservoir conditions (based on the thermal maturity in the oil window for the study area), a single hydrocarbon phase, oil, would be present in the subsurface. With the negligence of the correction for volume change in water and oil, oil saturation in the reservoir conditions would be 91.7%.

References

Handwerger, D.A., R. Suarez-Rivera, K.I. Vaughn, and J.F. Keller, 2012, Methods improve shale core analysis: The American Oil & Gas Reporter, December 2012.

Luffel, D.L., C.W. Hopkins, and P.D. Schettler Jr., 1993, Matrix permeability measurements of gas productive shales, SPE Paper 26633 presented at the SPE Annual Technical Conference and Exhibition, 3-6 October, Houston, TX, USA.

Table 5. SRP crushed core analysis data of the Brown Dense, Sessions #1 well.

Sample ID	Top Depth, feet	Bottom Depth, feet	A-R Bulk Density, gm/cc	A-R Water Saturation, % of PV	A-R Oil Saturation, % of PV	A-R Gas Saturation, % of PV	A-R Gas Saturation, % of BV	Dry Bulk Density, gm/cc	Dry Grain Density, gm/cc	Dry Helium Porosity, % of BV	Dry Press Decay Permeability, md
1-34 SRP	7408.45	7408.65	2.67	10.8	34.2	55.0	1.1	2.67	2.72	2.0	8.43E-05
1-45 SRP	7419.50	7419.80	2.69	5.5	37.5	57.0	0.8	2.68	2.72	1.3	1.50E-04
2-7-1 SRP	7441.30	7441.60	2.65	8.6	57.0	34.4	0.8	2.63	2.69	2.3	4.69E-04
Average values			2.67	8.3	42.9	48.8	0.9	2.66	2.71	1.9	2.34E-04

As-Received and vacuum dried at 212°F
As-received bulk volumes and bulk densities were determined on intact bulk sample material. The bulk material was crushed and all other analysis reported herein were conducted on the crushed material.
The following brine & oil densities were used to calculate H_2O & oil volumes respectively: 1.050g/cc & 0.850g/cc.
Mud/Fluid type: Water based mud

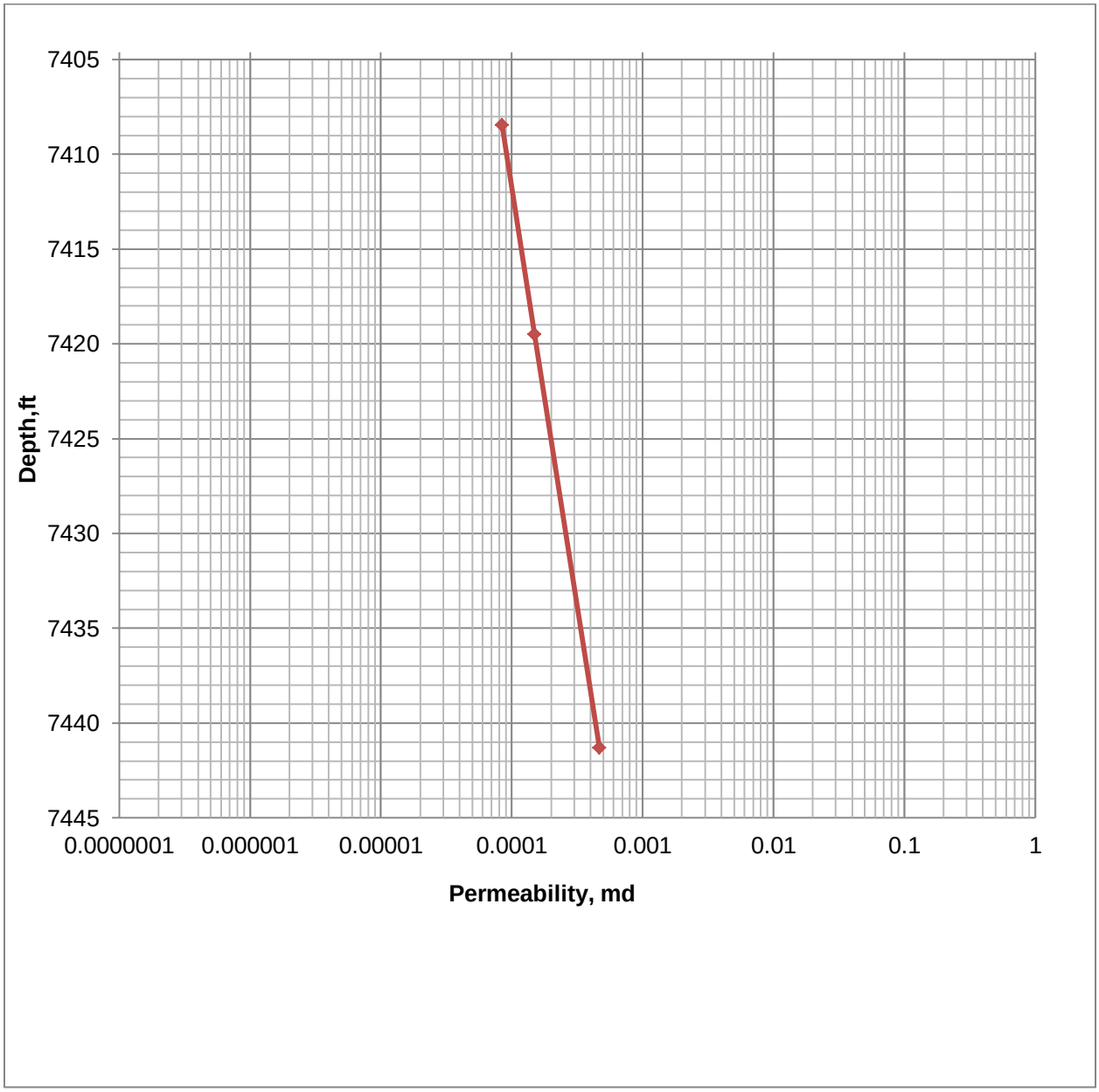

Figure 10. Permeability vs. depth of the Brown Dense, Sessions #1 well.

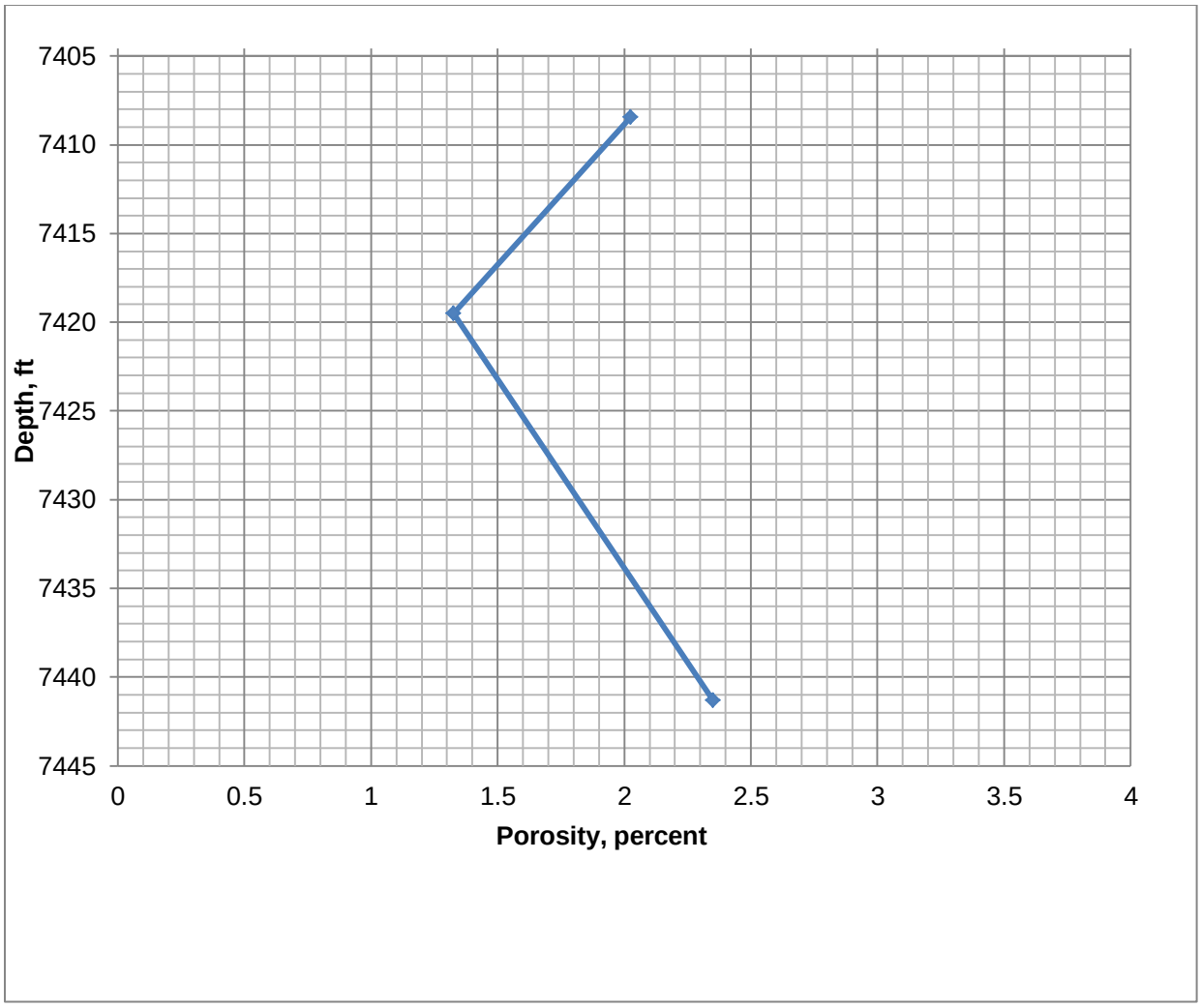

Figure 11. Porosity vs. depth of the Brown Dense, Sessions #1 well.

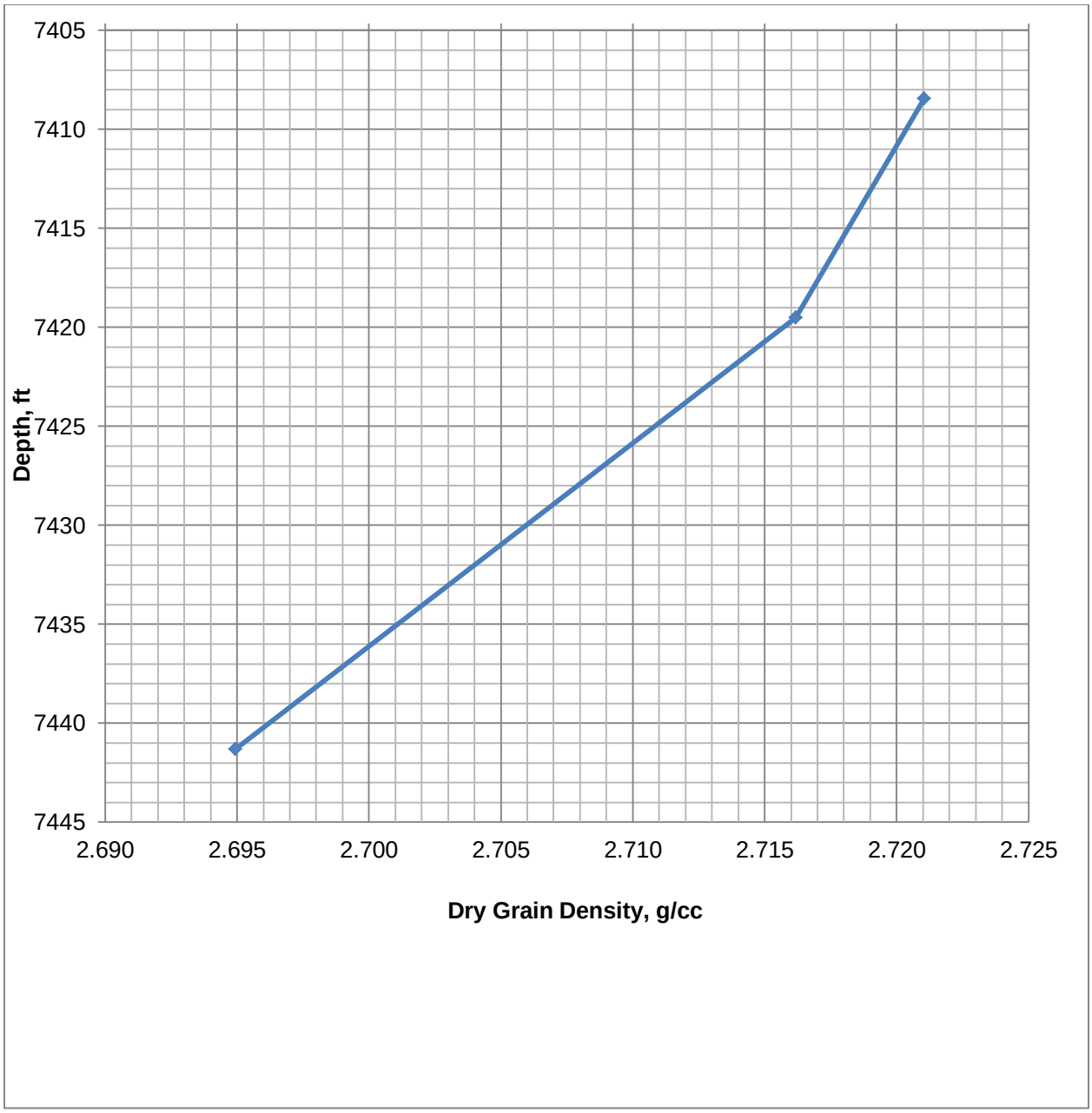

Figure 12. Dry grain density vs. depth of the Brown Dense, Sessions #1 well.

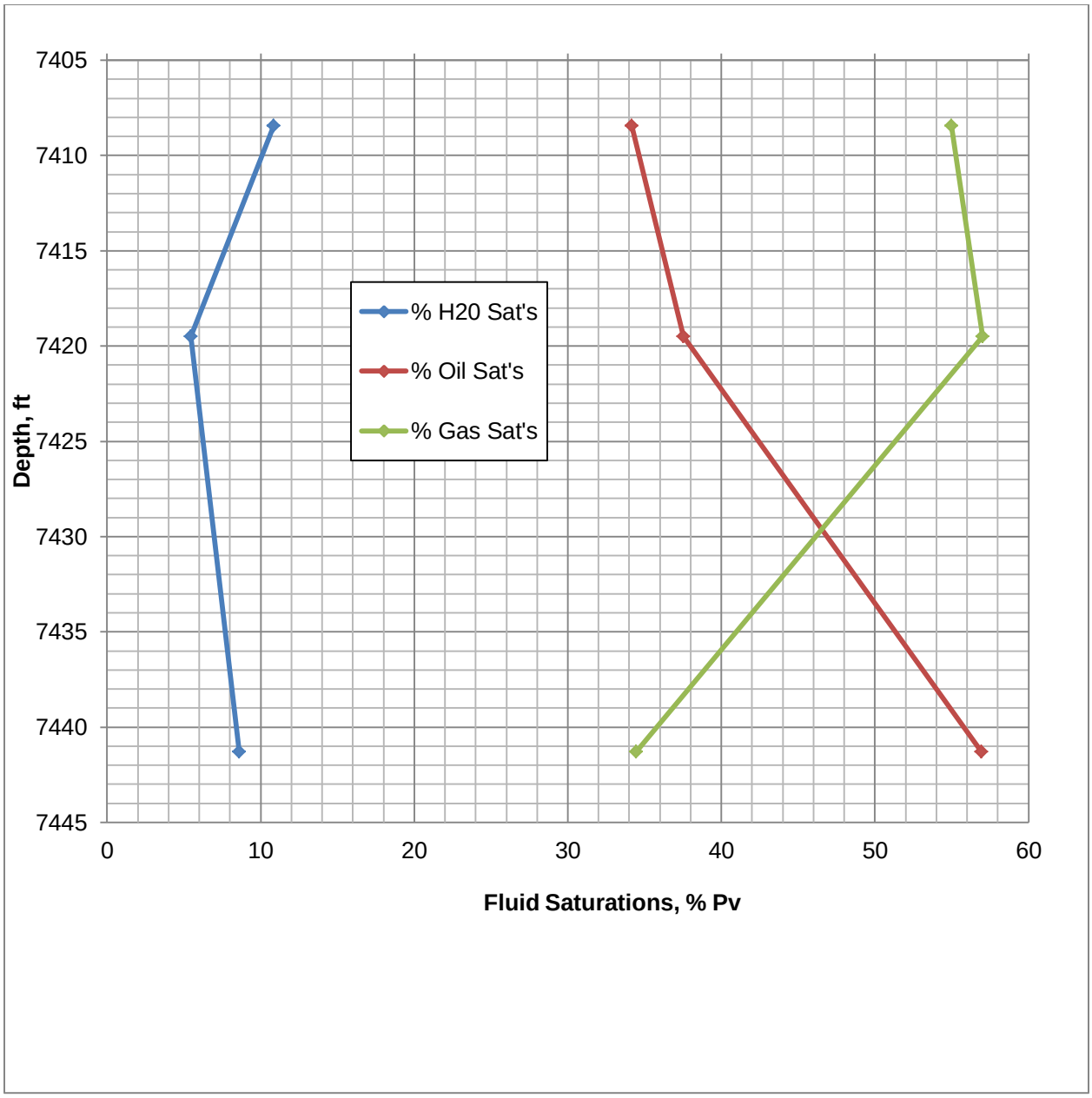

Figure 13. Fluid saturations vs. depth of the Brown Dense, Sessions #1 well.

Oil Organic Geochemical Analysis

Introduction

One oil sample was collected from the Sessions #1 well. The sample was sent to the Petroleum Geochemistry and Environmental Forensics Laboratory at the University of Oklahoma for organic geochemical analysis. The oil was separated into fractions with liquid chromatography, and whole oil, saturate, and aromatic fractions were analyzed with gas chromatography (GC) (Figures 14-16). Biomarkers in the Sessions oil were evaluated using the maltene fraction by gas chromatography-mass spectrometry (GC-MS). The mass/charge ratios of *m/z* 217.30/218.30 (Figure 17), *m/z* 231.20/232.20 (Figure 18), *m/z* 191.30 (Figure 19), *m/z* 123.20 (Figure 20), and *m/z* 133.20/134.20 (Figure 21) were monitored. Stable carbon isotope analysis was performed on the saturated fractions of the Sessions oil (Figure 22).

Depositional Environment Parameters

Saturates/aromatic

The oils from marine source rocks are typically richer in saturate hydrocarbons than aromatic hydrocarbons compared to those from terrestrial sediments. However, at low thermal maturity the aromatic content is higher and the S/A ratio increases with increasing thermal maturity. The low S/A ratio (<1) indicate immature to early mature in agreement with T_{max} and HI data. From 108.5 mg of the Sessions oil sample, 11.25 mg of asphaltens and 77.7 mg of maltenes were recovered. Then, 48.36 mg of maltens was fractioned by column chromatography and recovered the following weights: saturates (11.8 mg), aromatic (24.02 mg), and NSO (0.22 mg) (Figures 15-16). This unusually low NSO yield may be an artifact of the analysis, sample collection, or production fractionation. In the worst case for production it would suggest they were stripped off in the reservoir and possibly occluded the pore throats.

Normal Alkanes Distribution

The n-alkane distribution from the Sessions oil maximizes at n-C_{16} with low abundance in the high molecular-weight region (Figure 16). The increase in the n-C_{15} to n-C_{20} in the gas chromatography for the saturate hydrocarbons suggests marine organic matter with contribution to the biomass from algae and plankton (Peters and Moldowan, 1993).

Carbon Preference Index (CPI) and Odd-Even Preference (OEP)

The relative abundance of odd versus even carbon-numbered n-paraffins in the n-C_{20} to n-C_{30} range reflects the environment and lithofacies of source rock deposition. These measurements include the carbon preference index (CPI) and the improved odd-even preference (OEP). The OEP value of the Sessions oil is 0.96 indicative of a marine carbonate sourced oil (Figure 14).

Molecular parameters based on biomarker compounds are valuable for determining the nature of the source sediment. Since biomarkers can be traced back to specific biological compounds, they provide insight into the organisms that contribute organic matter to the source beds.

Pristane/Phytane Ratio

Pristane/phytane (Pr/Ph) ratios of oils are used to indicate the redox potential and organic matter type of the source sediments (Didyk et al., 1978). Pr/Ph < 1 indicates a strongly reducing depositional setting generally found in some type I, and most marine carbonates and often marine marls of type II, or II-S organic matter deposited in an anoxic environment. Pr/Ph of 1-3 suggests type II organic matter, and Pr/Ph > 3 indicates type III terrestrial organic matter under oxic conditions. The Pr/Ph ratio of the Sessions oil is 0.67, reflecting a strongly reducing depositional environment (Figure 14).

Steranes (*m/z* 217-218)

The Sessions oil is characterized by a predominance of C_{27} steranes and presence of C_{30} steranes, suggesting a marine source (Figure 17).

Steranes are valuable indicators of organic matter type in source rocks (Peters and Moldowan, 1993). Huang and Meinshein (1979) suggested that C_{27} sterols predominate in marine organic matter, whereas a predominance of C_{29} sterols is assumed to indicate a terrigenous organic matter. Sterane/hopane ratios reflect input of eukaryotic (mainly algae and higher plants) versus prokaryotic (bacteria) organisms to the source rock (Peters and Moldowan, 1993). The presence of C_{30} steranes is the most powerful parameter for identifying marine organic matter to the source rock (Moldowan et al., 1985; Peters et al., 1986). In general, high concentrations of C_{27} steranes, the existence of C_{30} steranes, along with high steranes/hopanes ratios (≥ 1) typify marine organic matter.

4-Methyl Steranes (*m/z* 231-232)

4-methyl steranes are generally associated with marine sources. A series of these biomarkers are observed in the Sessions oil further confirming its marine setting (Figure 18).

Diasteranes (*m/z* 127)

Diasteranes/steranes ratios are commonly used to distinguish petroleum from carbonate versus clastic source rocks (Mello et al., 1988). Low diasteranes/steranes ratios in oils indicate an anoxic, clay-poor, carbonate source rock. High diasteranes/steranes ratios are typical of petroleum derived from source rocks containing abundant clays. In the Sessions oil, diasteranes appear to be absent, indicating that the source of this oil is markedly from marine carbonates.

Terpanes (m/z 191)

C_{23} tricyclic and C_{24} tetracyclic terpanes are normally associated with carbonate depositional environment (Palacas et al., 1984). The high values of C_{23} tricyclic and C24 tetracyclic terpanes for the Sessions oil are typical of oils being generated by a carbonate source rock (Figure 19). The high C24 tetracyclic to C26 tricyclic ratio is also indicative of a marine carbonate sourced oil and contraindicative of a lacustrine sourced oil.

Hopanes (m/z 191)

Crude oils from organic-rich carbonate-evaporite rocks generally show higher values for the C_{29} norhopane compared with the C_{30} hopanes (Connan et al., 1986). A high C_{29}/C_{30} hopanes ratio (>1) in the Session oil indicates the oil sample was generated from carbonate source rocks (Figure 19).

Homohopanes (m/z 191)

Homohopanes (C_{31}-C_{35}) distribution has been used to evaluate redox conditions based on the homohopanes index (the ratio $C_{35}/(C_{31}$ to $C_{35})$ homohopanes). High C_{35} homohopanes are commonly associated with highly reducing marine conditions, whereas low C_{35} homohopanes concentrations are generally observed in oxidizing water conditions (Peters and Moldowan, 1991). In the Sessions oil sample, homohopanes are dominated by the C_{31} homohopanes with values decreasing through C_{35} homohopanes. The high homohopanes ratio is indicative of a highly reducing marine carbonate depositional environment (Figure 19).

Bicyclic Sesquiterpanes (m/z 123)

The occurrence of bicyclic sesquiterpanes such as drimane is sometimes reported as terrestrial markers. The drimane in the Sessions oil sample is indicative of microbial input to the oil's source rock (Figure 20).

Aryl Isoprenoids (m/z 133-134)

Aryl isoprenoids (1-alkyl, 2-, 3-, 6-trimethylbenzenes) are believed to derive from green sulfur bacteria Chlorobiaceae which perform photosynthesis with hydrogen sulfide (H_2S) rather than oxygen. The presence of aryl isoprenoids is used as an indicator of euxinic photic zone anoxia (Summons and Powell, 1987). A series of aryl isoprenoids is observed in the Sessions oil, indicating that deposition of source rock for this oil is possibly associated with oceanic anoxic events (Figure 21).

Thermal Maturity Parameters

Molecular rearrangements of biological marker compounds can also provide a series of sensitive thermal maturation parameters. All of these measurements rely on the comparison of the relative proportion of metastable reactive compounds to their more stable isomers or products.

17α (H)22S/(22S + 22R) Homohopanes (*m/z* 191)

Typically C_{31} or C_{32} homohopanes are used for calculations of the 22S/(22S + 22R) ratio. The 22S/(22S + 22R) ratio rises from 0 to about 0.6 during maturation (0.57 to 0.62 = equilibrium) (Seifert and Moldowan, 1978). The 22S/(22S + 22R) ratio for the Sessions oil sample is about 0.59, which suggests that it reached equilibrium for oil window (Figure 19).

Ts/(Ts + Tm) (*m/z* 191)

During catagenesis, C_{27} 17α (H)-trisnorhopane (Tm) shows lower relative stability than C_{27} 18α (H)-trisnorhopane II (Ts) (Seifert and Moldowan, 1978). Ts/(Ts + Tm) increases with increasing thermal maturity. However, it is also dependent on organofacies and kerogen type differences. The Ts/(Ts + Tm) ratio is 0.55 for the Sessions oil which indicates that this oil is in the oil window (Figure 19).

C_{29} 20S/(20S + 20R) Steranes & C_{29} ββ/(ββ + αα) Steranes (*m/z* 217)

Maturity levels of oils increase with the increase of the C_{29} sterane ratios (i.e. 20S/(20S + 20R) and ββ/(ββ + αα) (Seifert and Moldowan, 1986). These parameters are useful as a maturity indicator in early to middle oil window. The 20S/(20S + 20R) ratio rises from 0 to 0.5 (0.52 to 0.55 = equilibrium) with increasing maturity. The ββ/(ββ + αα) ratio increases from nonzero values to about 0.7 (0.67 to 0.71 = equilibrium). 20S/(20S + 20R) and ββ/(ββ + αα) C_{29} steranes ratios are 0.55 and 0.53, respectively for the Sessions oil, indicating that this oil was generated from a mature source rock but not yet in the condensate window (Figure 17).

Saturate Oil Carbon Isotope

Stable carbon isotopes have been used to characterize oil source characteristics. $\delta^{13}C$ value of the saturate oil averages -27.6‰ in the Sessions #1 well (Figure 22). Since there is only one oil sample available and no comparison can be made, the interpretation is limited. This value is slightly lighter (less mature) than many Smackover sourced oils in northeastern Texas where the Smackover averages around -25.5‰.

Conclusions

Geochemical characterization based on biomarker components and isotopic data was used to characterize the crude oil from the Brown Dense mudstone in the Sessions #1 well. The depositional environment parameters indicates the Sessions oil was derived from a carbonate source rock with no significant terrestrial organic matter contribution and deposited in a marine environment under highly reducing, anoxic conditions. The thermal maturity parameters suggest that the Sessions oil was generated from a source rock in the earliest oil window.

References

Connan, J., J. Bouroullec, D. Dessort, and P. Albrecht, 1986, The microbial input in carbonate-anhydrite facies of sabkha palaeoenvironment from Guatemala: A molecular approach: Organic Geochemistry, v. 10, p. 29-50.

Didyk, B.M., B.R.T. Simoneit, S.C. Brassell, and G. Eglinton, 1978, Organic geochemical indicators of paleoenvironmental conditions of sedimentation: Nature, v. 272, p. 216-222.

Huang W.Y., and W.G. Meinshein, 1979, Sterols as ecological indicators: Geochimica et Cosmochimica Acta, v. 43, p. 739-745.

Mello, M.R., N. Telnaes, P.C. Gagilianone, M.I. Chicarelli, S.C. Brassell, and J.R. Maxwell, 1988, Organic geochemical characterization of depositional paleoenvironments in Brazilian marginal basins: Organic Geochemistry, v. 13, p. 31-46.

Moldowan, J.M., W.K. Seifert, and E.J. Gallegos, 1985, Relationship between petroleum composition and depositional environment of petroleum source rocks: American Association of Petroleum Geologists Bulletin, v. 69, p. 1255-12268.

Palacas, J.G., D.E. Anders, and J.D. King, 1984: South Florida Basin-Prime example of carbonate source rocks of petroleum, *in* J. G. Palacas (*ed.*), Petroleum geochemistry and source rock potential of carbonate rocks: AAPG Studies in Geology 18, 71-96.

Peters, K.E., J.M. Moldowan, M. Schoell, and W.B. Hempkins, 1986, Petroleum isotopic and biomarker composition related to source rock organic matter and depositional environment: Organic Geochemistry, v. 10, p. 17-27.

Peters, K.E., and J.M. Moldowan, 1991, Effects of source, thermal maturity, and biodegradation on the distribution and isomerization of homohopanes in petroleum: Organic Geochemistry, v. 17, p. 47–61.

Peters, K.E. and J.M. Moldowan, 1993, The biomarker guide, interpreting molecular fossils in petroleum and ancient sediments: Englewood Cliffs, New Jersey, Prentice Hall, 363 p.

Seifert, W.K. and J.M. Moldowan, 1978, Applications of Steranes, Terpanes and Monoaromatics to the Maturation, Migration and Source of Crude Oils: Geochimica et Cosmochimica Acta, v. 42, p. 77-95.

Seifert, W.K. and J.M. Moldowan, 1986, Use of biological markers in petroleum exploration, *in* R. B. Johns, *ed*., Methods in Geochemistry and Geophysics, v. 24, p. 261-290.

Summons, R.E. and T.G. Powell, 1987, Identification of aryl isoprenoids in source rocks and crude oils: biological markers for the green sulphur bacteria: Geochimca et Cosmochimica Acta, v. 51, 557–566.

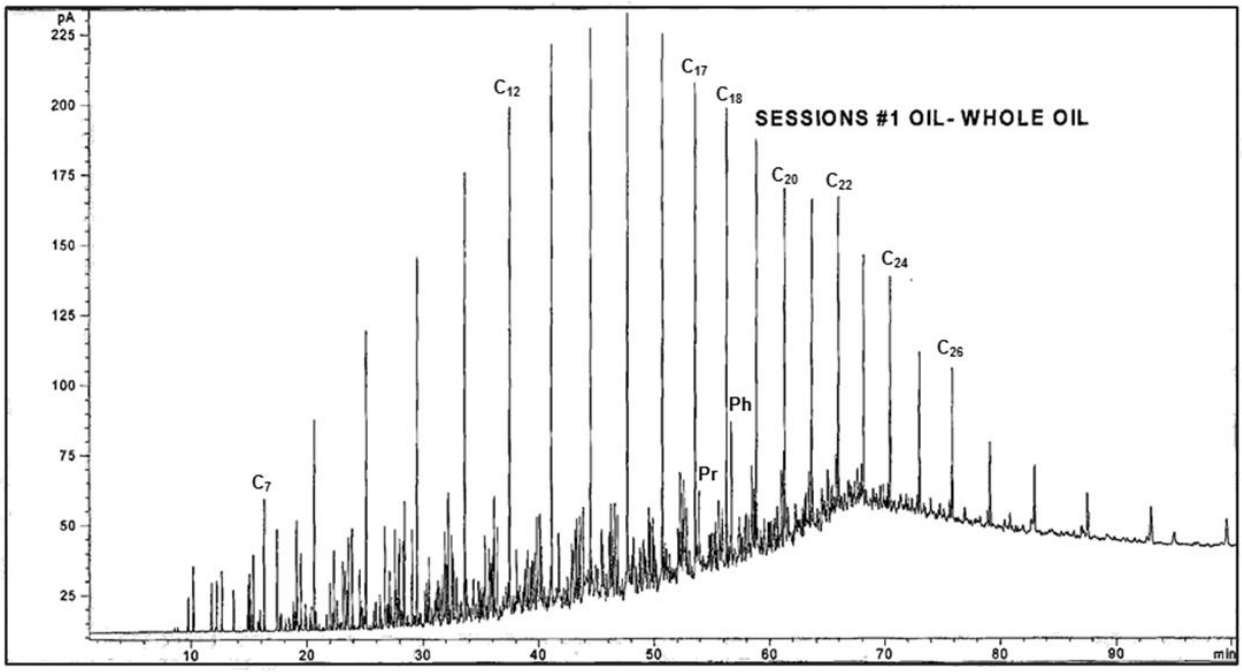

Figure 14. Gas chromatograph of whole oil from the Brown Dense, Sessions #1 well.

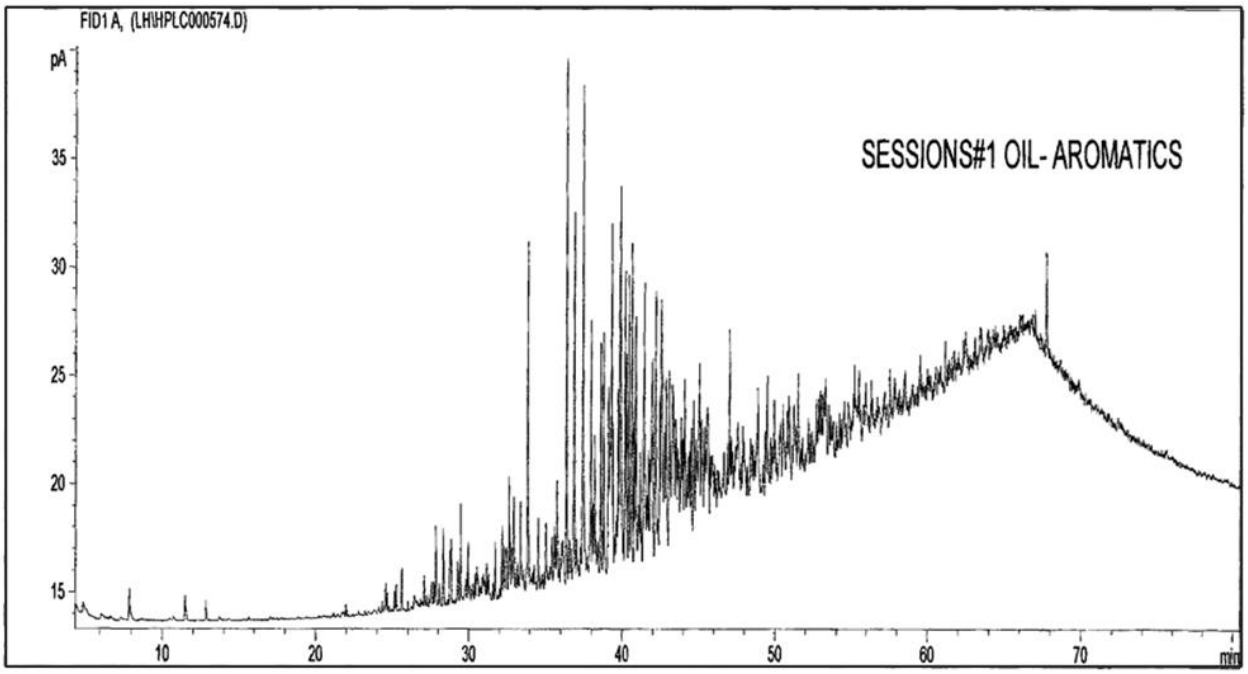

Figure 15. Gas chromatograph of aromatic hydrocarbon from the Brown Dense, Sessions # 1 well.

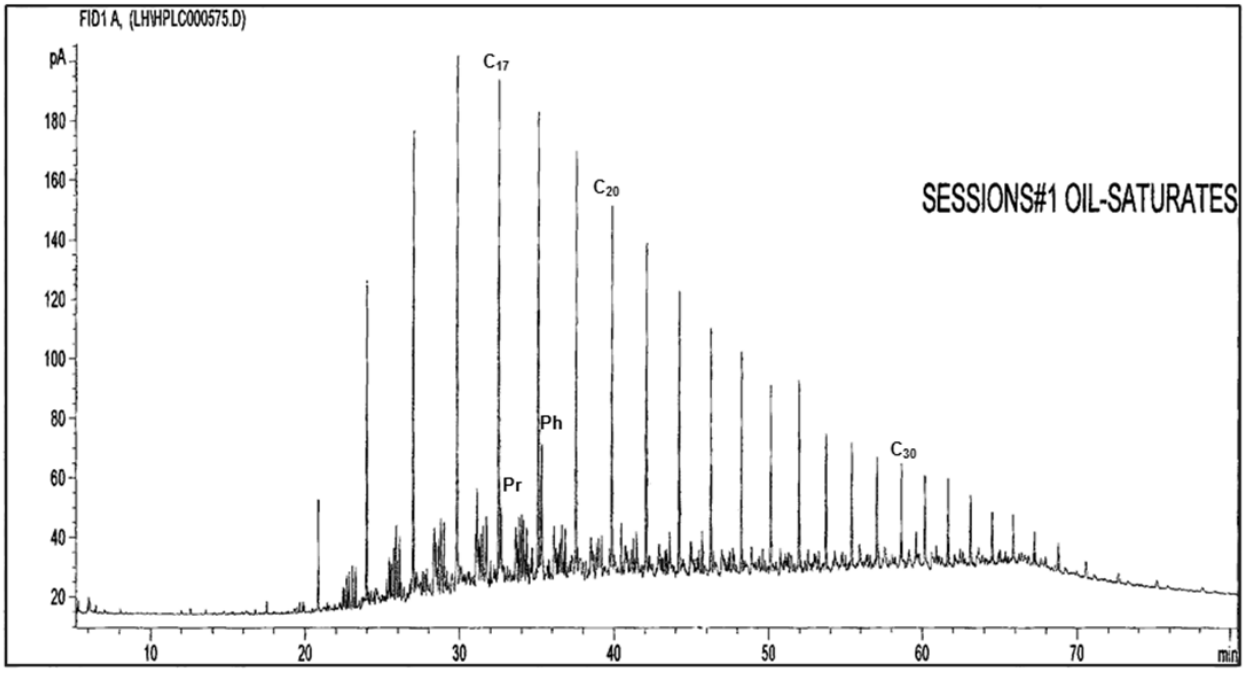

Figure 16. Gas chromatograph of saturated hydrocarbon from the Brown Dense, Sessions # 1 well.

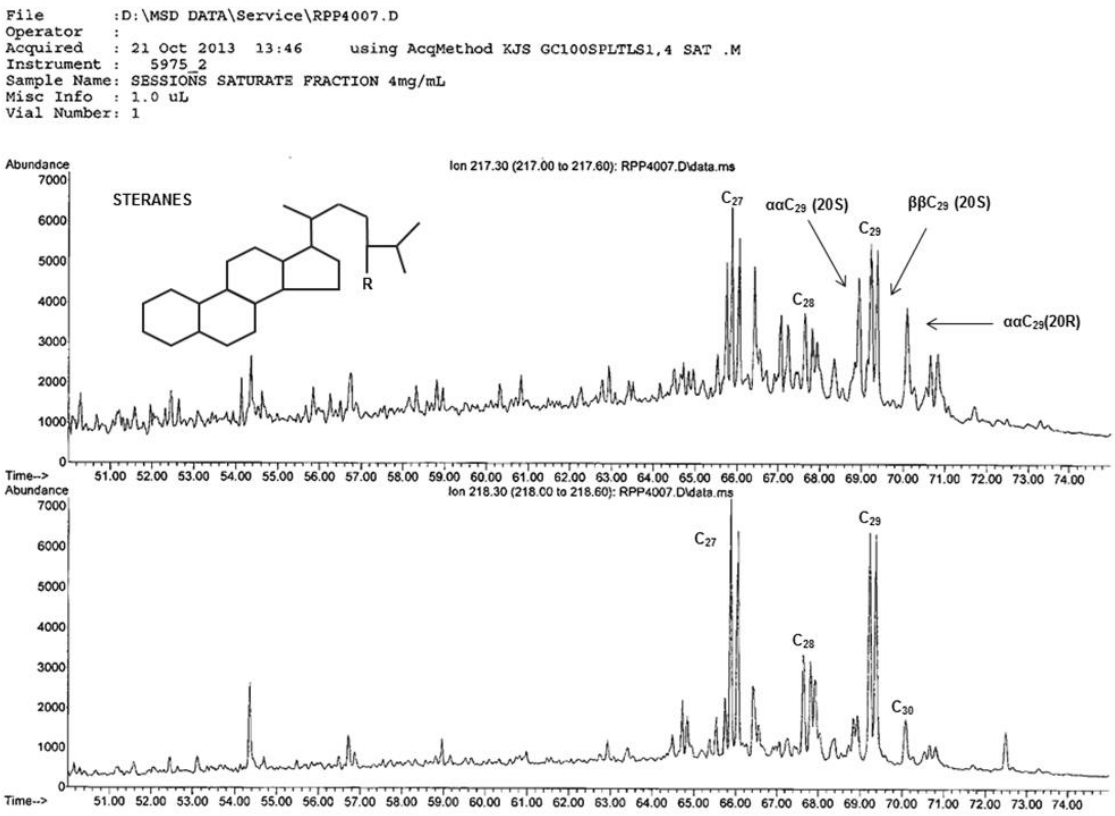

Figure 17. GCMS analysis of steranes in the saturate fraction of oil from the Brown Dense, Sessions #1 well.

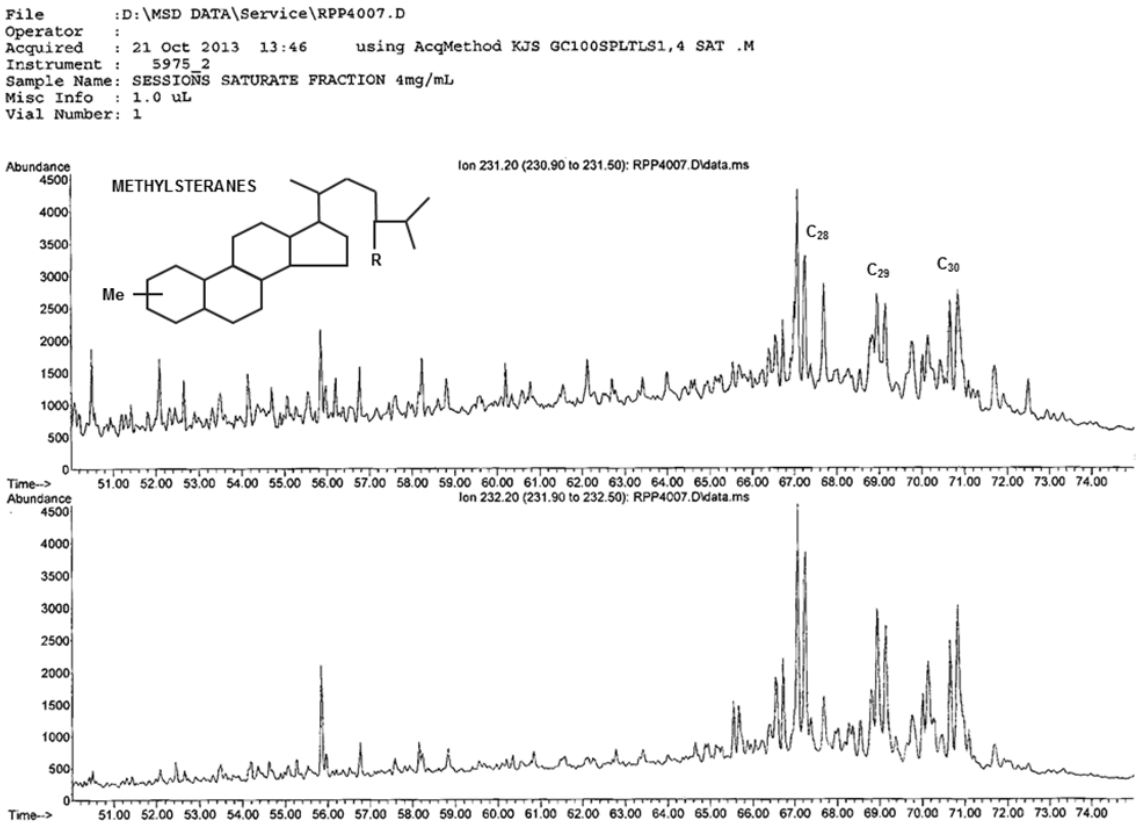

Figure 18. GCMS analysis of methyl steranes in the saturate fraction of oil from the Brown Dense, Sessions #1 well.

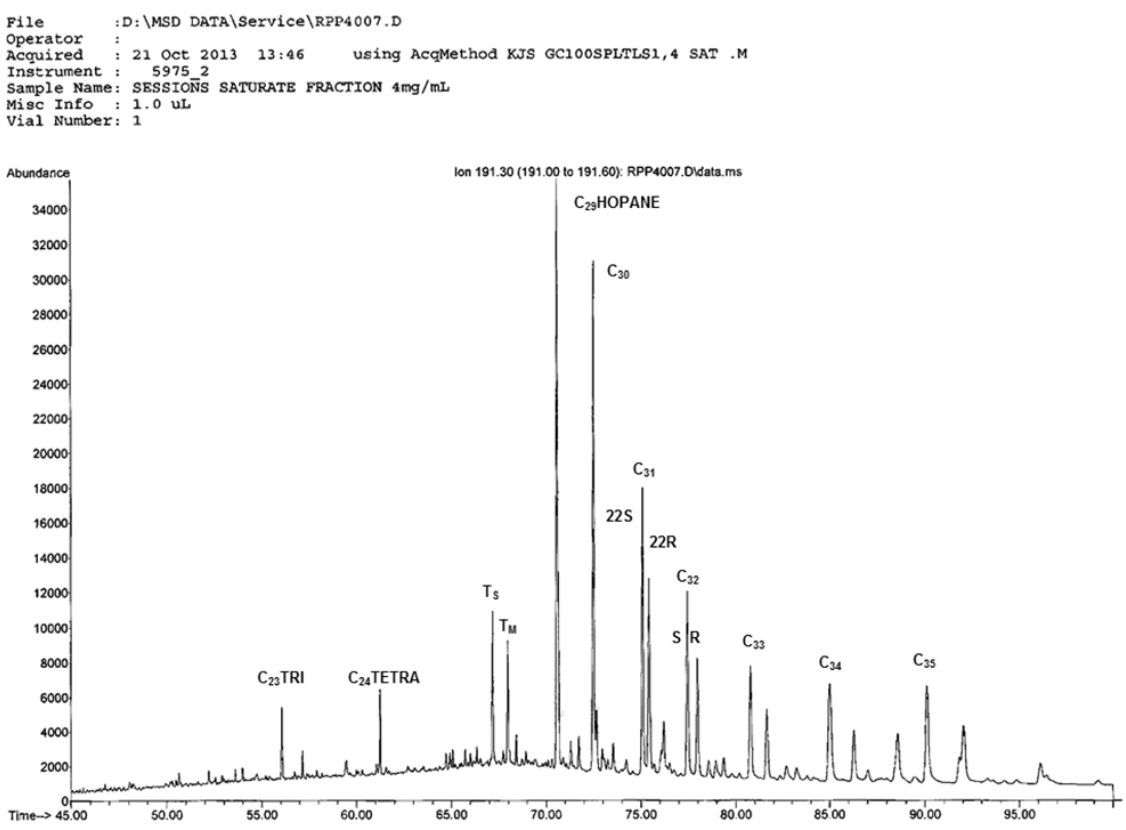

Figure 19. Terpane fingerprints (*m/z* 191) by GCMS for the saturate fraction of oil from the Brown Dense, Sessions #1 well.

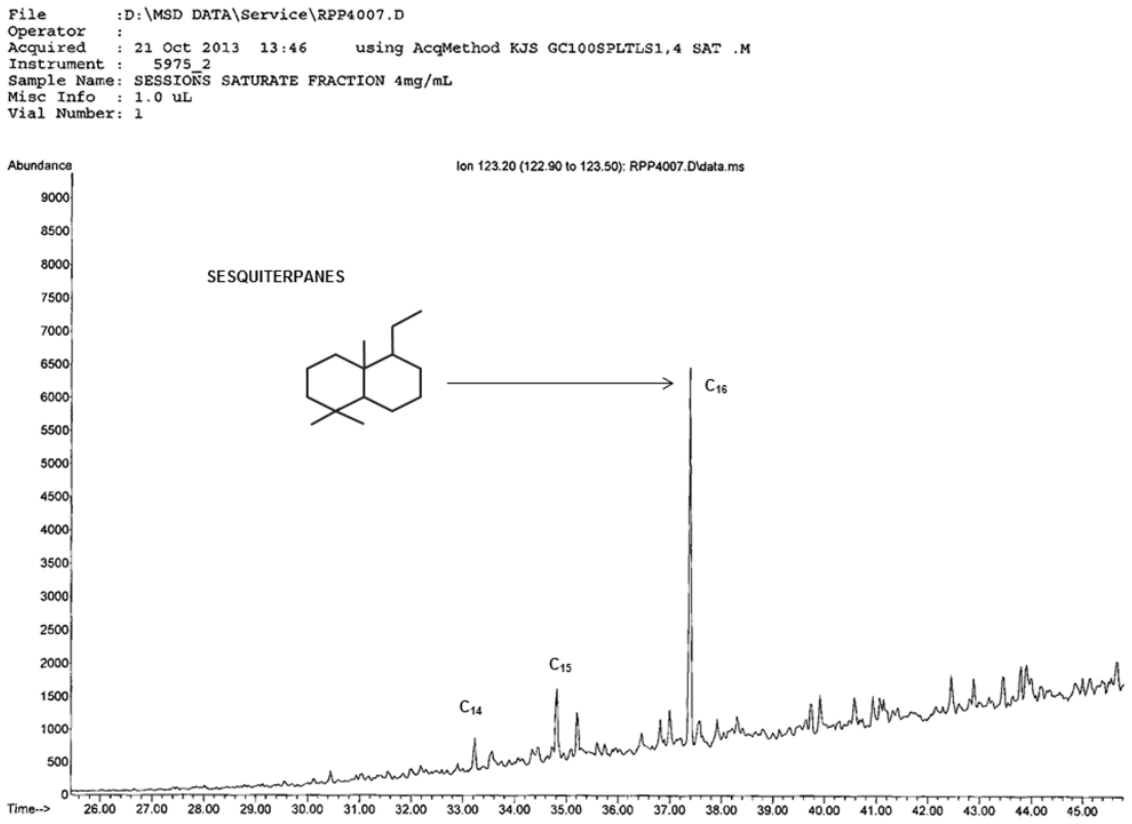

Figure 20. Sesquiterpane fingerprints (*m/z* 123) by GCMS for the saturate fraction of oil from the Brown Dense, Sessions #1 well.

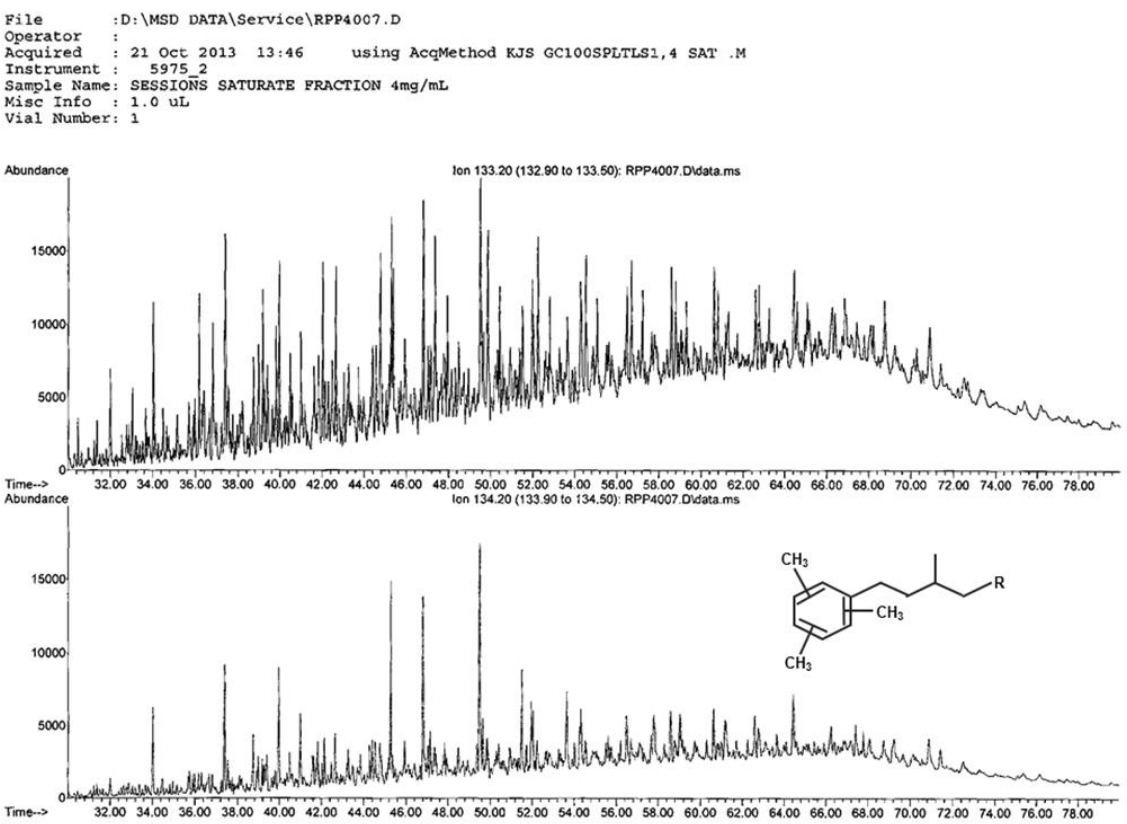

Figure 21. Aryl Isoprenoid fingerprints by GCMS for the saturate fraction of oil from the Brown Dense, Sessions #1 well.

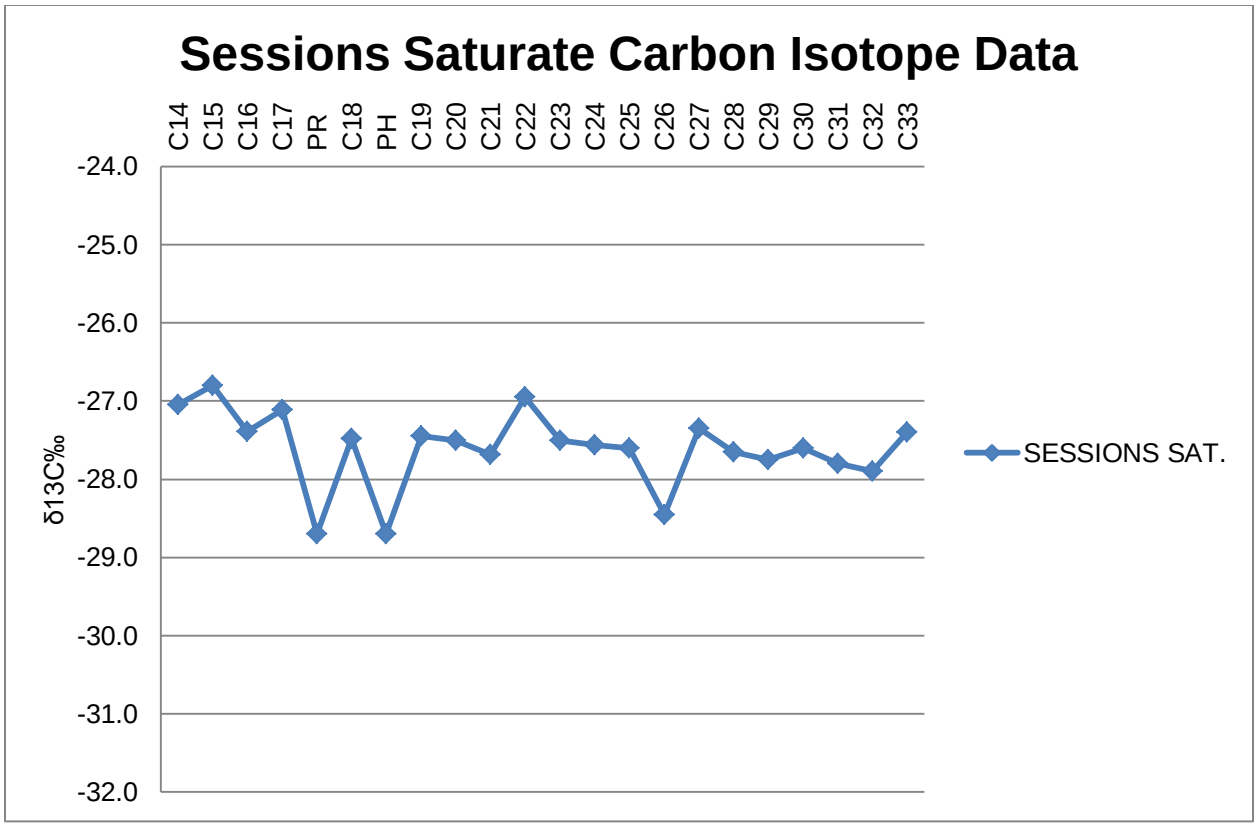

Figure 22. Carbon isotopic analysis of the saturate hydrocarbon from the Brown Dense, Sessions #1 well.

Conclusions

1. This work represents the comprehensive and integrated study of core and oil analysis of the Sessions No. 1 well, Union County, Arkansas for identifying and evaluating the unconventional resource characterization of the Upper Jurassic Lower Smackover Formation (Brown Dense Mudstone) in south Arkansas. To date, the unconventional reservoirs research work is predominately focused on the shale system. Very limited knowledge of calcareous mudstone in terms of the unconventional resources has been revealed. The question therefore arises as to the suitability and applicability of the methodology of assessing the shale systems to calcareous mudstones. Therefore, the results of this research on the Brown Dense Mudstone present an insight to understand the nature and reservoir characteristics of the calcareous mudstone, which can be used for the future unconventional exploration and research efforts in this type of lithology.
2. Using the terminology of the Dunham classification system for carbonate rocks, the lithology of the Brown Dense Mudstone observed in the thin sections and core description includes: (1) slightly silty/sandy limestone ranging in texture from mudstone to wackestone; (2) slightly silty/sandy, bioclastic limestone with texture ranging from crystalline, wackestone to packstone; (3) slightly silty limestone with an algal boundstone texture; (4) slightly sandy peloidal limestone with a wackestone texture; and (5) slightly sandy, oolitic limestone with a grainstone texture. Detrital grains are comprised of quartz sand/silt, feldspar, muscovite, and phosphatic fragments. Allochems include peloids, ooids, limestone lithoclasts, spherules, foraminifera, brachiopod fragments, echinoderm fragments, and algal fragments/laminites. The dominant depositional environments are interpreted to be in the range of inner, middle, outer ramp to basin, with a minor presence of ooid shoal.
3. The averaged TOC value suggests that the Brown Dense has fair to good source potential. Rock-Eval pyrolysis results indicate that the majority of organic matter of the sampled cores in the Sessions #1 well is Type II, oil-prone kerogen. The thermal maturity assessed from T_{max} indicates that the organic matter is in the oil window, which is consistent with the observations from biomarker data.
4. The dominant porosity is hosted within the OM. However, some intra/interparticle pores are present in the matrix of the Brown Dense Mudstone. All pore sizes observed in our samples fall into the micro to nanopore range. OM pores appear to be associated with the migrated OM which provides more contiguous permeability pathways than isolated depositional OM alone. The thermal maturity

of the samples with OM pores is in oil window, which indicates that OM pores begin to develop from oil-window-maturity level.

5. X-ray diffraction analysis shows that samples at depths of 7,379.90 and 7,418.05 ft contain similar compositions. They exhibit 97% of calcite, 2% of quartz and 1% of clays (primarily illite/mica). The sample from 7,441.90 ft showed a much more diverse composition with 31% of calcite, 26% of quartz, 18% of dolomite, and 13% of illite/mica. Other constituents include plagioclase, pyrite, mixed-layer illite/smectite, and kaolinite.

6. Rock mechanics testing shows that the Brown Dense samples are very dense and massive as indicated by high bulk density. High Young's moduli, low Poisson Ratios and high ultrasonic velocities suggest that the Brown Dense samples are pretty brittle. The correlation of dynamic and static Young's Moduli further supports the high brittleness of the Brown Dense Mustone in the Sessions #1 well.

7. Shale Rock Properties (SRP) analysis shows that porosity and permeability values measured from the crushed core samples are much lower than the routine ones. Both porosity and permeability from SRP are very low. Dry helium porosity is 1.9% on average ranging from 1.3 to 2.3%. Dry pressure decay permeability varies from 8.43×10^{-5} md (84.3 nanoDarcys) to 4.69×10^{-4} md (469 nanoDarcys) with an average of 2.34×10^{-4} md (234 nanoDarcys). As-received fluid saturations indicate average water saturation is 8.3%, oil saturation is 42.9%, and gas saturation is 48.8%.

8. Biomarker components of the crude oil are used to interpret the depositional environment and thermal maturation of the Brown Dense Mudstone from which the oil was generated and extracted. The Sessions oil was derived from a carbonate source rock with no significant terrestrial organic matter contribution and deposited in a marine environment under highly reducing, anoxic conditions. The oil was generated from a source rock in the earliest oil window.

Acknowledgments

This research was funded by the USGS under Grant/Cooperative Agreement No. G12AC20245. However, the views and conclusions contained herein are those of the authors and should not be interpreted as representing the opinions or policies of the USGS. Mention of laboratory names does not constitute their endorsement by the USGS. We thank Betsy Production Company for donating the core and oil samples and providing data and reports to the Arkansas Geological Survey. We are very appreciative of Dan Jarvie of Worldwide Geochemistry for providing the constructive reviews of the geochemical and biomarker analyses. Finally, we would like to thank the geologic staff of the AGS for reviewing the technical aspects of this report.

Arkansas Geological Survey
Bekki White, State Geologist and Director

Appendix 1: Well Location Map for Brown Dense (Lower Smackover) Play, Southern Arkansas

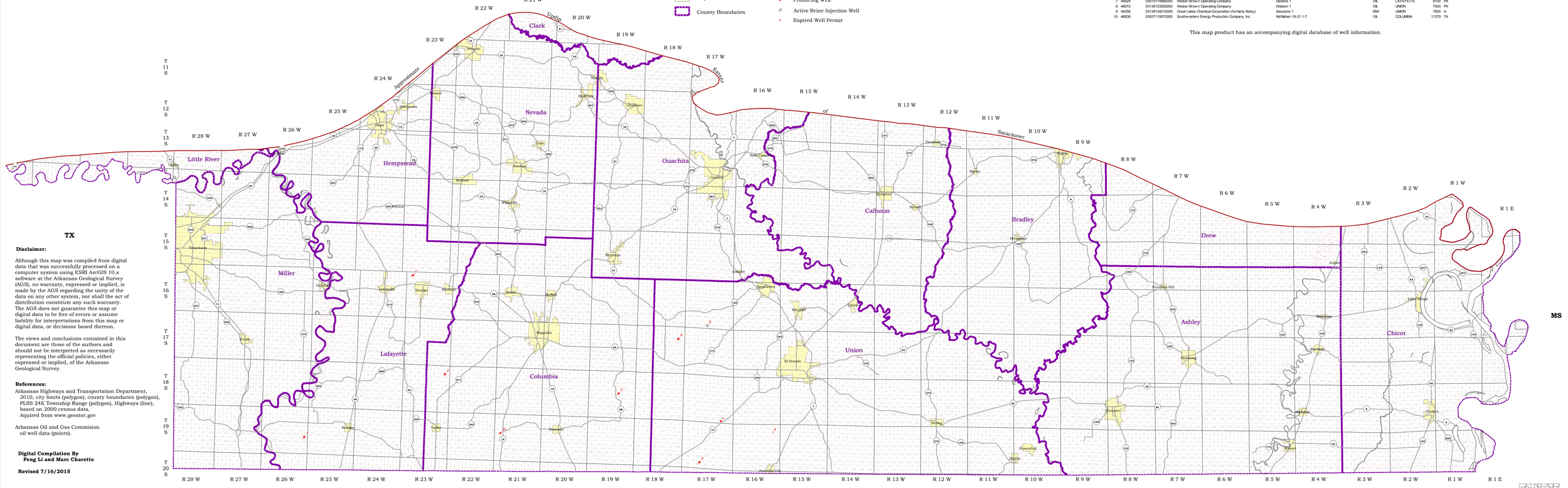

ID	Wl_Permit	API_WellNo	CoName	Well_Nm	Well_Typ	County	DepthToBeD	Wl_Status
1	42463	0307311464000	Border Exploration, LLC	Endsley 1-24H	OIL	LAFAYETTE	12000	PA
2	43826	0302711785000	Brammer Engineering, Inc	Watson-Fullerw ider Properties Ltd 1-12H	OIL	COLUMBIA	9950	PA
3	45015	0302711543000	Southw estern Energy Production Company, Inc.	Roberson 18-19 1-15H	OIL	COLUMBIA	8927	TA
4	45178	0313913301000	Cabot Oil & Gas Corporation	Denny 1-32H	OIL	UNION	9550	PA
5	45417	0313913370000	Rsl Energy, LLC (formerly Weiser-Brow n)	SWF Red River Land 1	OIL	UNION	9500	PR
6	45569	0313913360000	Southw estern Energy Production Company, Inc.	James, Dick 19-16 1-1H	OIL	UNION	8500	SX
7	45929	0307311488000	Weiser-Brow n Operating Company	Dickens 1	OIL	LAFAYETTE	8700	PA
8	46072	0313913320000	Weiser-Brow n Operating Company	Watson 1	OIL	UNION	7500	PA
9	46258	0313913410000	Great Lakes Chemical Corporation (formerly Betsy)	Sessions 1	SW	UNION	7600	A
10	46836	0302711957000	Southw estern Energy Production Company, Inc.	McMahen 19-21 1-7	OIL	COLUMBIA	11370	TA

This map product has an accompanying digital database of well information.

Disclaimer:

Although this map was compiled from digital data that was successfully processed on a computer system using ESRI ArcGIS 10.x software at the Arkansas Geological Survey (AGS), no warranty, expressed or implied, is made by the AGS regarding the unity of the data on any other system, nor shall the act of distribution constitute any such warranty. The AGS does not guarantee this map or digital data to be free of errors or assume liability for interpretations from this map or digital data, or decisions based thereon.

The views and conclusions contained in this document are those of the authors and should not be interpreted as necessarily representing the official policies, either expressed or implied, of the Arkansas Geological Survey.

References:

Arkansas Highways and Transportation Department, 2010, city limits (polygon), county boundaries (polygon), PLSS 24K Township Range (polygon), Highways (line), based on 2000 census data. Aquired from www.geostor.gov

Arkansas Oil and Gas Commision oil well data (points).

Digital Compilation By
Peng Li and Marc Charette

Revised 7/16/2015

Map Projection:
North American Datum of 1983
UTM Zone 15 North

Scale 1:250,000

0 5 10 20 30 40 Miles

0 5 10 20 30 40 Kilometers

N

Appendix 2: Whole Core CT Number and Bulk Density Plots with CT Longitudinal Images

CT NUMBER PLOT WITH LONGITUDINAL

7375.00-7376.00 feet

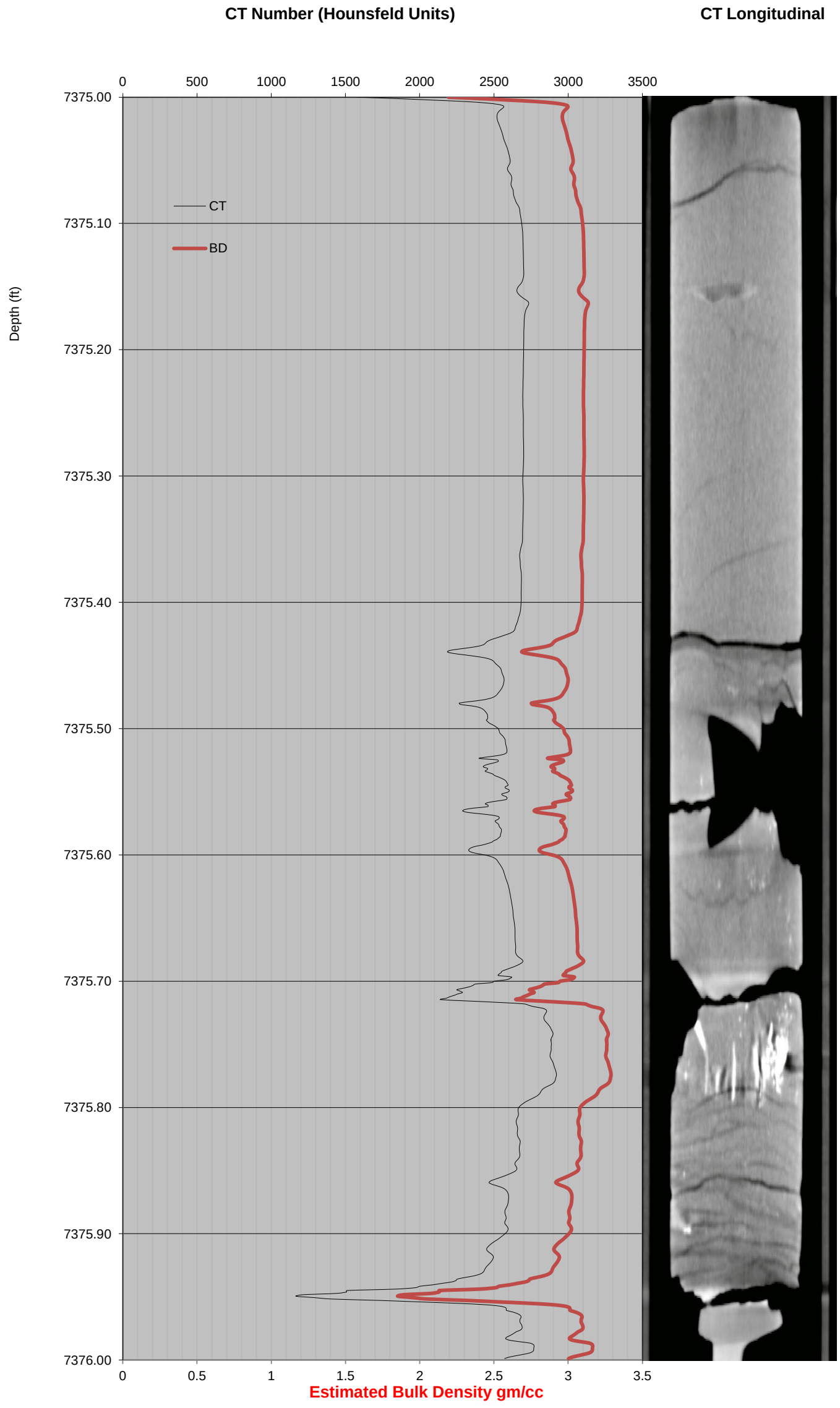

CT NUMBER PLOT WITH LONGITUDINAL

7376.00-7379.00 feet

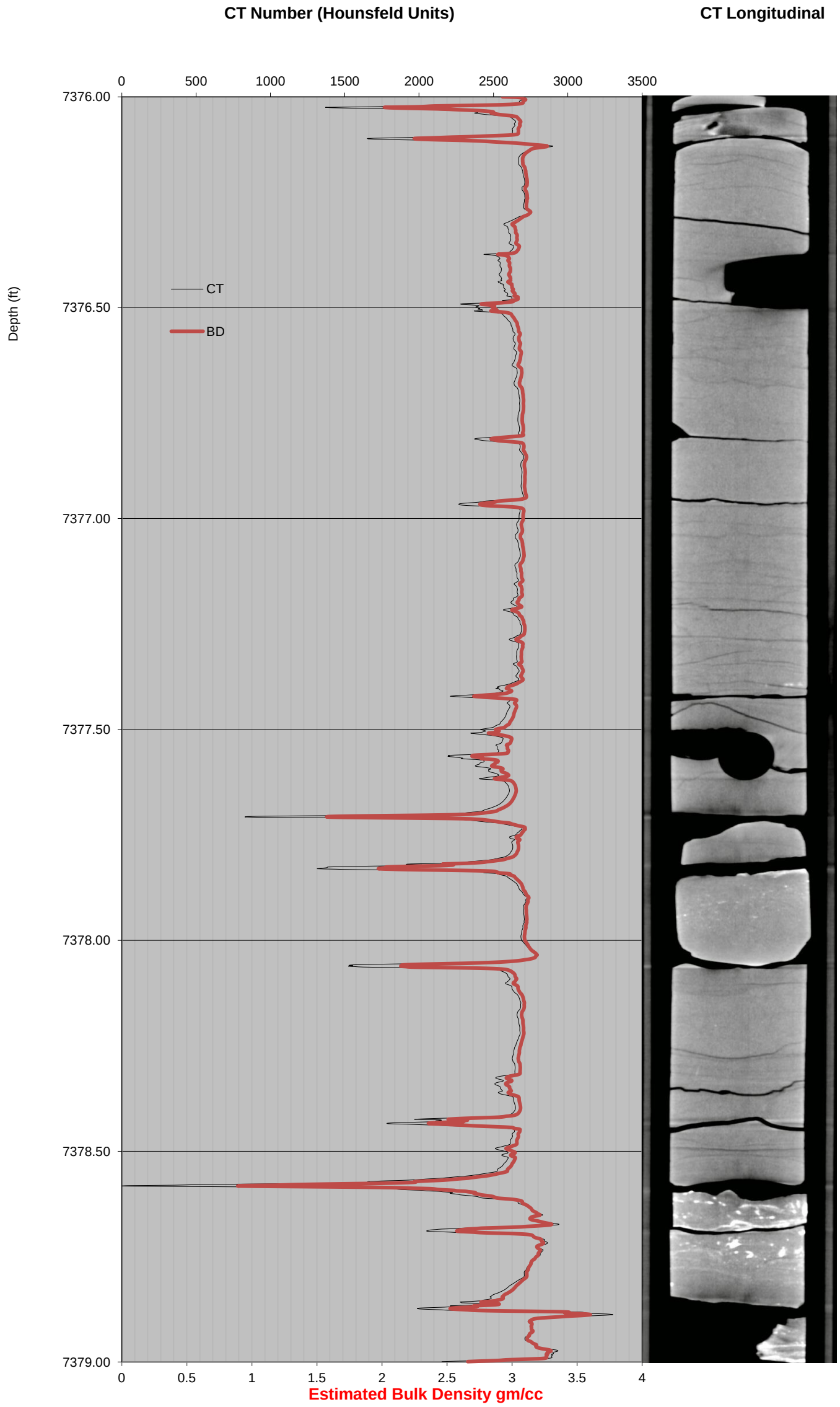

CT NUMBER PLOT WITH LONGITUDINAL

7379.00-7382.00 feet

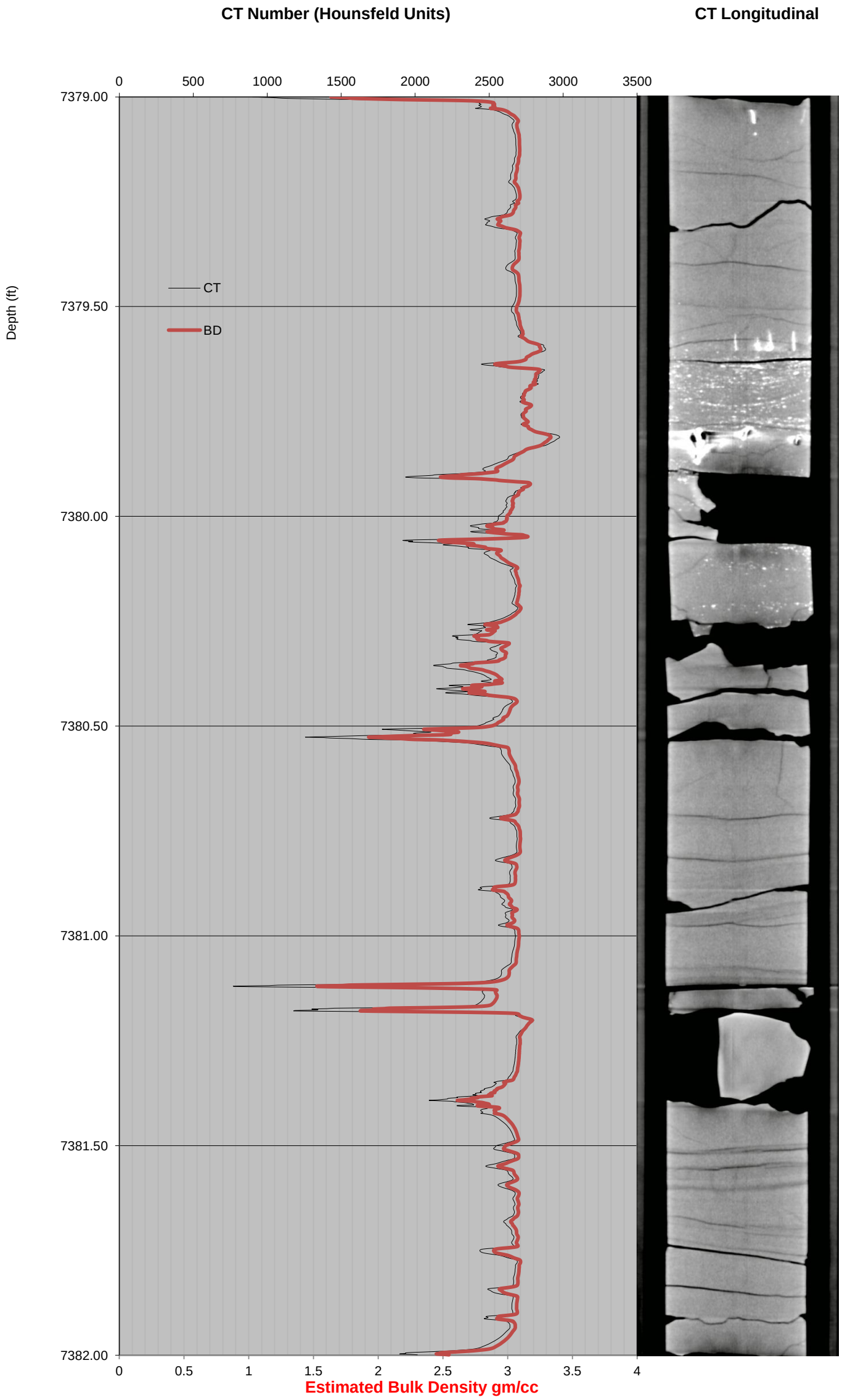

CT NUMBER PLOT WITH LONGITUDINAL

7382.00-7385.00 feet

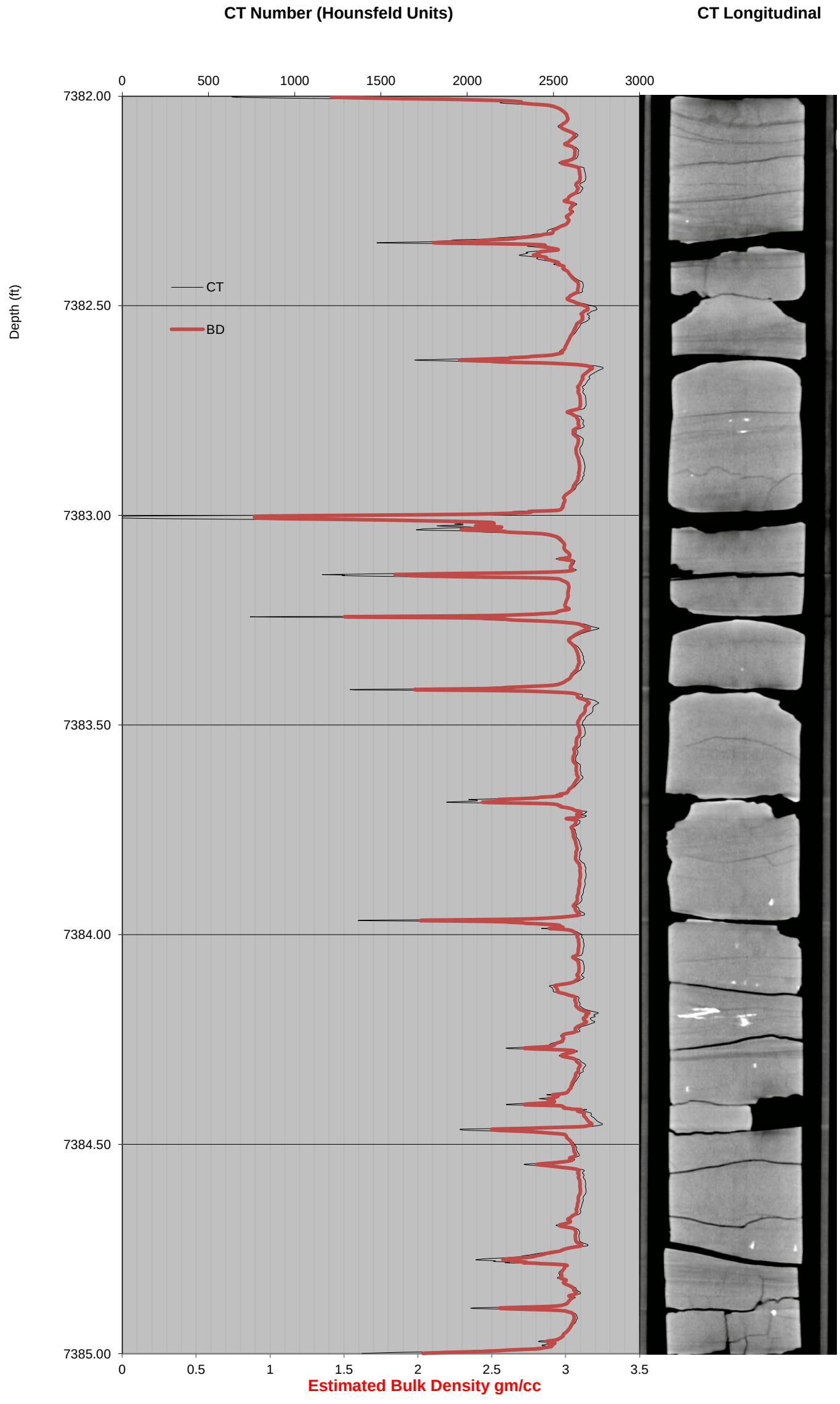

CT NUMBER PLOT WITH LONGITUDINAL

7385.00-7388.00 feet

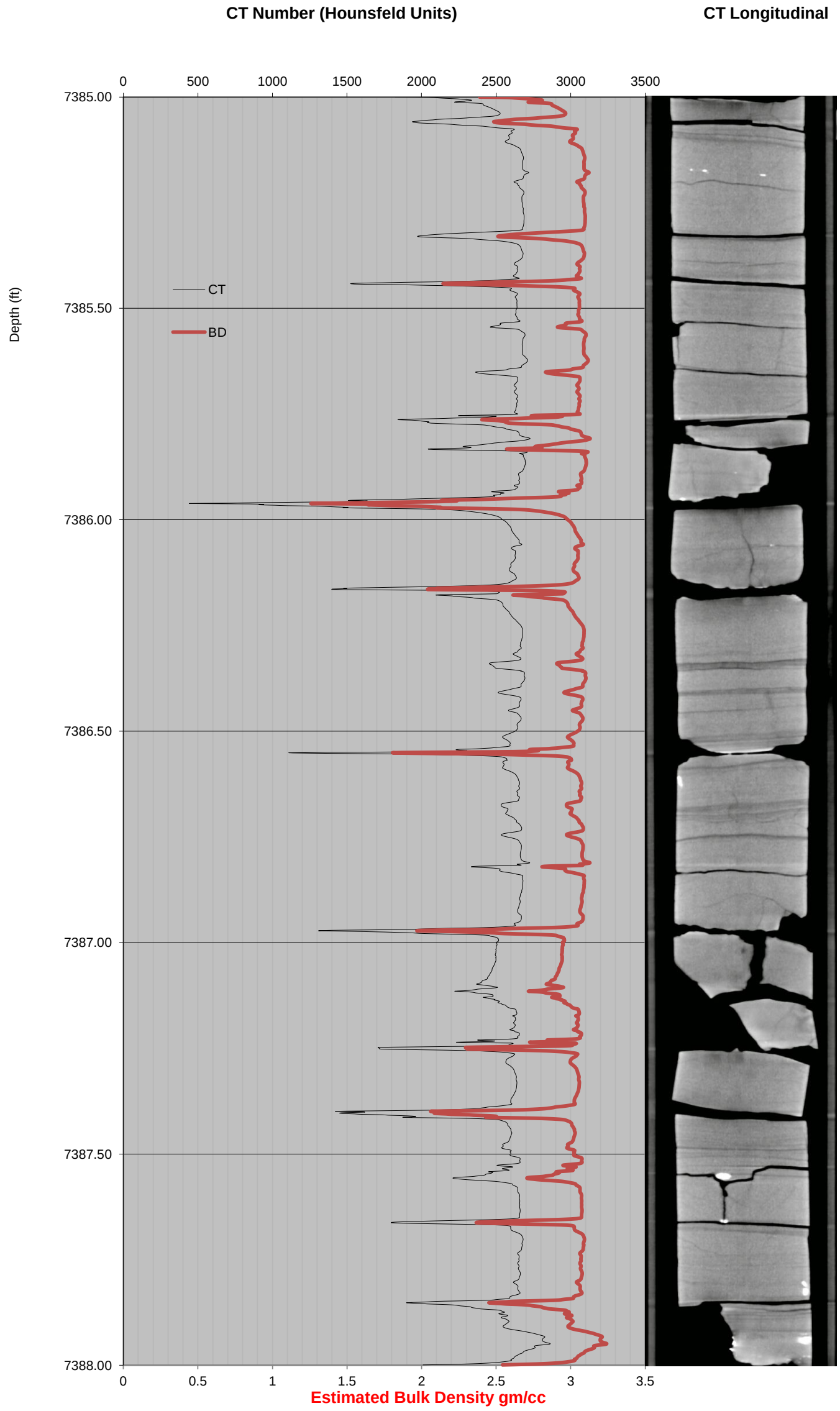

CT NUMBER PLOT WITH LONGITUDINAL

7388.00-7390.50 feet

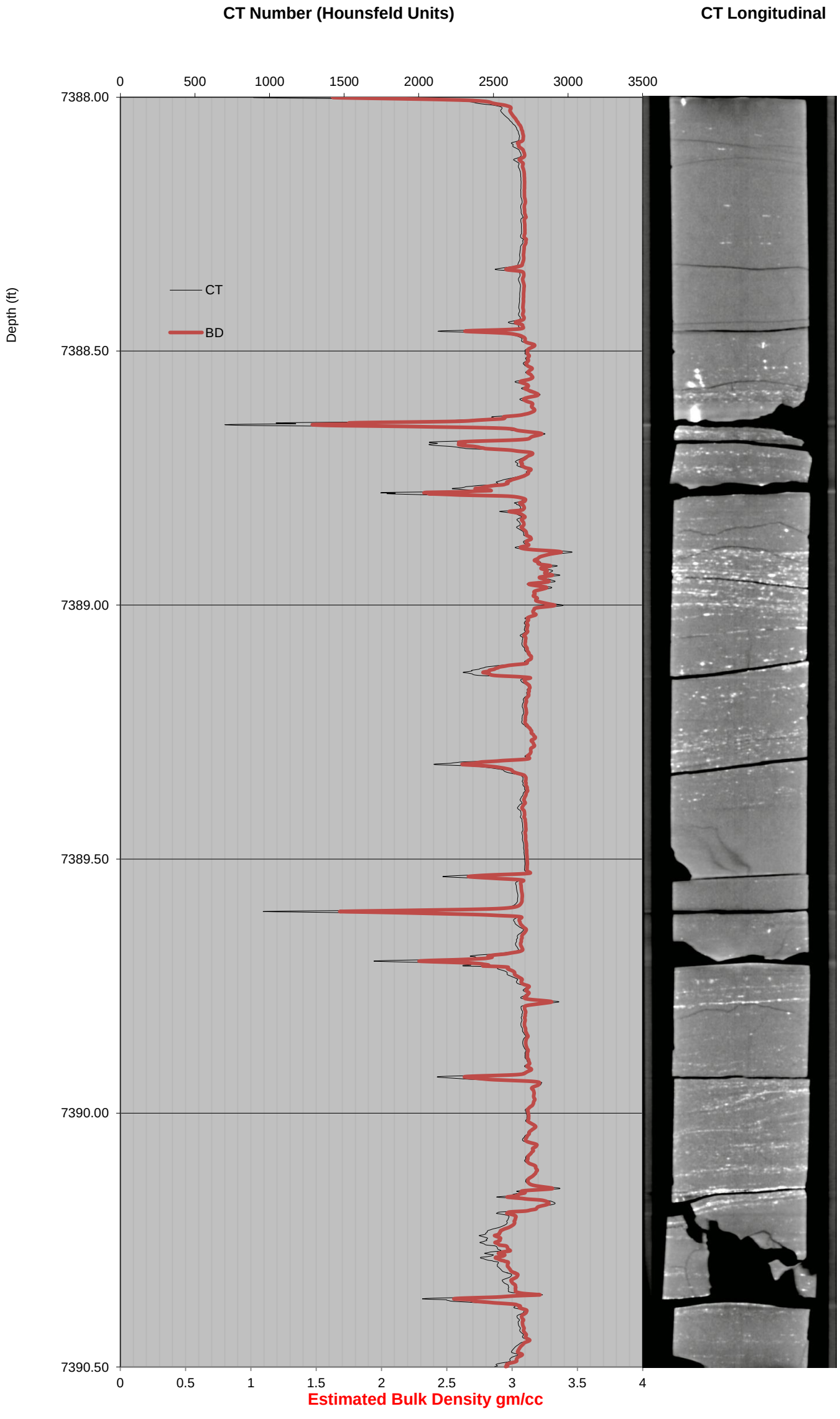

CT NUMBER PLOT WITH LONGITUDINAL

7390.50-7393.50 feet

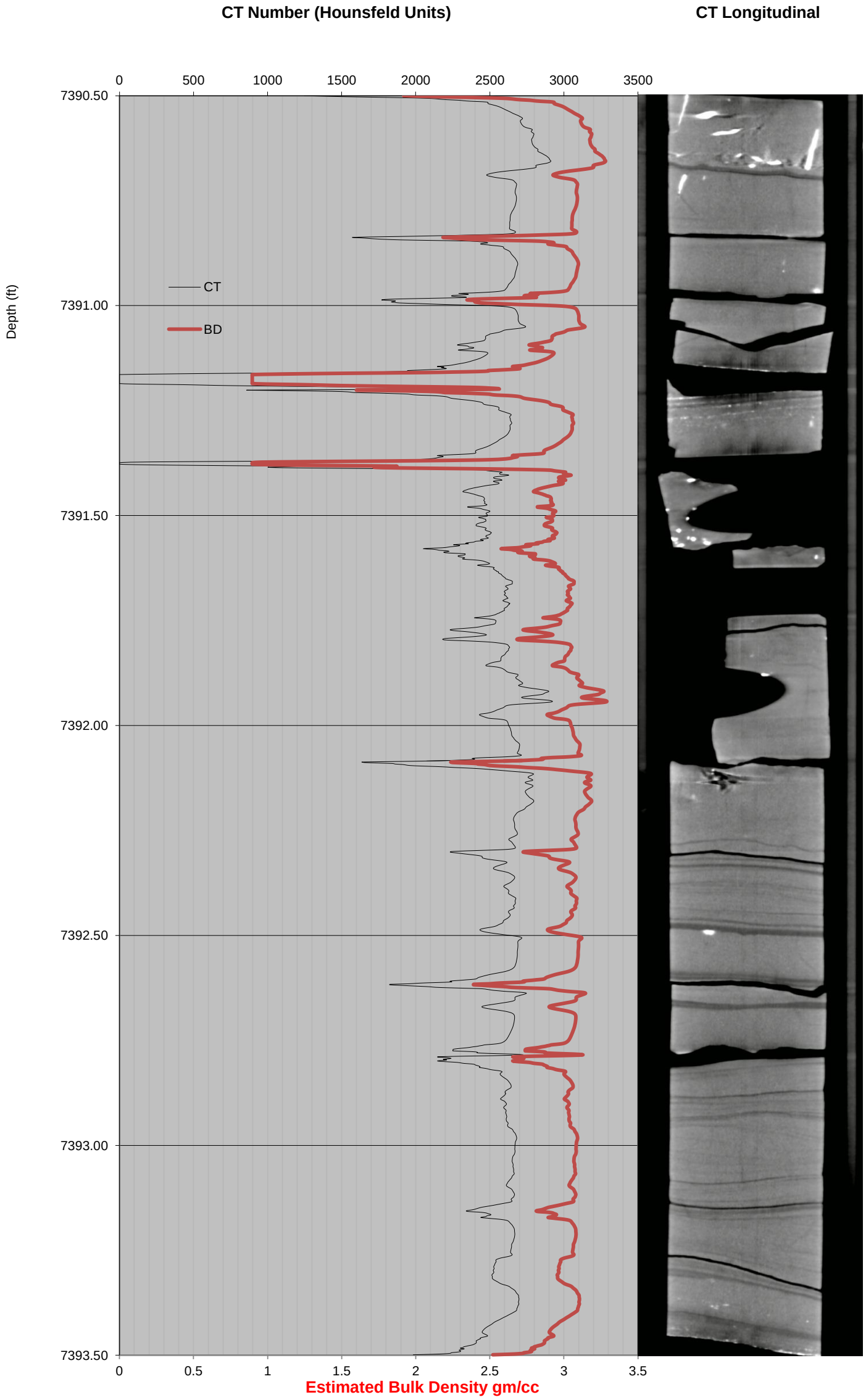

CT NUMBER PLOT WITH LONGITUDINAL

7393.50-7396.00 feet

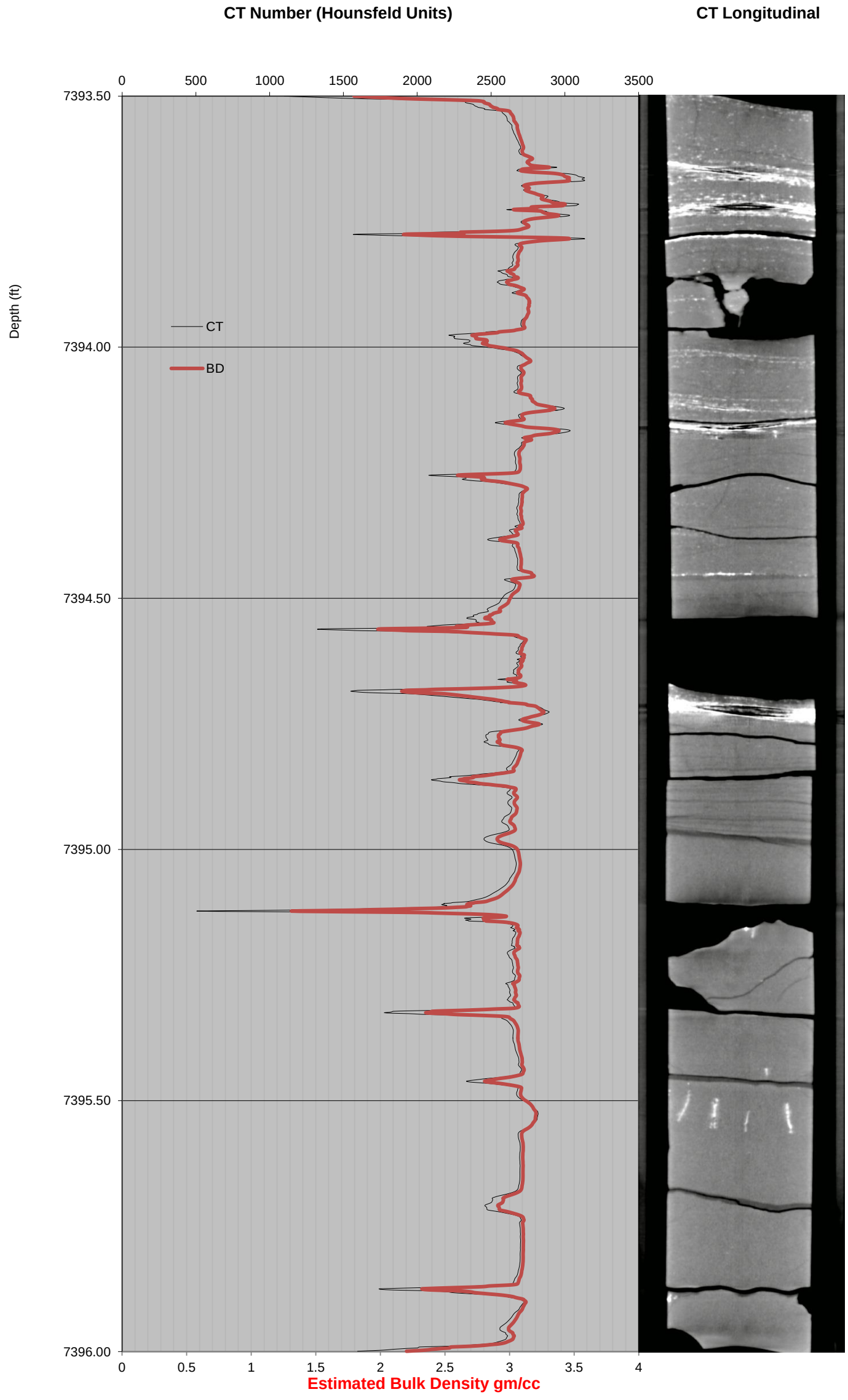

CT NUMBER PLOT WITH LONGITUDINAL

7396.00-7399.00 feet

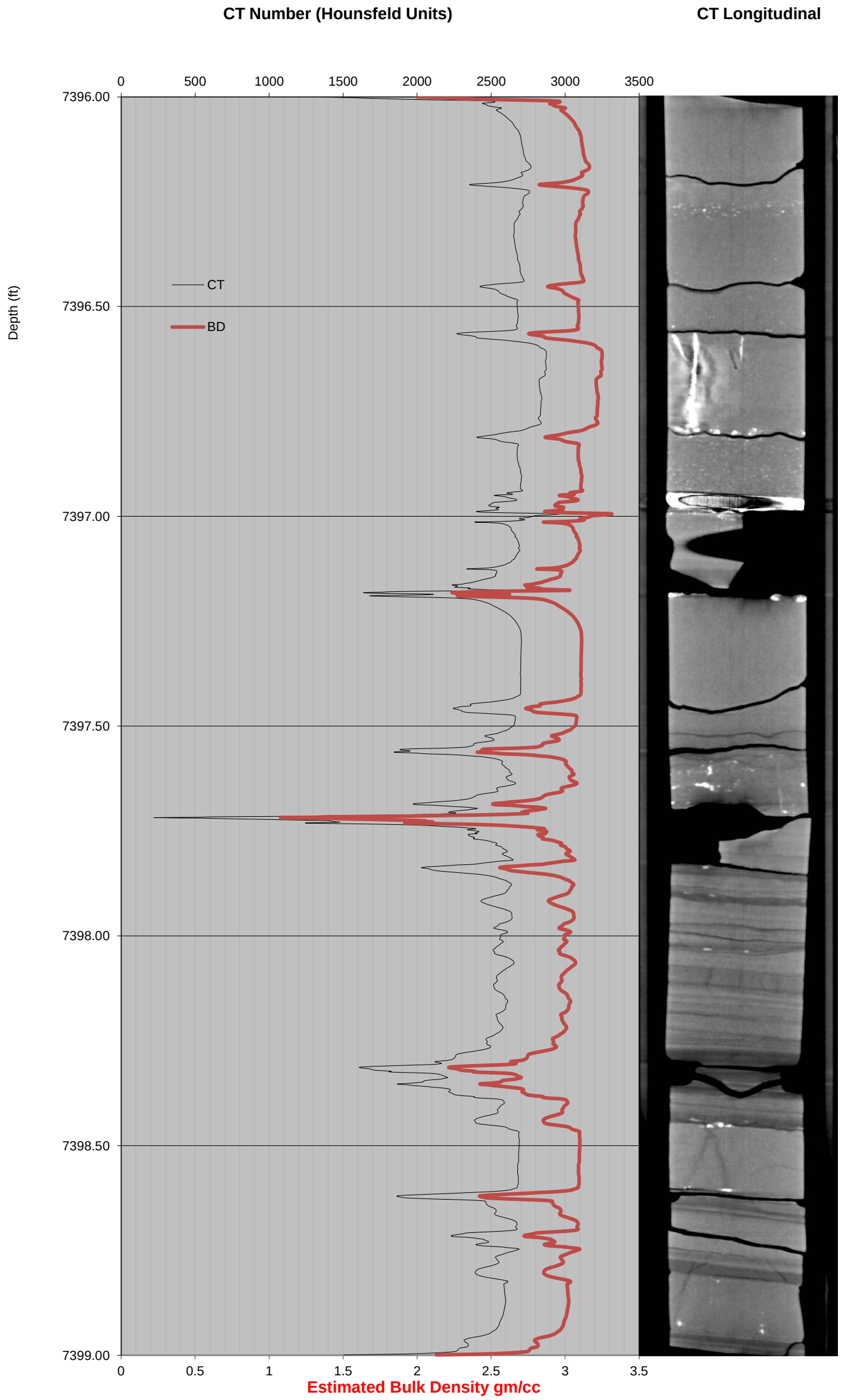

CT NUMBER PLOT WITH LONGITUDINAL

7399.00-7402.00 feet

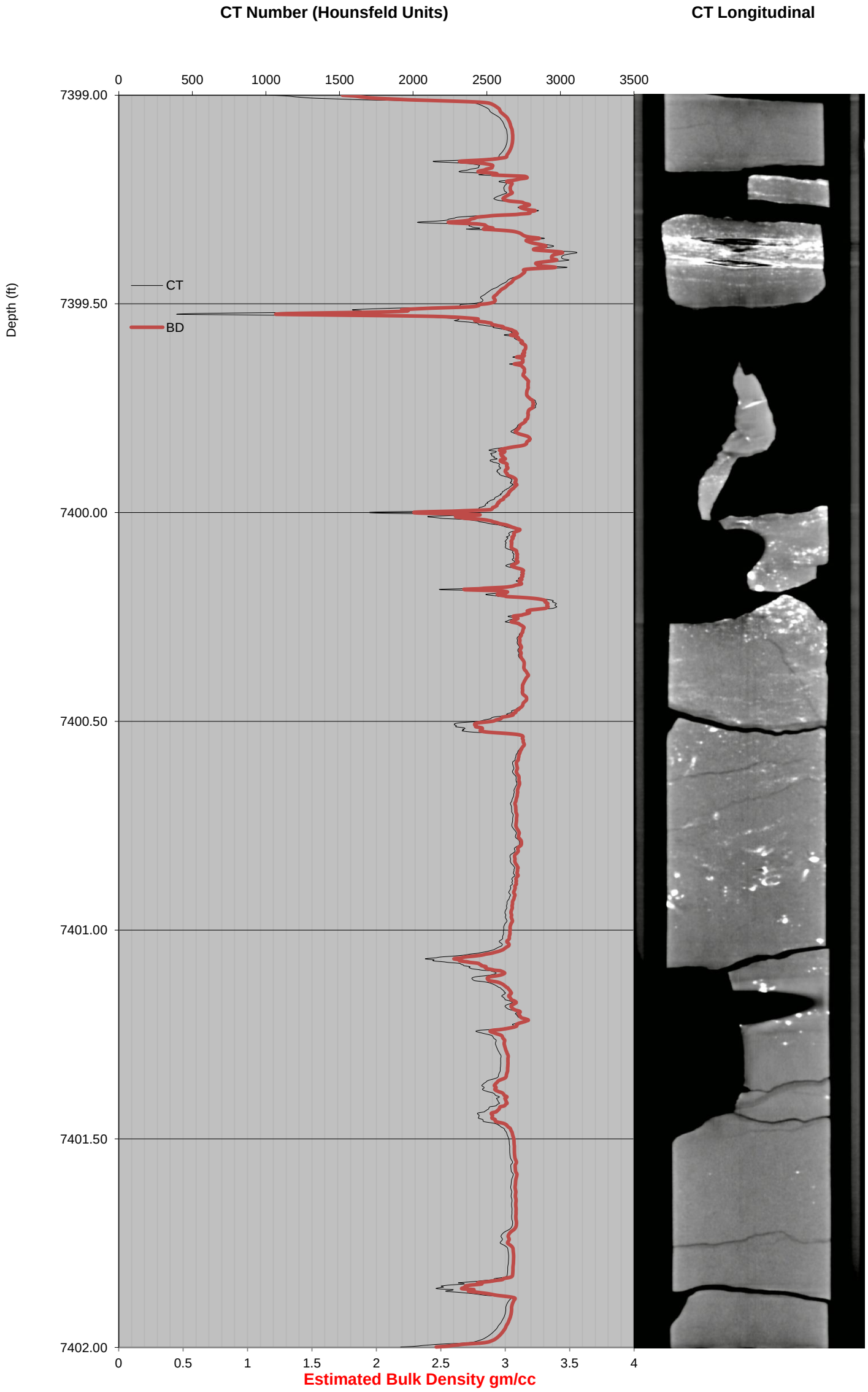

CT NUMBER PLOT WITH LONGITUDINAL

7402.00-7405.00 feet

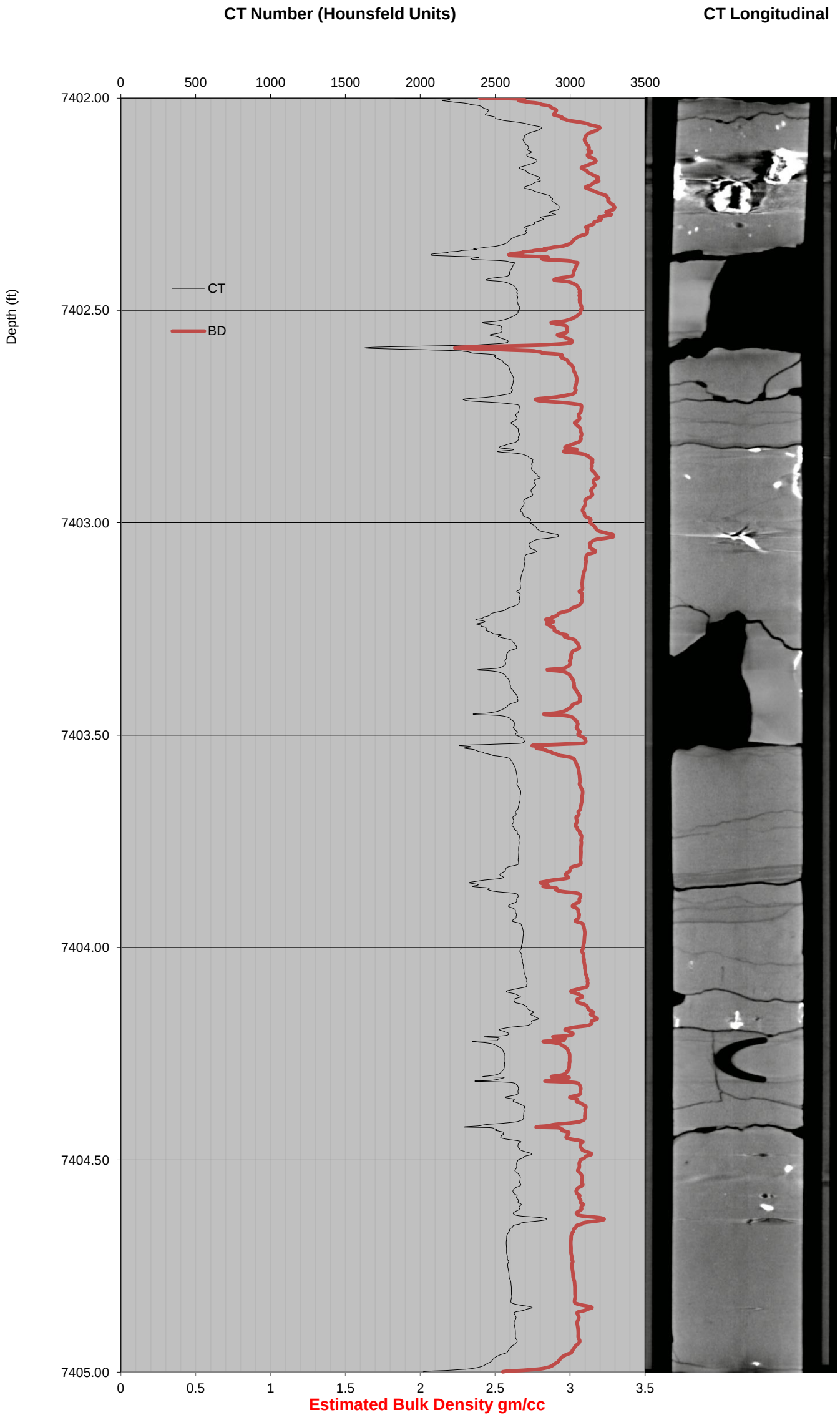

CT NUMBER PLOT WITH LONGITUDINAL

7405.00-7408.00 feet

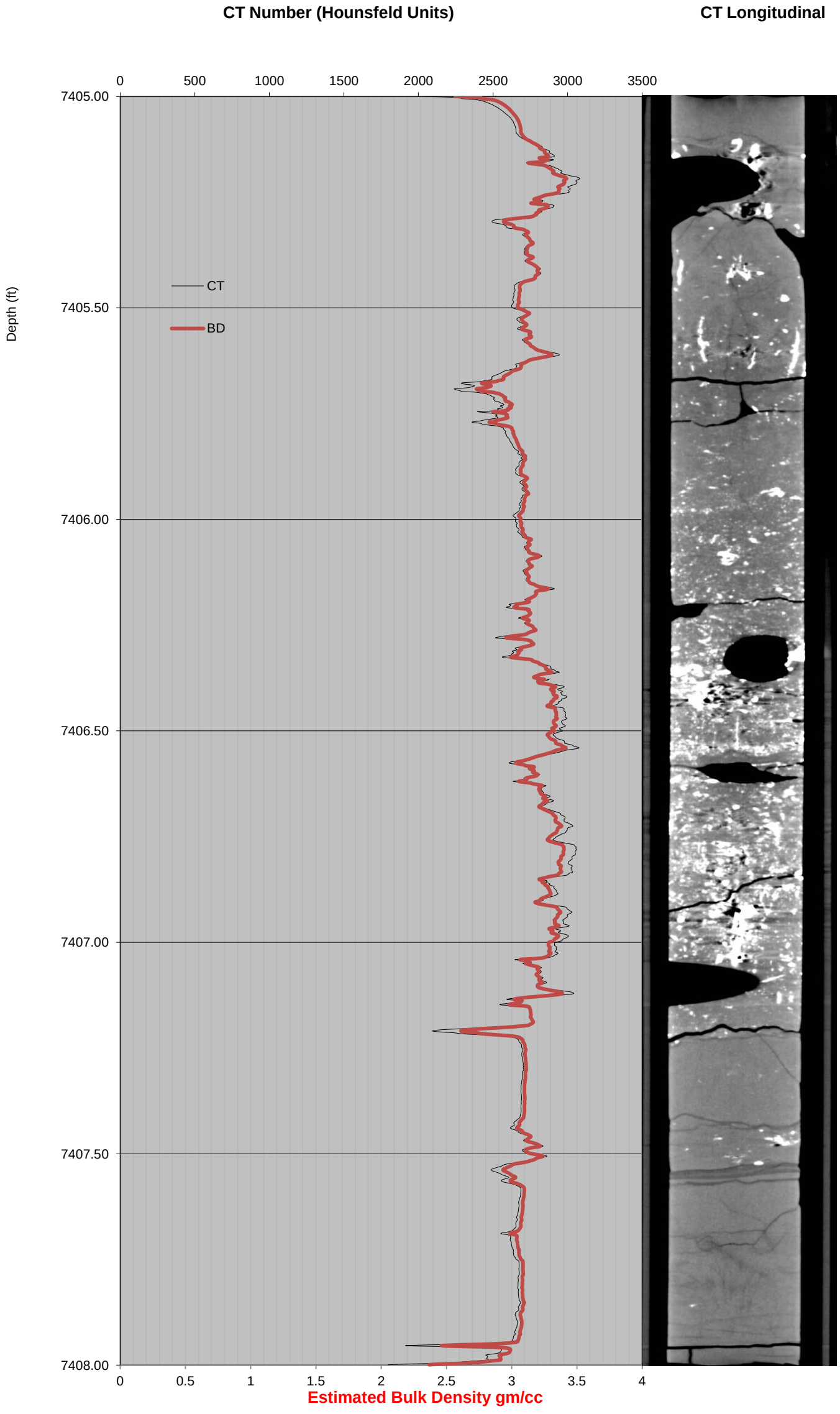

CT NUMBER PLOT WITH LONGITUDINAL

7408.00-7411.00 feet

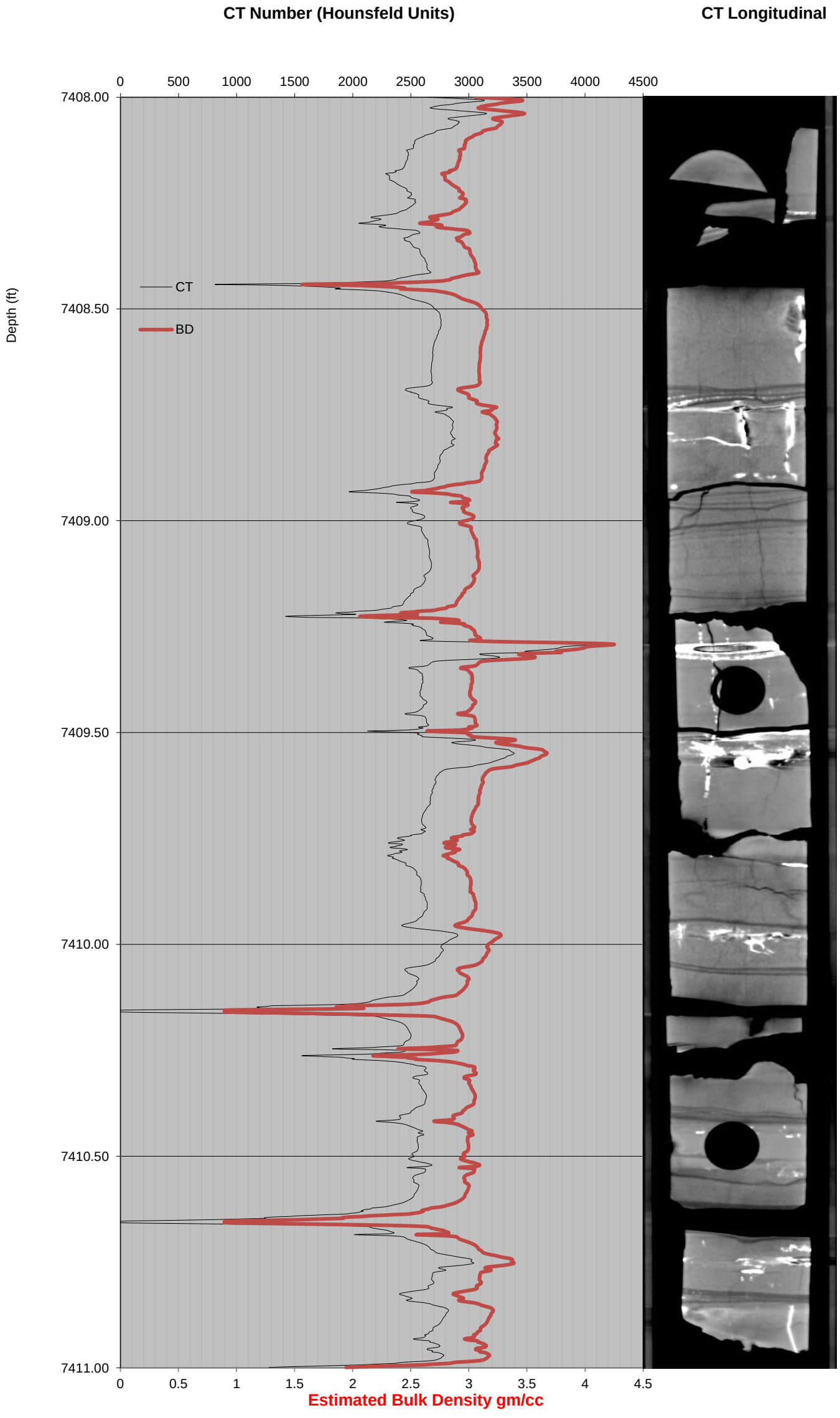

CT NUMBER PLOT WITH LONGITUDINAL

7411.00-7414.00 feet

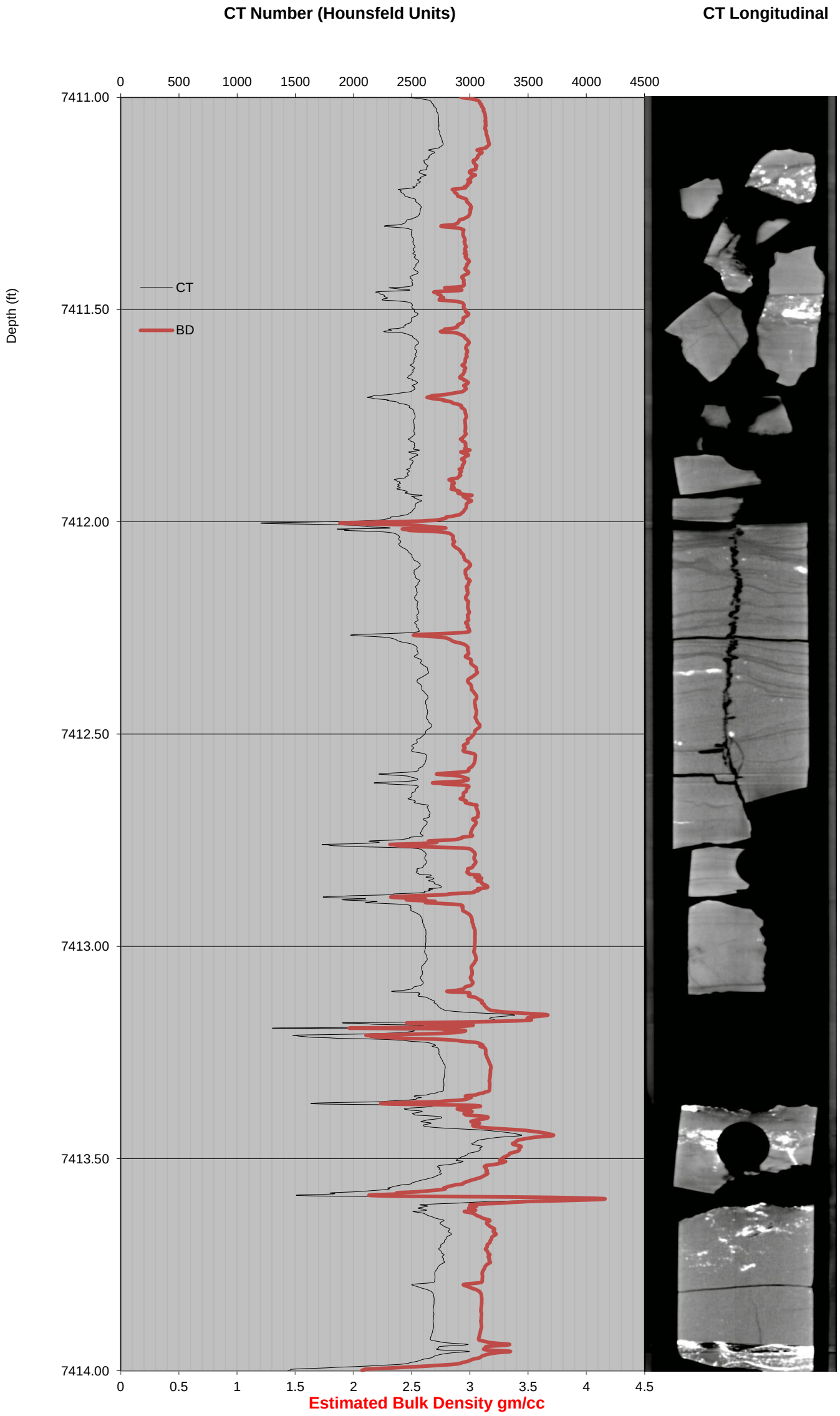

CT NUMBER PLOT WITH LONGITUDINAL

7414.00-7417.00 feet

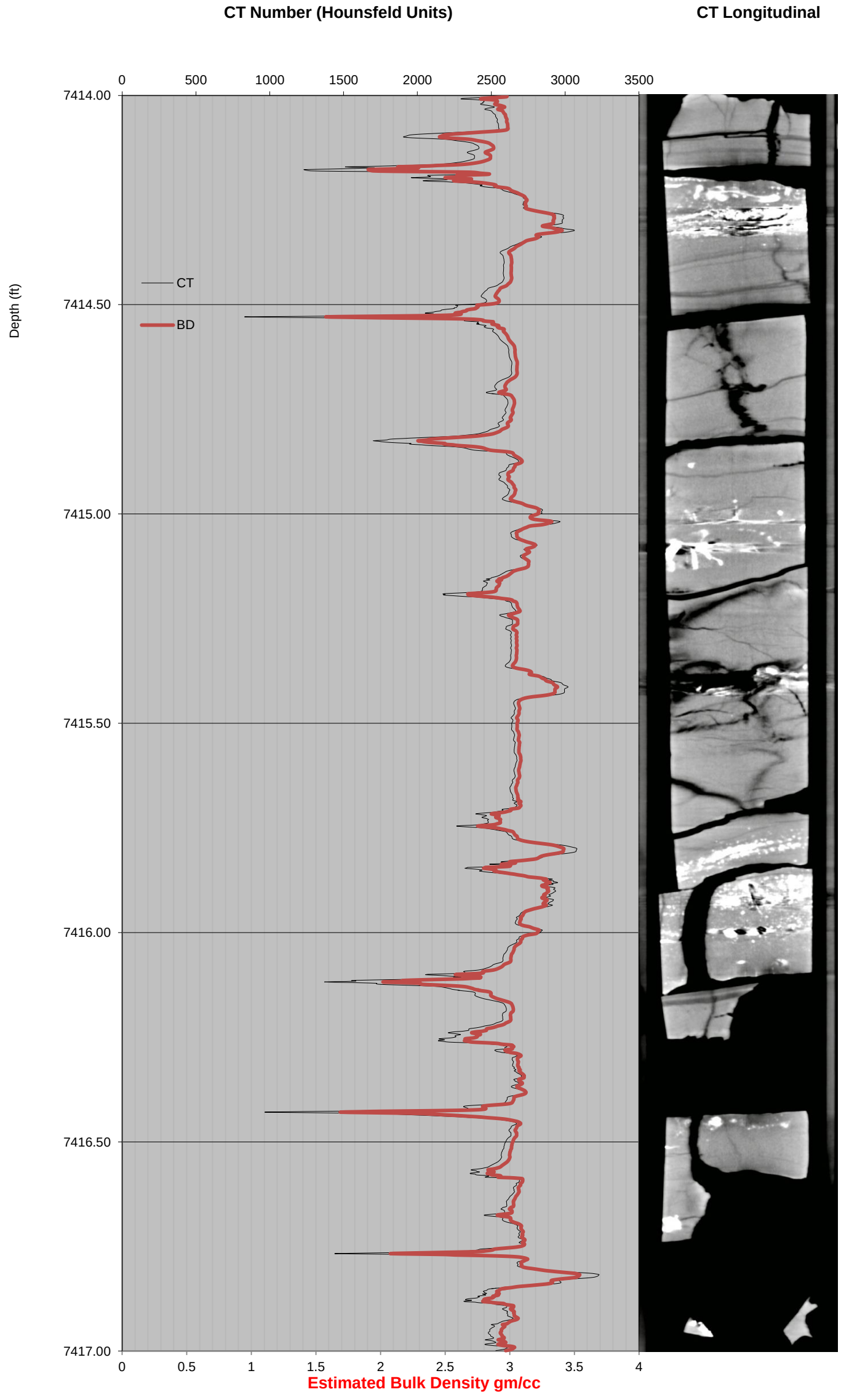

CT NUMBER PLOT WITH LONGITUDINAL

7417.00-7419.80 feet

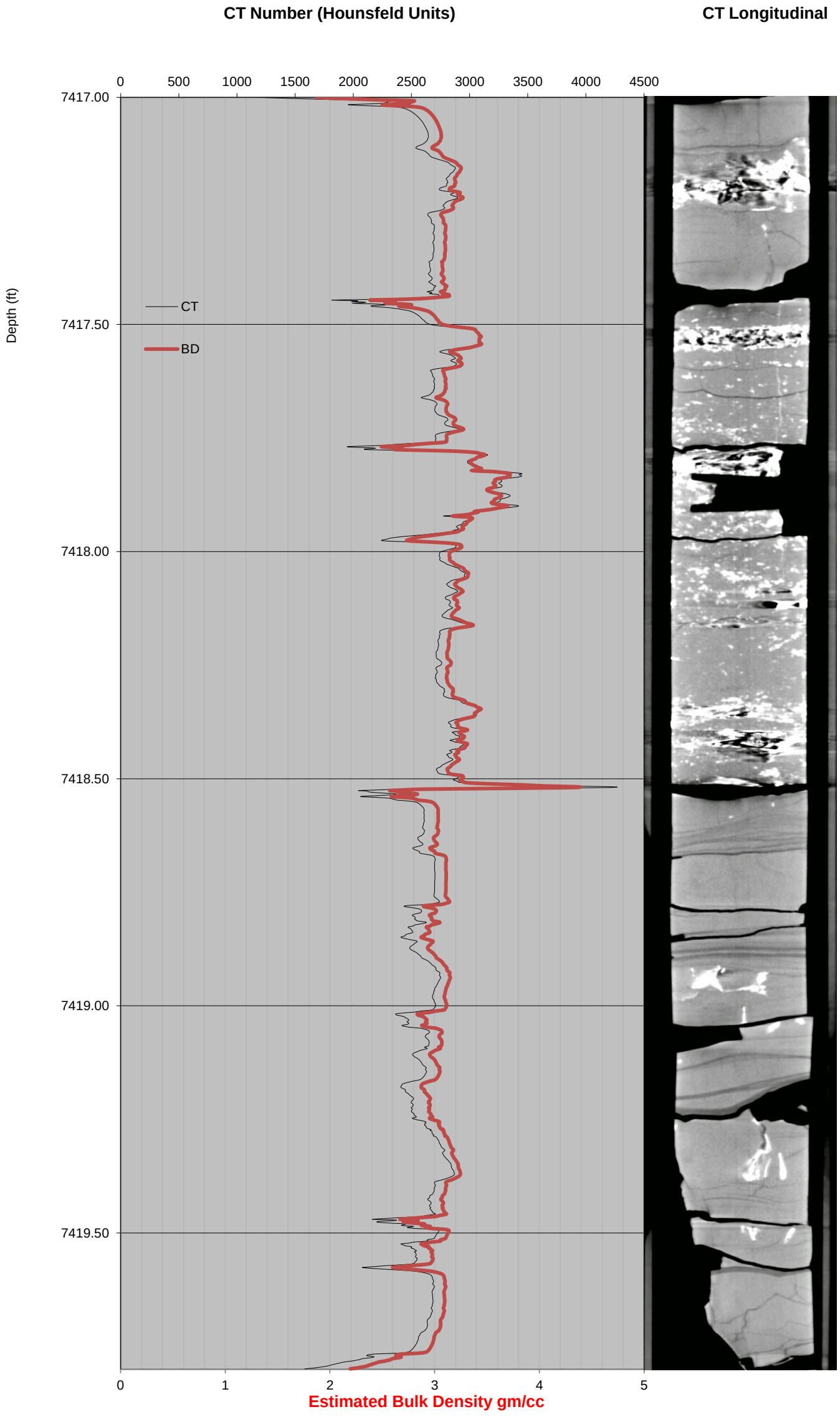

CT NUMBER PLOT WITH LONGITUDINAL

7435.00-7436.00 feet

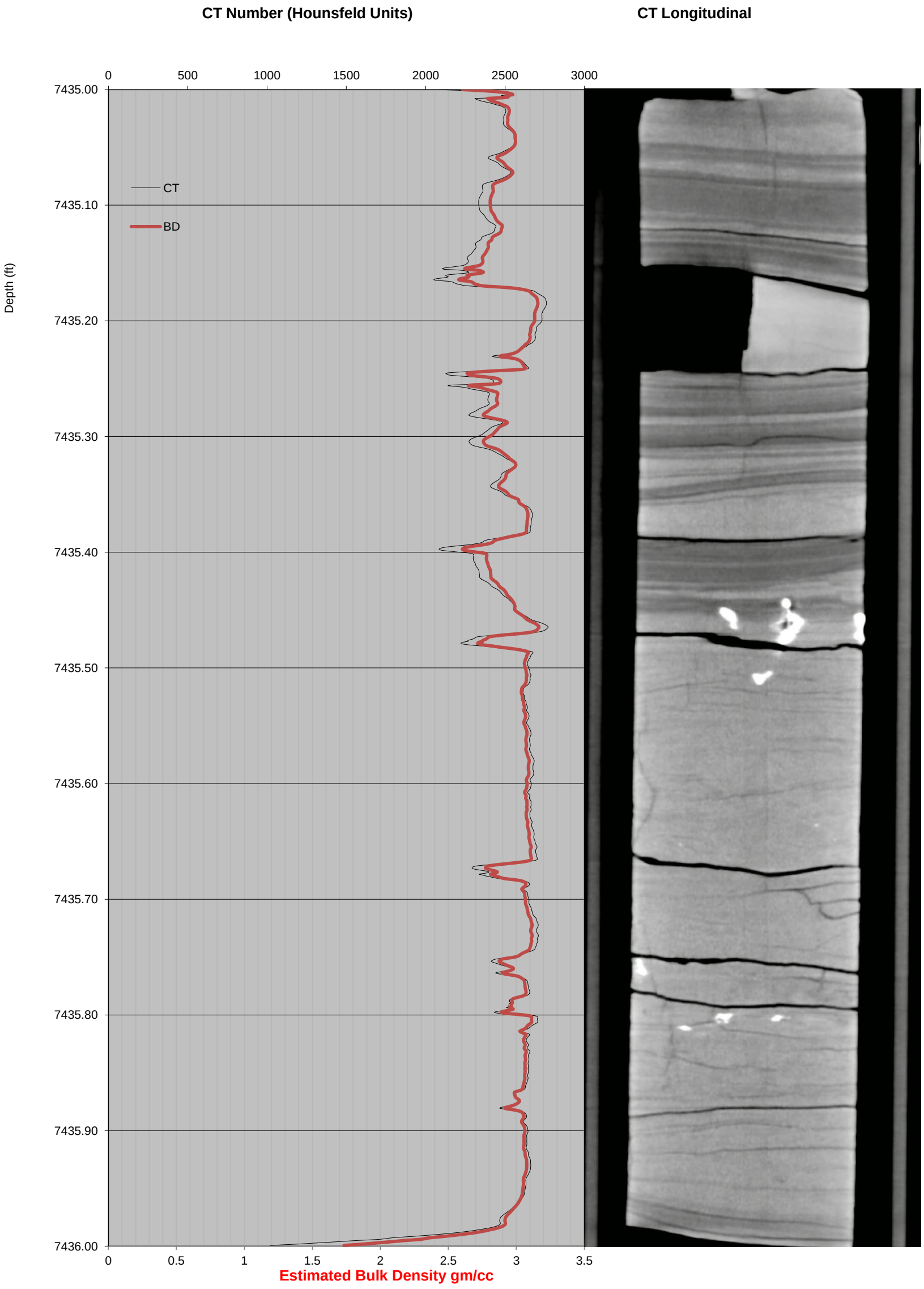

CT NUMBER PLOT WITH LONGITUDINAL

7436.00-7439.00 feet

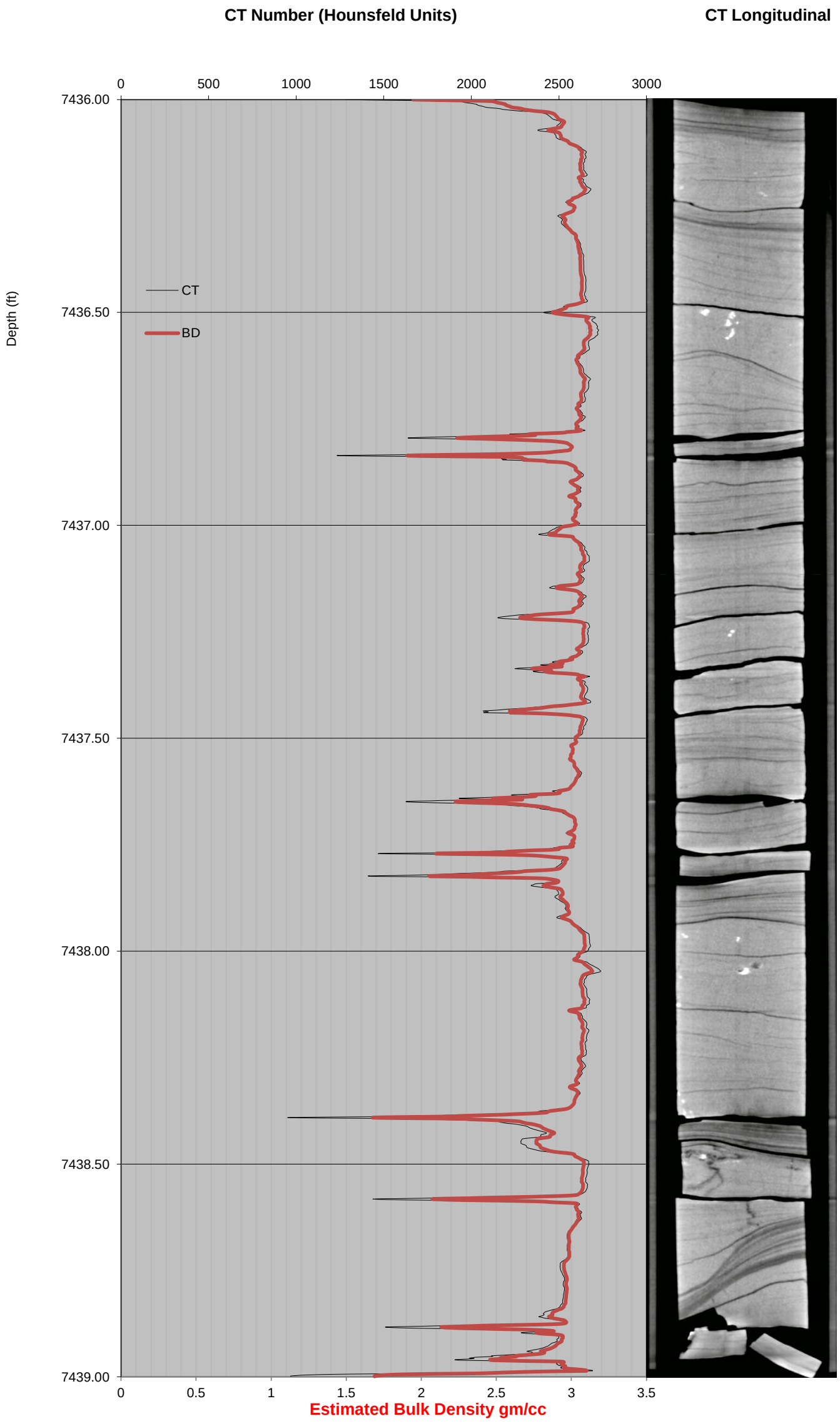

CT NUMBER PLOT WITH LONGITUDINAL

7439.00-7442.00 feet

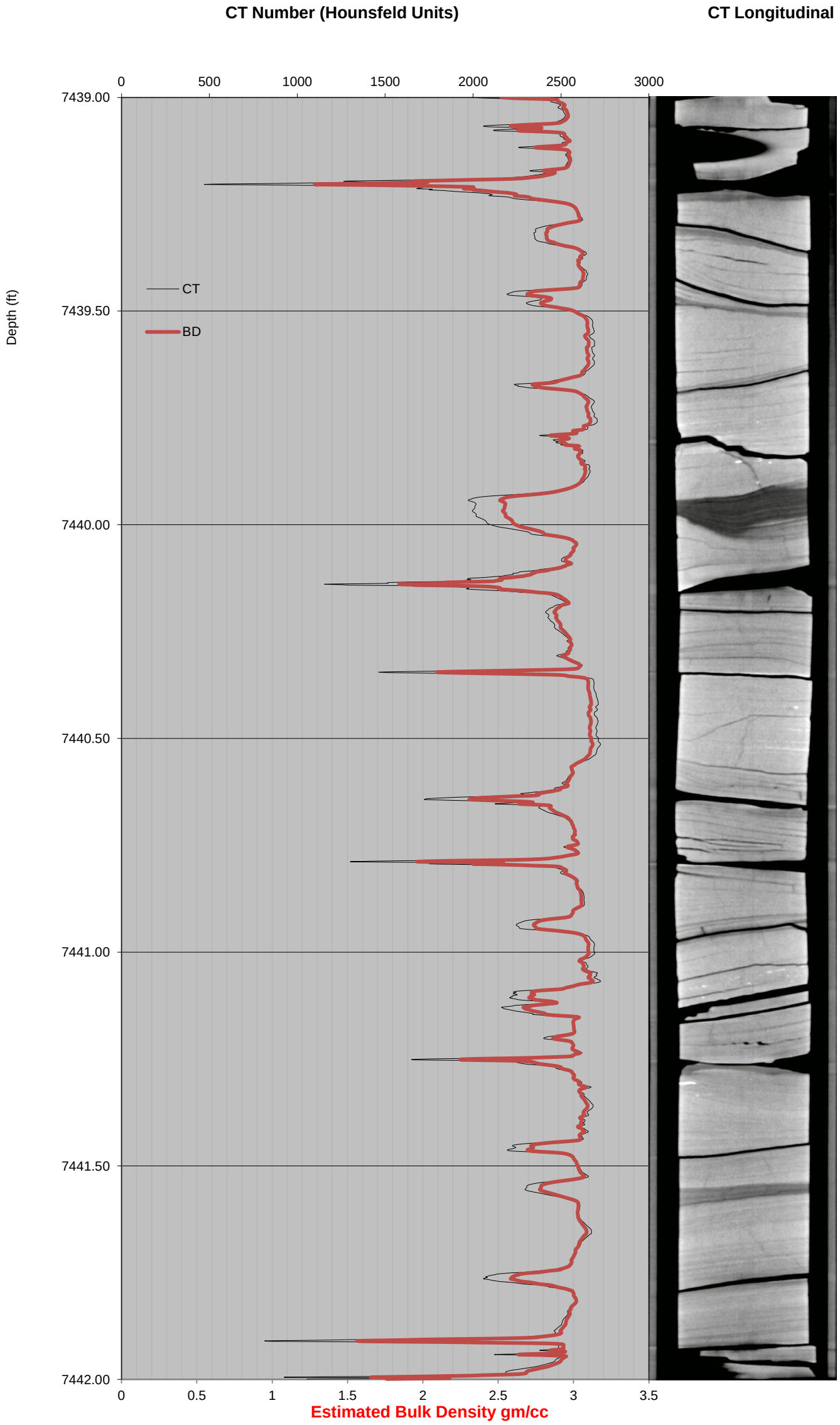

CT NUMBER PLOT WITH LONGITUDINAL

7442.00-7445.00 feet

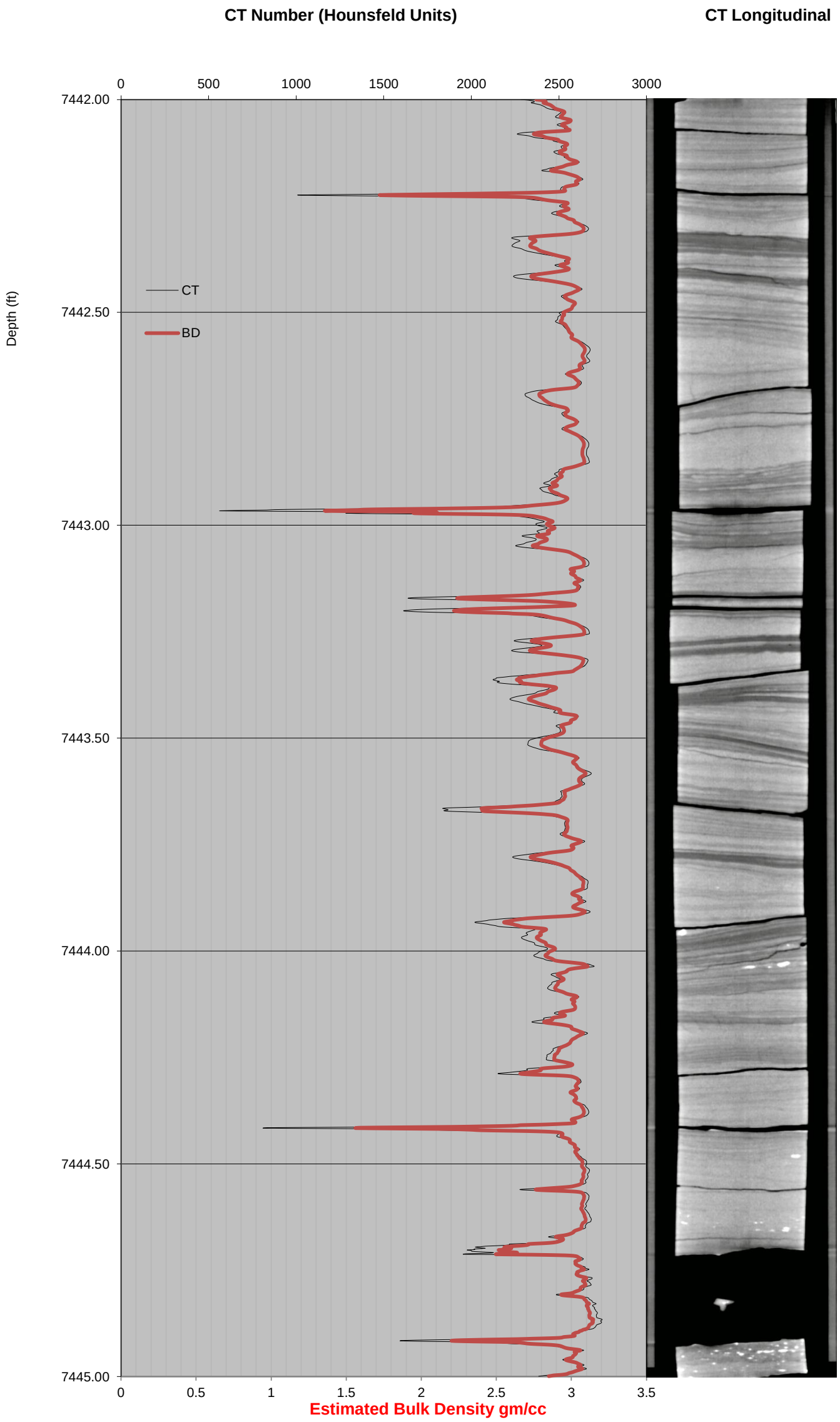

CT NUMBER PLOT WITH LONGITUDINAL

7445.00-7448.00 feet

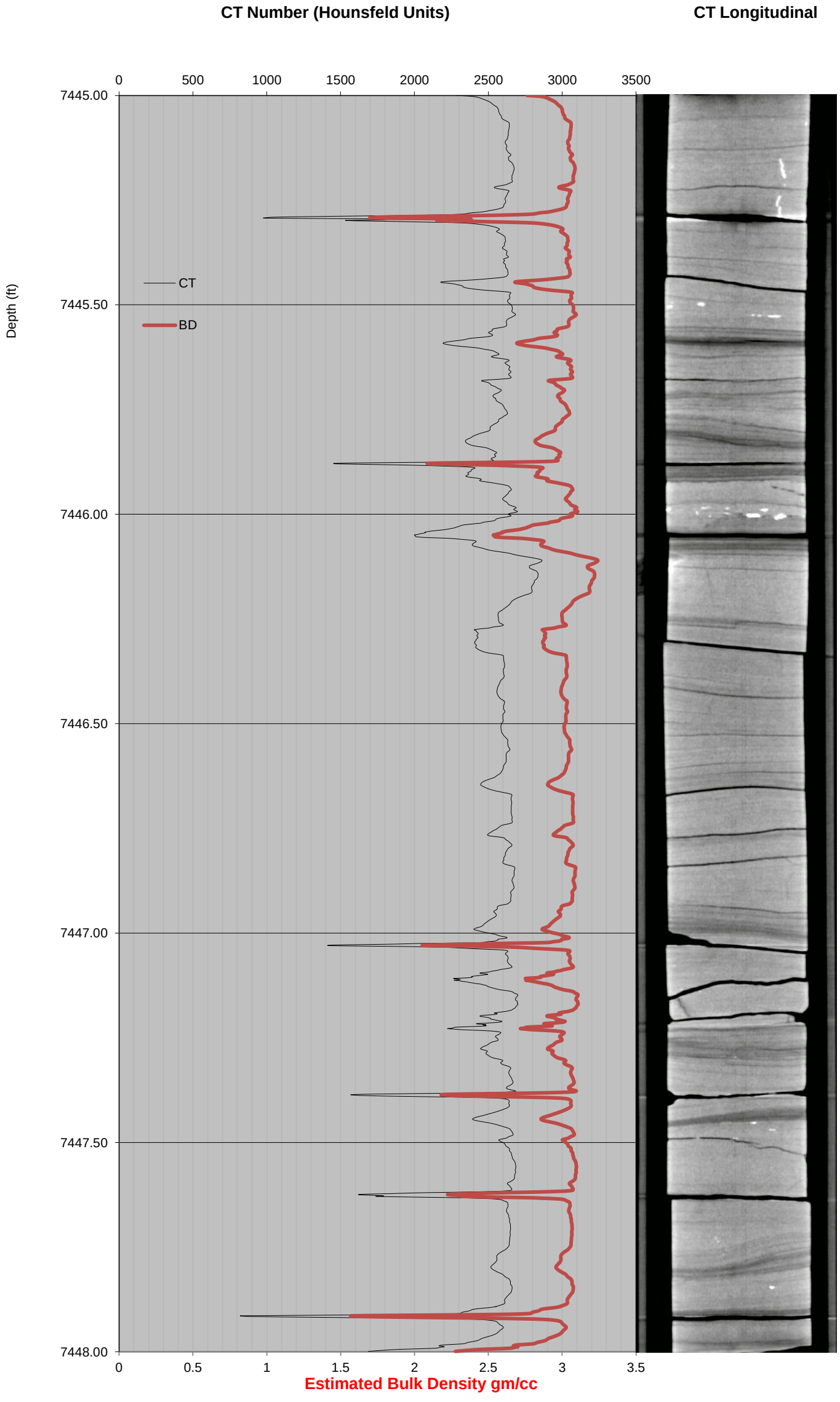

CT NUMBER PLOT WITH LONGITUDINAL

7448.00-7451.00 feet

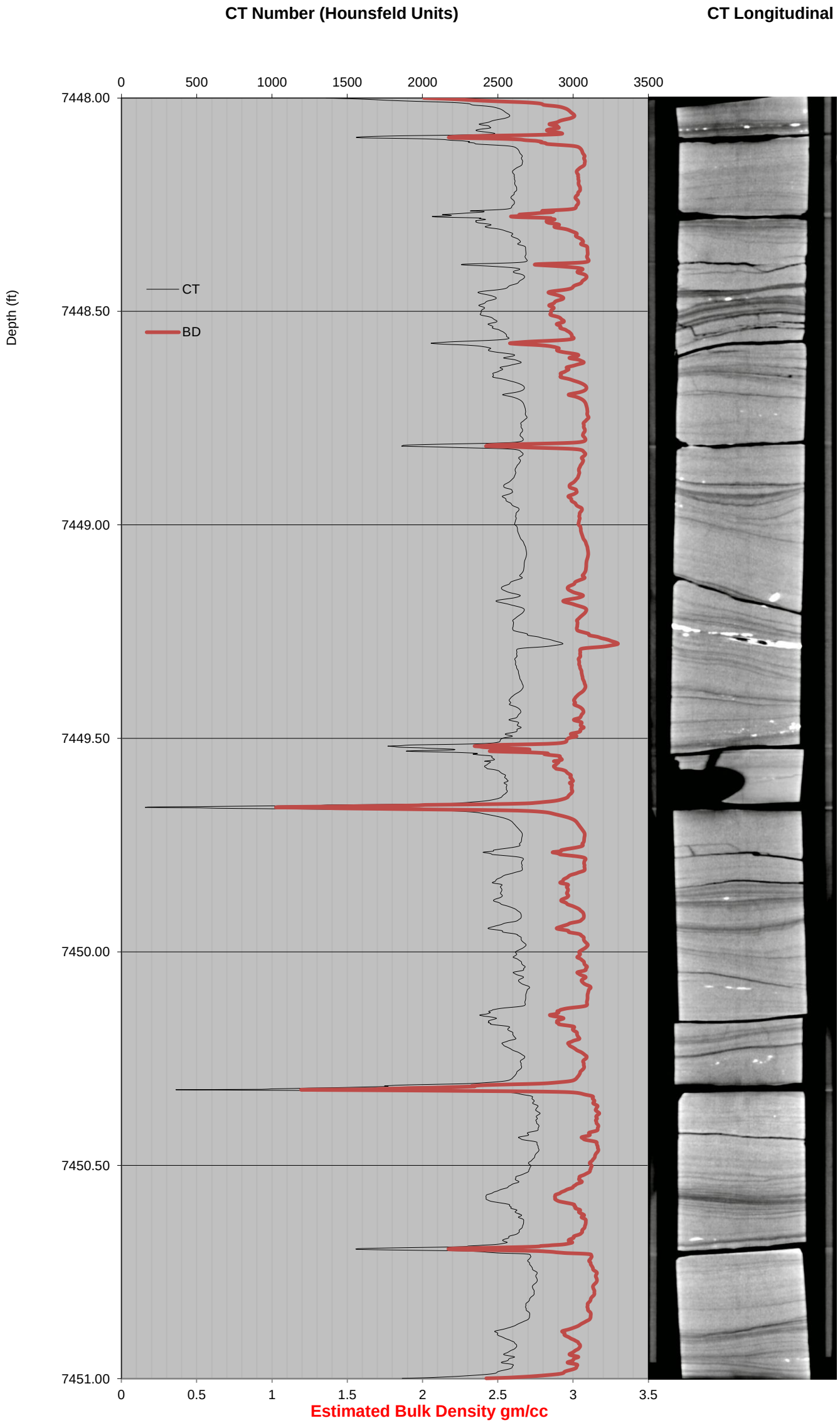

CT NUMBER PLOT WITH LONGITUDINAL

7451.00-7454.00 feet

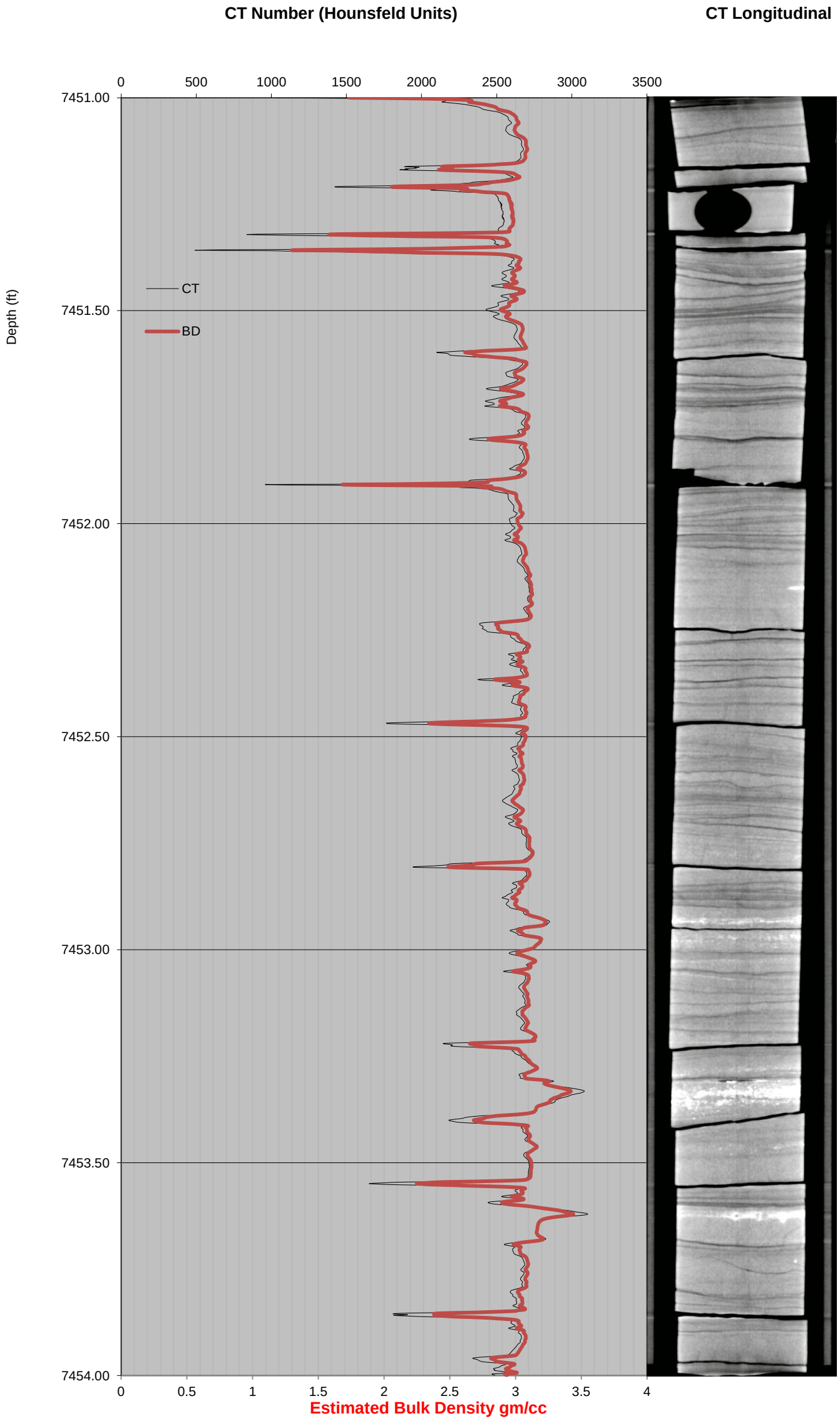

CT NUMBER PLOT WITH LONGITUDINAL

7454.00-7457.00 feet

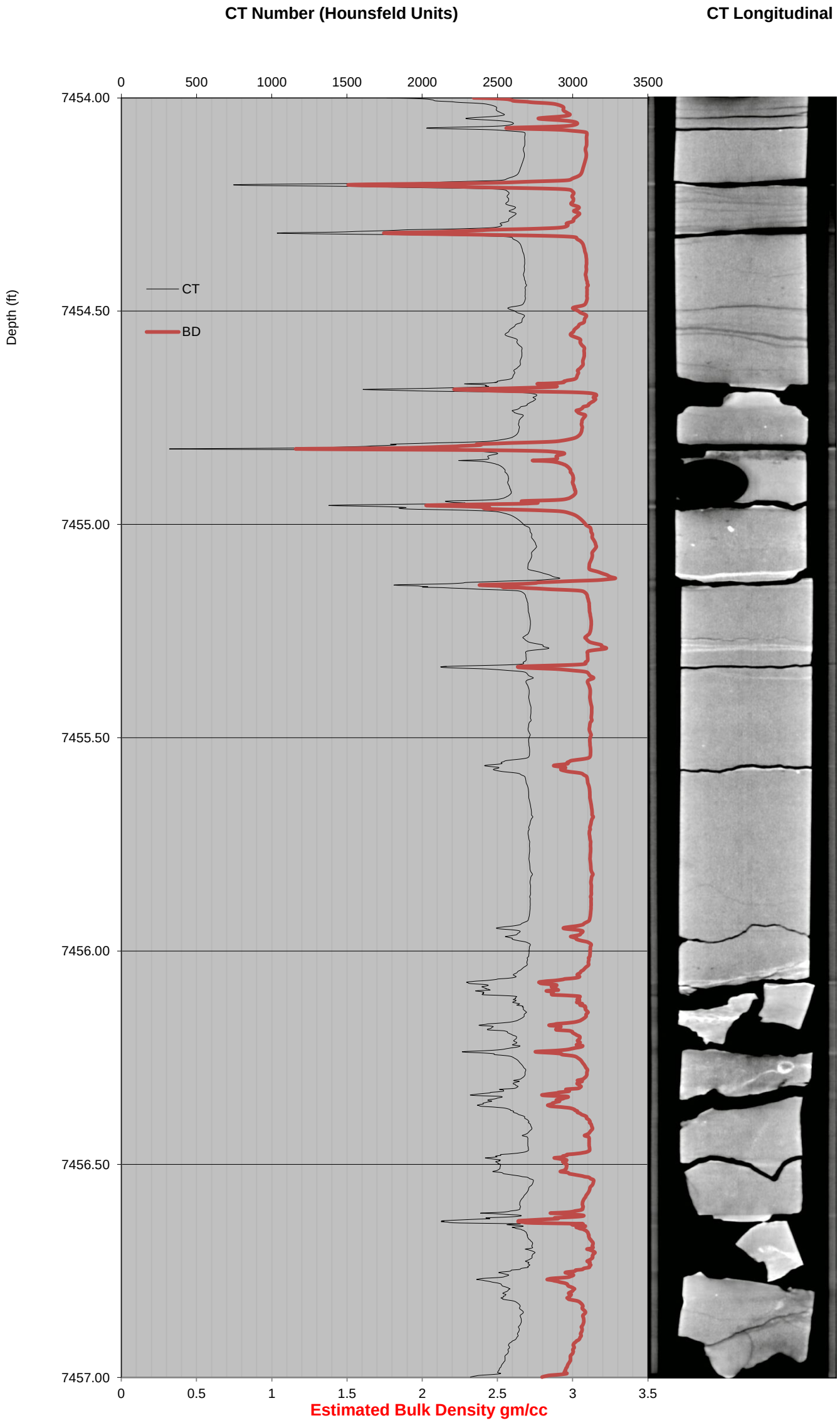

CT NUMBER PLOT WITH LONGITUDINAL

7457.00-7460.00 feet

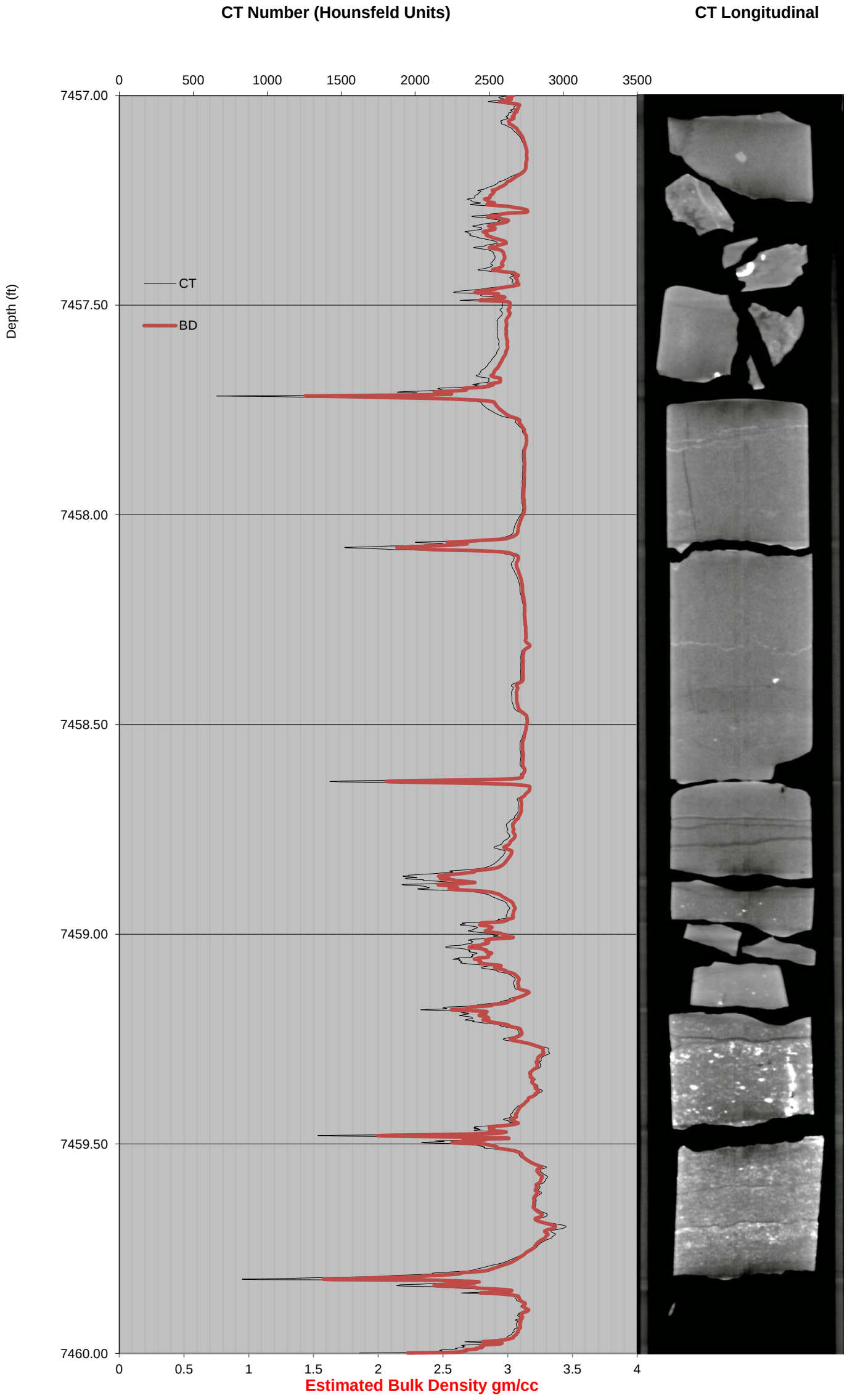

CT NUMBER PLOT WITH LONGITUDINAL

7460.00-7464.00 feet

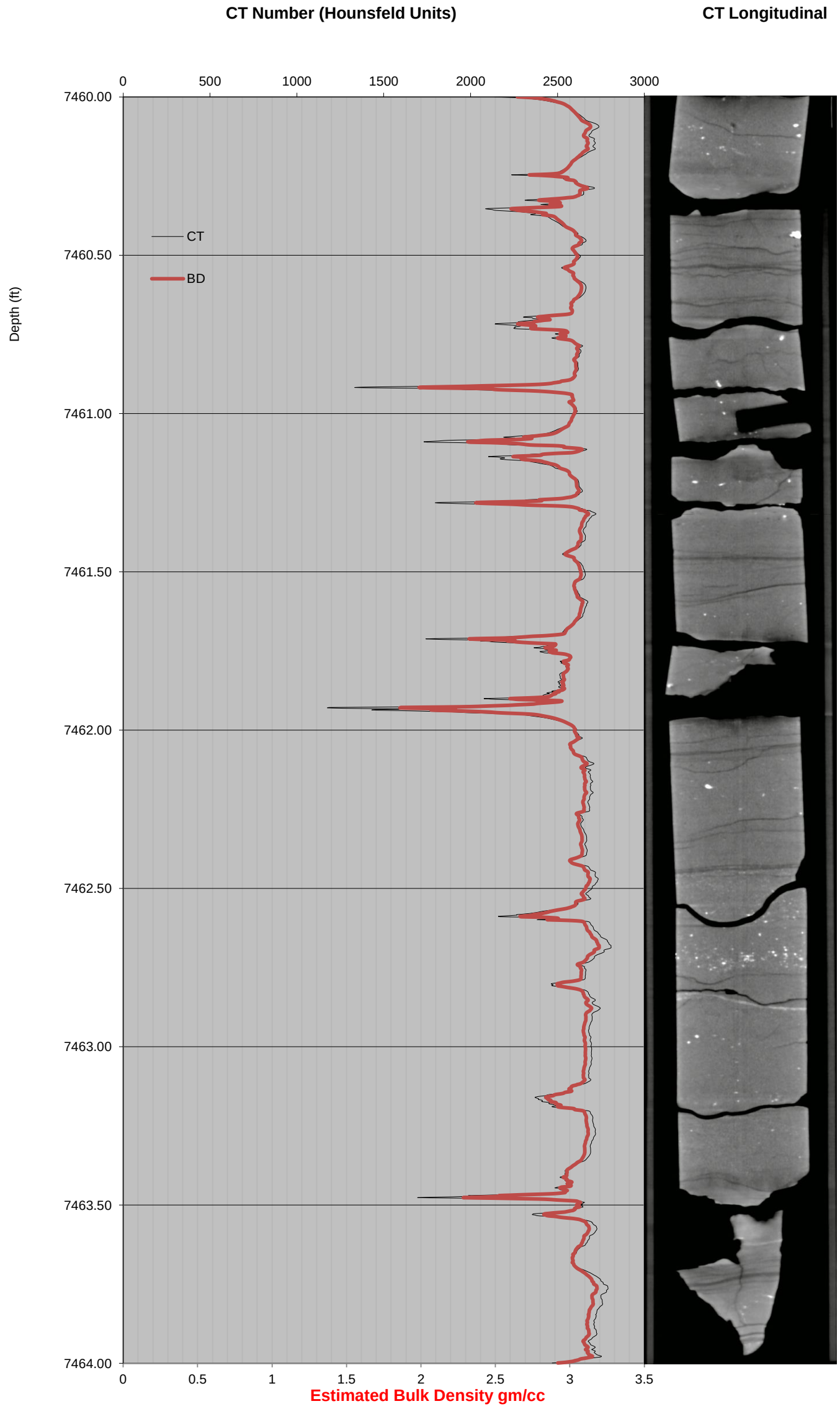

CT NUMBER PLOT WITH LONGITUDINAL

7464.00-7466.70 feet